AUBURN UNIVERSITY

Samuel Ginn College of Engineering

Research Report

ULTRA-HIGH-PERFORMANCE CONCRETE FOR THE ALABAMA TRANSPORTATION INDUSTRY

Submitted to

The Alabama Department of Transportation

Prepared by

Segun J. Osibodu

Daniel M. Coleman

Anton K. Schindler

APRIL 2026

Highway Research Center

Harbert Engineering Center

Auburn, Alabama 36849

1. Report No. 931-069	2. Government Accession No.	3. Recipient Catalog No.
4. Title and Subtitle Ultra-High-Performance Concrete for the Alabama Transportation Industry		5. Report Date April 2026
		6. Performing Organization Code
7. Author(s) Segun J. Osibodu, Daniel M. Coleman, and Anton K. Schindler		8. Performing Organization Report No. 931-069
9. Performing Organization Name and Address Highway Research Center Department of Civil and Environmental Engineering 238 Harbert Engineering Center Auburn University, AL 36849		10. Work Unit No. (TRAIS)
		11. Contract or Grant No.
12. Sponsoring Agency Name and Address Alabama Department of Transportation 1409 Coliseum Boulevard Montgomery, Alabama 36130-3050		13. Type of Report and Period Covered
		14. Sponsoring Agency Code
15. Supplementary Notes Project performed in cooperation with the Alabama Department of Transportation.		

16. Abstract

Ultra-high-performance concrete (UHPC) offers exceptional compressive strength, sustained post-cracking tensile capacity, and inherent durability that makes it well suited for transportation applications such as closure pours, deck overlays, and precast element connections. The objective of this study was to develop, characterize, and field-validate non-proprietary UHPC using Alabama materials that satisfies Federal Highway Administration (FHWA) structural requirements for cast-in-place applications at a significantly lower cost when compared to proprietary UHPC. During the laboratory-testing phase, UHPC mixtures were produced using a planetary high-shear mixer to systematically evaluate five constituent variables: steel fiber dosage (0% to 2.0% by volume), fine aggregate gradation, cementitious blend type (binary versus ternary), silica fume content (9% to 15% of total binder), and water-to-binder ratio (0.18 to 0.22). Each mixture was evaluated in compression, flexure per ASTM C1609, and direct tension per AASHTO T 397 at 28 and 91 days, with select mixtures further tested for freeze-thaw durability through 300 cycles. A refined testing protocol for AASHTO T 397 was developed that improved the direct-tension test success rate from 44% to 75% using a 220-kip universal testing machine with wedge grips. A forward analysis was also performed to establish equivalent flexural stress acceptance criteria corresponding to the FHWA tensile stress requirements. During the field-testing phase, three production trials were performed where two cubic yards of UHPC were produced in a ready mixed concrete plant. During each full-scale trial the mixing and loading sequence was progressively adjusted to eliminate cement balling during mixing. The non-proprietary UHPC, proportioned with standard AASHTO M 6 river sand, Type IL cement, slag cement, 9% silica fume, and 1.5% steel fibers by volume, exceeded the FHWA minimum post-cracking tensile strength of 750 psi at an estimated material cost of $640 to $760 per cubic yard, representing less than 40% of the cost of proprietary alternatives. All mixtures tested were inherently freeze-thaw resistant without air entrainment, and field-produced UHPC achieved tensile performance comparable to laboratory specimens, confirming the viability of full-scale production. A draft ALDOT special provision with performance-based acceptance criteria was developed from these findings. This work provides ALDOT with the technical basis and specification framework needed to implement non-proprietary UHPC using materials already available within the Alabama concrete industry.

17. Key Words Direct-tension testing, flexural testing, steel fibers, full-scale, non-proprietary UHPC, proportions		18. Distribution Statement No restrictions.	
19. Security Classification (of this report) Unclassified	20. Security Classification (of this page) Unclassified	21. No. of Pages 143	22. Price None.

Research Report

ULTRA-HIGH-PERFORMANCE CONCRETE FOR THE ALABAMA TRANSPORTATION INDUSTRY

Submitted to

The Alabama Department of Transportation

Prepared by

Segun J. Osibodu

Daniel M. Coleman

Anton K. Schindler

APRIL 2026

DISCLAIMERS

Anton K. Schindler, Ph.D., P.E.

Research Supervisor

ACKNOWLEDGEMENTS

Material contained herein was obtained in connection with a research project "Ultra-High-Performance Concrete for the Alabama Transportation Industry" ALDOT Project 931-069, conducted by the Auburn University Highway Research Center. Funding for the project was provided by the Alabama Department of Transportation (ALDOT). The funding, cooperation, and assistance of many individuals from each of these organizations are gratefully acknowledged. The authors particularly acknowledge the contributions of the following individuals:

Scott George	ALDOT, State Materials and Tests Engineer
Stacey Glass	ALDOT, State Construction Engineer
Brad Williams	ALDOT, State Bridge Engineer
Paul Froede	ALDOT, Miscellaneous Structures and Bridge Design
Kidada Dixon	ALDOT, State Research and Development Engineer
Steven Ingram	ALDOT, Deputy State Materials and Tests Engineer
Ryan Kelley	ALDOT, Concrete Engineer
Dr. Benjamin Graybeal	FHWA, Team Leader–Bridge Engineering Research
Dr. Rafic El-Helou	FHWA, Research Structural Engineer
Scott Kelley	Heidelberg Materials, Concrete Technical Services
Nicholas Bailey	Heidelberg Materials, Sr. Tech Service Manager, S.E. Concrete
Jim Van Keuren	Heidelberg Materials, Sr. Quality Control Specialist, S.E. Concrete
Nick Shortridge	Master Builders Solutions, Sales Representative

ABSTRACT

Ultra-high-performance concrete (UHPC) offers exceptional compressive strength, sustained post-cracking tensile capacity, and inherent durability that makes it well suited for transportation applications such as closure pours, deck overlays, and precast element connections. The objective of this study was to develop, characterize, and field-validate non-proprietary UHPC using Alabama materials that satisfies Federal Highway Administration (FHWA) structural requirements for cast-in-place applications at a significantly lower cost when compared to proprietary UHPC.

During the laboratory-testing phase, UHPC mixtures were produced using a planetary high-shear mixer to systematically evaluate five constituent variables: steel fiber dosage (0% to 2.0% by volume), fine aggregate gradation, cementitious blend type (binary versus ternary), silica fume content (9% to 15% of total binder), and water-to-binder ratio (0.18 to 0.22). Each mixture was evaluated in compression, flexure per ASTM C1609, and direct tension per AASHTO T 397 at 28 and 91 days, with select mixtures further tested for freeze-thaw durability through 300 cycles. A refined testing protocol for AASHTO T 397 was developed that improved the direct-tension test success rate from 44% to 75% using a 220-kip universal testing machine with wedge grips. A forward analysis was also performed to establish equivalent flexural stress acceptance criteria corresponding to the FHWA tensile stress requirements.

During the field-testing phase, three production trials were performed where two cubic yards of UHPC were produced in a ready mixed concrete plant. During each full-scale trial the mixing and loading sequence was progressively adjusted to eliminate cement balling during mixing.

The non-proprietary UHPC, proportioned with standard AASHTO M 6 river sand, Type IL cement, slag cement, 9% silica fume, and 1.5% steel fibers by volume, exceeded the FHWA minimum post-cracking tensile strength of 750 psi at an estimated material cost of $640 to $760 per cubic yard, representing less than 40% of the cost of proprietary alternatives. All mixtures tested were inherently freeze-thaw resistant without air entrainment, and field-produced UHPC achieved tensile performance comparable to laboratory specimens, confirming the viability of full-scale production. A draft ALDOT special provision with performance-based acceptance criteria was developed from these findings. This work provides ALDOT with the technical basis and specification framework needed to implement non-proprietary UHPC using materials already available within the Alabama concrete industry.

TABLE OF CONTENTS

LIST OF TABLES

LIST OF FIGURES

CHAPTER 1
INTRODUCTION

1.1 OVERVIEW

Ultra-high-performance concrete (UHPC) is a class of cementitious composite materials distinguished not by a single constituent or mixture proportions, but by a combination of performance-based mechanical and durability criteria that far exceed those of conventional and high-performance concretes – including a minimum compressive strength of 17,500 psi (120 MPa), a minimum uniaxial tensile cracking strength of 750 psi (5.2 MPa), and a low permeability from the dense cementitious matrix (ACI PRC-239.1-24, Graybeal and El-Helou 2023). The combination of tensile ductility, toughness, and durability that characterizes UHPC makes it particularly well suited for demanding transportation applications, where these properties give bridge design, construction, maintenance, and materials engineers the tools to pursue design solutions that are generally not achievable with conventional materials. UHPC is also a self-consolidating material, which facilitates placement in geometrically complex or congested conditions (Graybeal 2014a). Figure 1-1 illustrates one such application, where UHPC is used to fill the joint between two full-depth bridge deck panels as part of an Accelerated Bridge Construction (ABC) project.

Figure 1-1: UHPC placement operation in a deck-level connection (Haber 2016)

There are currently limited suppliers of UHPC and due to their proprietary nature, their cost can exceed \$2,000/yd^3 (Stewart et al. 2022). In this study, literature was reviewed and both laboratory and full-scale testing were performed to determine means to reduce the cost of UHPC by using locally and regionally available materials and still meet the requirements of the Alabama transportation industry. Only materials that are compliant with the Build America, Buy America Act were considered. Because of its increased durability and excellent performance, many state departments of transportation across the nation are currently exploring and implementing the use of UHPC in various bridge construction and maintenance applications. The performance of non-proprietary UHPC made with Alabama materials is yet to be established; therefore, the primary objective of this project was to use as much raw materials from locally available sources as possible to produce non-proprietary UHPC that meets the desired performance requirements for various ALDOT cast-in-place applications.

1.2 BACKGROUND

The proportions of UHPC are very different when compared to conventional high-performance concrete. UHPC with optimized gradation has been reported to contain portland cement, silica fume, fine sand, high-range water-reducing (HRWR) admixture, steel fibers, and water, with a typical water-to-cement ratio of approximately 0.22 (Russell and Graybeal 2013). The portland cement content often exceeds 1,100 lbs/yd^3. Wille et al. (2011a) concluded that the optimal amount of silica fume is 25 percent by cement weight, which is very high compared to conventional concrete. Since dense packing of particles is required, the nominal maximum aggregate size less than 0.25 in. (ASTM C1856 2017) and the aggregates could include ground quartz, glass, or basalt that has a specific gradation to ensure dense particle packing. Research will be performed to evaluate if locally available fine aggregates could provide the required performance when used to produce non-proprietary UHPC. A high volume of steel fibers (some report 2.0 percent by volume) is often used to add sufficient ductility and toughness (Floyd et al. 2023), but the use of this large amount of steel fibers significantly increases cost and impacts the workability of the UHPC.

As mentioned earlier, commercially available UHPC are proprietary products and typically costs about \$2,000/yd^3, whereas depending on the fiber dosage some have reported success in developing non-proprietary UHPC ranging from about \$350 to \$850/yd^3 (Graybeal 2014b). Therefore, in this study the type and quantity of steel fibers used will be carefully selected to minimize material cost while meeting the UHPC performance requirements desired for various typical ALDOT applications. The unique properties of UHPC come at a significantly increased material cost, however, when used in appropriate applications, the increased long-term durability and performance obtained from using UHPC could be economically justified based on reduced maintenance and life-cycle cost.

Because of the large amount of binders (cement, silica fume, etc.), the low water-to-cementitious materials ratio, and the rapid increase in temperature due to heat of hydration, Sbia et al. (2017) found that during field applications it can be a challenge to retain sufficient workability over the period required to transportation, place, consolidate, and finish the UHPC. Therefore, in this study the workability retention of UHPC under field-scale conditions was also evaluated by producing UHPC in a local ready mixed concrete plant. The evaluation of UHPC production at a ready mixed concrete plant allowed the research team to evaluate the feasibility of the non-proprietary UHPC developed during this project.

1.3 Project Objectives

The primary objective of this project is to use raw materials from locally and regionally available sources to produce non-proprietary UHPC that meets the desired performance requirements for various ALDOT cast-in-place applications. To achieve this primary objective, the following secondary objectives are part of this proposed project:

1. Identification of locally and regionally available materials that can be used to produce non-proprietary UHPC.
2. Laboratory-scale testing to evaluate the fresh and hardened properties of various non-proprietary UHPC made with locally and regionally available materials.
3. Field-scale testing of UHPC made with Alabama materials to determine its cost, workability, placeability, and performance.
4. Development of a draft ALDOT Special Provision for UHPC.

The research focused on testing and developing UHPC for field-cast applications where UHPC is used to either connect precast concrete elements or for maintenance applications (e.g., joint repair). Typical applications where states have used UHPC to connect precast concrete elements include (Graybeal 2014a; Graybeal 2018):

a. Closure pours for precast deck panels (examples are shown in Figure 1-1);
b. Connections for composite action between precast deck panels and girders that are often used in ABC;
c. Longitudinal joint connections between various bridge elements, including adjacent box beams, deck-bulb-tee girders, and NEXT beams;
d. Precast abutment connections; and
e. Pier column to cap connections.

1.4 Research Approach

The work was conducted in two main phases. Phase 1 consisted of laboratory material characterization, and Phase 2 consisted of field-scale production trials.

In Phase 1, more than twenty-five batches of non-proprietary UHPC were produced at laboratory scale using a planetary high-shear mixer. Five constituent variables were systematically investigated: steel fiber dosage, fine aggregate gradation, cementitious blend type, silica fume dosage, and water-binder ratio. Each batch was tested for flow immediately after mixing. Hardened property testing included compressive strength at five ages (1, 7, 28, 56, and 91 days), flexural strength per ASTM C1609 at 28 and 91 days, direct-tension testing per AASHTO T 397 at 28 and 91 days, and freeze-thaw durability per AASHTO T 161 on select batches. A parallel effort was undertaken to develop a refined testing protocol for AASHTO T 397 to improve the reliability of the direct-tension test. An analytical approach, called *forward analysis*, was also developed to establish equivalent flexural stress acceptance criteria corresponding to the FHWA tensile stress requirements.

In Phase 2, three field-scale trials were conducted at an Alabama ready mixed concrete plant, each requiring two cubic yards of UHPC that was produced in a ready mixed concrete truck. The trials progressively refined the loading sequence to address the formation of cement balling, which was the primary challenge encountered during the transition from laboratory to field production. Specimens were extracted from field-scale slabs and tested alongside conventionally molded specimens to compare field-scale and laboratory-scale hardened properties. The findings from both phases were used to develop implementation recommendations and a draft ALDOT special provision for the use of UHPC.

1.5 Report Outline

Chapter 2 presents a literature review covering the history, properties, constituent materials, testing methods, mixing procedures, field-scale production, and specification landscape for UHPC in the United States. Chapter 3 covers the experimental plan for the laboratory phase, including the locally sourced materials, mixture proportions, batching procedure, and testing program. Chapter 4 documents the development of a refined direct-tension testing protocol for AASHTO T 397, including the challenges encountered and the systematic improvements made to improve the test success rate from 44% to 75% when using AASHTO T 397. Chapter 5 presents the material characterization results from the laboratory testing phase, including the effects of the five constituent variables on fresh and hardened properties, the forward analysis relating flexural and direct-tension results, freeze-thaw durability results, and the cost analysis. Chapter 6 documents the field-scale production trials, including the development of an improved UHPC mixing procedure and sequence. Chapter 6 also contains the fresh and hardened property results of the field-scale trials, and a comparison between the results obtained from the field-scale and laboratory specimens. Chapter 7 provides implementation recommendations for ALDOT, covering materials, mixing, placement, curing, testing, quality control, and cost considerations. Chapter 8 presents the summary, conclusions, and recommendations for future research. Appendix A contains the complete draft special provision. The MATLAB code developed to perform the forward analysis, including the sectional equilibrium, moment calculation, and displacement transformation, is provided in Appendix B.

CHAPTER 2
LITERATURE REVIEW

2.1 BRIEF HISTORY OF UHPC

Conventional concrete is the most widely used construction material in the world. The precursor to UHPC was developed by H.H. Bache in the 1980s, who developed densified systems with ultra-fine particles that achieved very high strength through optimized particle packing (Bache 1981). The French developed Reactive Powder Concrete (RPC) eliminating coarse aggregates while using optimized particle packing density and the use of small steel fibers to achieve improved compressive strengths (Richard and Cheyrezy 1995). The term "ultra-high-performance concrete" was first used by de Larrard and Sedran (1994), who employed optimized particle packing and a special selection of fine and ultrafine particles to develop a low-porosity, high-durability, self-compacting concrete (de Larrard and Sedran 1994; Martínez 2017).

RPC technology led to the development of the commercial product Ductal® through the coordinated work of three French companies: Lafarge, Bouygues, and Rhodia (Martínez 2017). The first field application of UHPC was the Sherbrooke Pedestrian Bridge in Quebec, Canada in 1997 (Blais and Couture 1999). According to Russell and Graybeal (2013), UHPC became commercially available in the United States around 2000. Shortly thereafter, the Federal Highway Administration (FHWA) initiated research on UHPC in 2001 (Graybeal 2008), and state DOTs began investigating the use of UHPC. In the United States, research on UHPC began in the late 1980s by the United States Army Engineer Research and Development Center (ERDC) for civil and military applications (Green et al. 2015). In 2013, FHWA published some examples of UHPC mixtures for different regions and a cost estimate (Graybeal 2013). Additionally, Wille and Boisvert-Cotulio (2013) provided recommendations for the material ratios to use when developing a non-proprietary UHPC mixture. The first U.S. highway bridge using UHPC was the Mars Hill Bridge in Wapello County, Iowa, which opened to traffic in 2006 using precast, prestressed UHPC modified Iowa bulb-tee beams (Russell and Graybeal 2013).

2.2 PROPRIETARY VERSUS NON-PROPRIETARY UHPC

Commercially available UHPC has historically been supplied as a proprietary blend in which the type and proportions of powder constituents, including cement, silica fume, ground quartz, and fine sand, are not disclosed by the manufacturer (Graybeal et al. 2020). This absence of transparency means that engineers and contractors working with proprietary products have limited ability to adjust the material to meet project-specific performance requirements. The blend's characteristics are fixed, and owners accept whatever strength and workability properties the product delivers. Non-proprietary UHPC removes that constraint entirely. Since the mixture proportions of non-proprietary UHPC are determined and controlled by the producer, the proportions can be adjusted to target a specific compressive strength, tensile performance, or workability demand, making non-proprietary formulations considerably more adaptable across the range of applications where UHPC offers structural advantages.

Cost has been an equally significant barrier to adoption. Proprietary UHPC has been reported at approximately \$2,000/yd^3 (Stewart et al. 2022; Wille and Boisvert-Cotulio 2013). At roughly 10 to 15 times the cost of conventional concrete, this premium has largely led to the use of proprietary UHPC in specialized or high-profile applications. As Shafei and Karim (2022) observed, "Due to cost considerations, use of proprietary UHPC in conventional projects has been limited." Research into non-proprietary alternatives has consistently demonstrated that material costs can be substantially reduced while still meeting the mechanical and durability thresholds that define UHPC. Wille and Boisvert-Cotulio (2013) developed non-proprietary fiber-reinforced formulations using locally available materials across three U.S. regions, reporting composite material costs in the range of \$750 to \$850/yd^3, with fiber reinforcement representing roughly half of the total material cost. Stewart et al. (2022) developed a Georgia-specific non-proprietary mixture estimated at approximately \$700/yd^3, a reduction of nearly 70% relative to proprietary product pricing at the time. These studies establish that cost-competitive non-proprietary UHPC is achievable, though the specific cost outcome depends on regional material pricing, fiber dosage, and mixture proportions. A detailed cost analysis based on the mixture developed in this study is presented in Section 5.10.

Beyond cost, the practical feasibility of producing non-proprietary UHPC has also been demonstrated at the field and plant scale. El-Tawil et al. (2018) confirmed that non-proprietary UHPC can be successfully batched using components sourced from multiple suppliers and concluded that field application of non-proprietary UHPC is viable. Giesler et al. (2016) showed that non-proprietary UHPC can be produced in an existing precast facility without modifications to equipment or procedures, which removes a potential barrier for producers considering the use of UHPC for the first time.

Advancements have also been made in material specifications that cover UHPC. The 2023 FHWA Structural Design Guide for UHPC relies on performance-based requirements and does not require the use of proprietary products, further reinforcing that non-proprietary UHPC formulations are a credible and supported option for bridge applications (Graybeal and El-Helou 2023). AASHTO T 397 (2022) "Uniaxial Tensile Response of Ultra-High-Performance Concrete" was also released to help characterize the tensile performance of UHPC.

2.3 UNIQUE PROPERTIES OF UHPC

UHPC is unique because of its excellent hardened properties. The FHWA design guide notes minimum property values of a compressive strength of 17,500 pounds per square inch (psi) (120 Megapascals (MPa)) and an effective cracking strength of 750 psi (5.2 MPa) (Graybeal and El-Helou 2023). UHPC has several properties that are commonly specified for concrete, such as its compressive strength. UHPC also has some innate properties that conventional concrete must be specifically designed for, such as its freeze-thaw resistance (Riding et al. 2019; Shafei and Karim 2021). Finally, UHPC has some properties that are typically not measured for conventional concrete, such as tensile strength, ductility, and toughness.

2.3.1 COMPRESSIVE STRENGTH

Compressive strength is a common property used to specify and design conventional concrete. The major difference between UHPC and conventional concrete is the magnitude of the specified compressive strength. UHPC is defined as having 17,500 psi while conventional concrete is often in the range of 4,000 to 8,000 psi according to Russell and Graybeal (2013). Rahman et al. (2005) said that the higher compressive strength of UHPC offers “advantages such as the use of less material, lighter structures and longer life of structures.” One method that allows UHPC to gain a high compressive strength is the particle packing technology it employs. In other instances, steam curing has also proven beneficial. According to Graybeal, “Steam-based treatment of UHPC tends to significantly enhance its material properties” (Graybeal 2006). Steam curing is only viable in precast plants, and since this project is limited to cast-in-place applications, steam curing will not be covered in this report.

2.3.2 TENSILE STRENGTH

The tensile strength of UHPC is the property that differentiates it most from conventional concrete. Conventional concrete has little to no post-cracking tensile strength. The reason UHPC has significant tensile strength is due to the addition of steel fibers (Alkaysi et al. 2016). The orientation of these steel fibers also affect the tensile strength of UHPC (Huang et al. 2021). Riding et al. (2019) stated that any tensile test result should also include a measure of toughness or ductility of the UHPC tested because tensile strength alone does not indicate significant post-cracking strength. Voss et al. (2022) also emphasized that a peak tensile strength alone is insufficient to assess UHPC. Instead, Voss et al. suggested that either the “overall behavior, a stress at a defined post-cracking strain or a toughness calculated up until a specified post-cracking strain can be used along with a maximum stress value.” This proposed approach captures the ductile response of the UHPC, rather than simply relying on its maximum tensile strength.

2.3.3 DUCTILITY AND TOUGHNESS

Ductility and toughness are closely related properties of UHPC that both result from its post-cracking, tensile load-carrying capacity. ACI CT (2025) defines ductility as the “ratio of displacement at ultimate strength to the displacement at which yield of the flexural reinforcement occurs”. This definition indicates how one of UHPC’s unique properties differentiates it from conventional concrete because conventional concrete requires reinforcing steel to have any ductility, while the steel fibers provide ductile behavior to UHPC.

According to ACI CT (2025) toughness is defined as “the ability of a material to absorb energy without rupturing.” Toughness can be calculated as the area under the curve of the load or stress versus displacement or strain response. A greater displacement or strain before failure is indicative of a higher toughness. Unlike ductility, toughness only captures the energy required to cause deformation or failure of the concrete. The FHWA Guide Specifications for Structural Design with UHPC (Graybeal and El-Helou 2023) quantify the ductile response of UHPC through the crack localization strain, requiring a minimum value of 0.0025 in./in. This provides a quantitative requirement that did not previously exist for fiber-reinforced concrete**.**

2.3.4 DURABILITY

Graybeal and Baby (2013) stated that UHPC is designed to "exhibit exceptional mechanical and durability properties." Some of these durability properties include excellent freeze-thaw resistance and very low permeability. Conventional concrete uses entrained air to provide freeze-thaw resistance. However, UHPC does not require entrained air as it absorbs a minimal quantity of water (Graybeal 2006). A well-designed UHPC mixture is unlikely to experience issues with freeze-thaw resistance, as Thomas et al. (2012) achieved 1,500 cycles of freezing and thawing without any appreciable loss of mechanical properties in a marine environment. This feat is impressive because AASHTO T 161 (2022) defines testing as complete after 300 cycles. This is not an isolated occurrence, as Graybeal (2006) had specimens that had a minimal decrease of the relative dynamic modulus after more than 600 cycles. The reason for this innate freeze-thaw resistance is the densely packed microstructure and very low porosity of UHPC (Graybeal 2006).

Russell and Graybeal (2013) state that in the United States of America, the permeability of concrete is typically evaluated by either AASHTO T 277 or its counterpart ASTM C1202. Due to the low water-binder ratio, particle packing, and low porosity, UHPC is resistant to "chloride ion permeability, carbon resistance and wear-resisting performance" (Zhou et al. 2018). The resistance to chloride ion penetration can be an important factor in using UHPC, as chloride ion penetration causes reinforcing steel to corrode, reducing the service life of concrete structures in a high chloride ion environment. Alkaysi et al. (2016) used ASTM C1202 to test the chloride ion penetration of UHPC and their results fell into either the rating of very low or negligible.

2.4 UHPC MIXTURE PROPORTIONS

There are a few unique factors that need to be considered when proportioning UHPC as compared to conventional concrete. This section addresses both the individual constituent materials used and the principles governing how they are proportioned for UHPC. The general material types required for UHPC are cementitious materials, fine aggregate, steel fibers, chemical admixtures, and water.

2.4.1 CEMENTITIOUS MATERIALS

The primary cementitious material in UHPC is portland cement. The cementitious materials used in concrete vary across literature because the material locally available behave differently in various regions.

Mendonca et al. (2020) stated that most researchers use Type I/II cement, though some researchers have tried using Type III cement. The supplementary cementitious materials (SCM) used in research have also varied. Some commonly used materials include silica fume, slag cement, and fly ash (Mendonca et al. 2020). Silica fume is a key component in UHPC because of its extreme fineness, which helps to eliminate voids between particles and improve particle packing. It also results in higher later-age strength due to its contribution to the pozzolanic reaction (Stewart et al. 2022; Wu et al. 2019). El-Tawil et al. (2018) showed that partial replacement of cement by slag cement can improve the workability of UHPC paste, lead to favorable self-consolidating characteristics, and reduce air voids and porosity.

2.4.2 FINE AGGREGATE

Unlike conventional concrete, UHPC contains only fine aggregates and no coarse aggregates because dense particle packing is a key component of UHPC proportioning. For conventional concrete, the fine aggregate used would meet the requirements for AASHTO M 6 (2022) as it provides criteria for its gradation. For UHPC, a target particle packing method dictates the desired gradation of all materials. For standard concrete fine aggregate, there is AASHTO M 6 (2022) while masonry fine aggregate should meet AASHTO M 45 (2024). To achieve better particle packing, some have blended different types of fine aggregate. An example is how Khayat and Valipour (2018) used a blend of Missouri River sand and masonry sand. Other researchers like Shafei and Karim (2021) have simply modified the fine aggregate by sieving to achieve improved particle packing for their UHPC.

Research performed for Georgia DOT (Stewart et al. 2022) evaluated multiple sand sources from across the state and found significant performance variation. Only the masonry sand and river sand from southern Georgia met their 18,000 psi compressive strength target. The northern Georgia masonry sand performed poorly due to platy minerals and organic inclusions, and the central Georgia sand also fell short of strength requirements despite somewhat better workability (Stewart et al. 2022).

2.4.3 STEEL FIBERS

Steel fibers is a key ingredient that provide UHPC with its unique tensile strength, resistance to crack propagation, and strain-hardening properties (Zhou et al. 2018; Shafei and Karim 2021). As the steel fibers control these properties, the amount, length, shape, and even orientation of the fibers play a role in obtaining high-strength UHPC. Graybeal (2006) found that fiber orientation affects tensile strength, while Huang et al. (2021) found that fiber orientation affected the strength and toughness. The reason steel fibers are used for UHPC is, as Abokifa and Moustafa (2021) said, “is responsible for various aspects of the unparalleled mechanical properties such as higher tensile strength and ductility…” Many researchers use straight steel fibers that have various lengths and diameters (Graybeal 2006; Riding et al. 2019). Graybeal (2006) stated that the steel fibers require a high tensile strength to function properly. Table 2-1 lists some of the various kinds of fibers various researchers have used and what fiber dosages they tested. From Table 2-1, it is apparent that a common fiber length is 0.5 inches (13 mm) while a common fiber dosage is 2%. Figure 2-

1 shows that increasing the fiber dosage increases the tensile/flexural strength of UHPC. This increase is due to the steel fibers bridging microcracks that develop during tensile testing (Shafei and Karim 2021). A major factor when selecting the fiber dosage of UHPC is the cost of fibers. Graybeal (2013) gave a cost estimate of $472.39 per cubic yard for just steel fibers, which was more than 50% of the total cost of the UHPC price estimate when assuming a 1.5% by volume fiber dosage.

Table 2-1: Fiber Properties from Literature

Source	Fiber Type (Steel)	Fiber Length (in.)	Fiber Diameter (in.)	Fiber Strength (ksi)	Fiber Dosage (%)
Graybeal (2013)	Straight	0.51	0.0078	Not Reported	1.0 – 2.0
Graybeal and Baby (2013)	Straight	0.5, 0.8	0.008, 0.012	Not Reported	2, 2.5
Shafei and Karim (2021)	Straight, Twisted, Hooked macrofibers	0.5, 1, 1.37	0.008, 0.02, 0.021	290, 246.5, 159.5	0.5, 1.0, 1.5, 2.0, 2.5, 3
Wille et al. (2011b)	Hooked, Twisted, Straight	1.18, 1.18, 0.51	0.015, 0.015, 0.008	420, 304 – 449, 377	1, 1.5, 2.5, 3, 5/8
Looney et al. (2019)	Deformed	0.98	0.021	Not Reported	2
Berry et al. (2017)	Straight	0.51	0.0079	400	2
Mendonca et al. (2020)	Straight, Twisted	0.51, 0.51 – 0.98	0.078, 0.02	399, 247	2

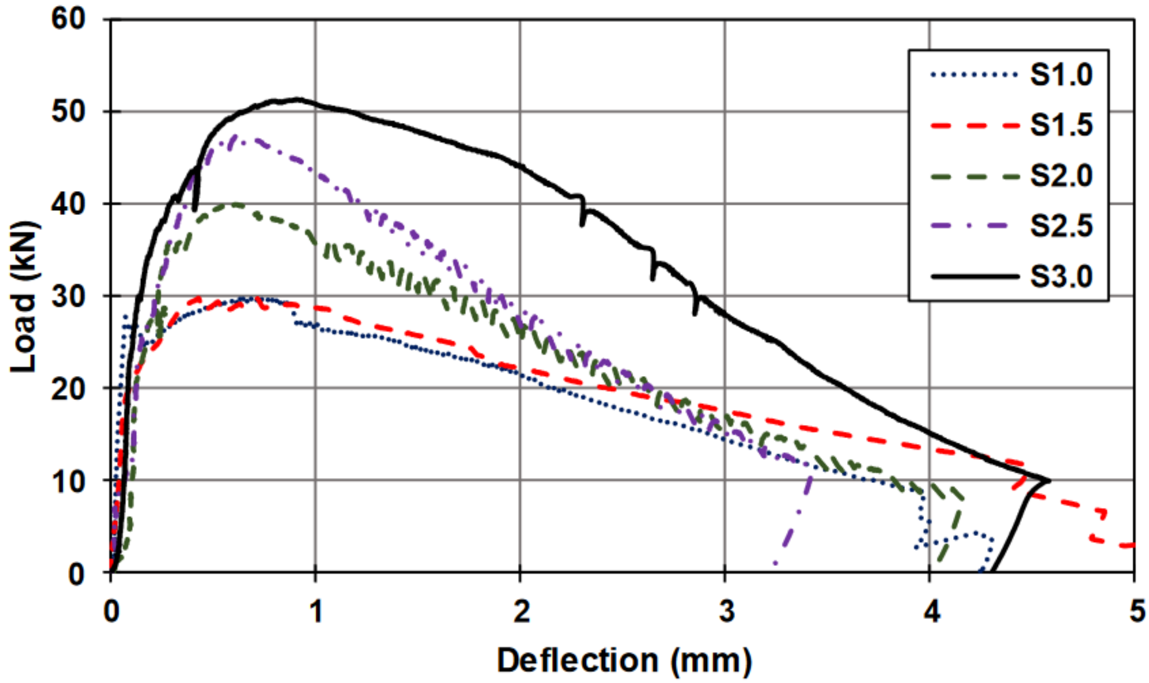

Figure 2-1: Flexural Load-Deflection Curve of Third-Point Bending Test (Shafei and Karim 2021)

(Note: S stands for straight steel fibers, while the numbers correspond to percent steel fibers by volume.)

2.4.4 HIGH-RANGE WATER-REDUCING (HRWR) ADMIXTURES

As UHPC is produced with a very low water-to-cementitious material ratio, it is necessary to use chemical admixtures to increase its workability. Without chemical admixtures it would not be possible to achieve flowable UHPC, which would prevent fibers from achieving a proper orientation (Mendonca et al. 2020). A typical admixture used in UHPC is a high-range water-reducing (HRWR) admixture, also called a superplasticizer. Khayat and Valipour (2018) used an HRWR admixture to "enhance the workability." This can be seen in Table 2.2 below, where Khayat and Valipour (2018) were able to increase the fiber dosage while still achieving their desired flow despite the fibers reducing the flow. They also reported the compressive strength and flexural response shown in Table 2-2. The flexural response detailed in Table 2-2 includes the first-peak flexural stress and deflection, peak flexural stress and deflection, and total toughness for the entire test. An important consideration when using an admixture to improve workability is the cost. According to Graybeal (2013), the cost of HRWR admixture was about $13-$20 per gallon in 2013. According to Wille et al. (2011a), the HRWR admixture has a large influence on the fresh properties of UHPC. Additionally, Wille et al. (2011a) found that there was an optimum range for HRWR admixture that led to an "optimized packing of the paste," which increased the compressive strength and flowability of UHPC.

Table 2-2: UHPC with Various Fiber Contents (Khayat and Valipour 2018)

Code	V_f (%)	HRWR demand (%)	Slump flow (mm)	Flow time (sec.)	28 d compressive strength (MPa)	f_1 (MPa)	d_1 (mm)	f_p (MPa)	d_p (mm)	T_{150} (J)
Ref.-no fiber	0.0	0.28	29.0	12	123	13.7	0.10	13.7	0.10	1.0
Steel-0.5%	0.5	0.28	29.0	20	124	14.9	0.10	14.9	0.10	24.5
Steel-1.0%	1.0	0.28	28.5	22	124	15.9	0.07	16.5	0.61	38.4
Steel-1.5%	1.5	0.29	28.0	24	125	16.2	0.11	19.6	0.77	41.3
Steel-2.0%	2.0	0.40	28.0	18	125	16.5	0.08	20.3	1.05	50.2
Steel-2.5%	2.5	0.69	28.0	35	126	12.7	0.07	19.7	1.65	49.7

Note: 1 mm = 0.039 in., 1MPa = 145 psi

2.4.5 Hydration Controlling Admixtures

Hydration controlling admixtures (HCA) are used to delay the setting time and extend the workability window of concrete and are stronger than convention retarding admixtures. Like other admixtures, there is a variety when it comes to the time that the setting can be delayed. Han and Han (2010) worked with a HCA that could delay “the setting and hardening of concrete from several hours to several days without having a detrimental effect on strength development”. One of the key reasons a hydration controlling admixture could be beneficial to UHPC is that it prolongs the workability if placement is delayed. An example of retarding admixture is MasterSet® DELVO that is an ASTM C494/C494M Type B retarding and Type D water-reducing and retarding, admixture (Master Builders Solutions 2024). The biggest benefit of an admixture like MasterSet® DELVO is the ability to maintain workability for very low w/cm mixtures such as UHPC. Hydration controlling admixtures are particularly important for field-scale production of UHPC, where transit time from plant to site and the duration of placement operations require extended working times.

2.4.6 Particle Packing and Proportioning

Particle packing is one of the factors that allows UHPC to achieve a low water-to-cementitious material ratio (Shafei and Karim 2021). One proportioning method for UHPC is utilizing a particle packing method to attain optimal particle packing (Yu et al. 2014). Riding et al. (2019) summarized the general format of particle packing methods, stating, “Most particle packing methods used today utilize a particle size distribution, which is shown with an equation instead of a set of distinct particle sizes and quantities.” From the literature review, many researchers utilize a variation of the Andreasen and Andersen method for particle packing (Berry et al. 2017; Shafei and Karim 2021; Wille and Boisvert-Cotulio 2013; Andreasen and Andersen 1930). The Andreasen and Andersen method (Andreasen and Andersen 1930) is shown in Equation 2-1.

$$P(D) = \frac{D^q}{D_{max}^q} \qquad \text{(Equation 2-1)}$$

where D_{max} represents the largest particle size in the mixture, *P(D)* represents the percent of particles finer than the particle size *D*, *q* represents the distribution modulus and is dependent on the desired size of the particles, with a lower value of q corresponding with a finer blend. Andreasen and Andersen (1930) determined that the optimal value for q, the distribution modules, was between 0.33 and 0.5.

One issue with the basic Andreasen and Andersen particle packing model is that it does not account for the minimum particle size present in the UHPC. Funk and Dinger (2013) modified the Andreasen and Andersen particle packing equation so that it accounts for both the minimum and maximum particle size present in UHPC as shown in Equation 2-2.

$$P(D) = \frac{D^q - D_{min}^q}{D_{max}^q - D_{min}^q} \qquad \text{(Equation 2-2)}$$

where D is the particle size. D_{min} and D_{max} represent the smallest and largest particle sizes. The distribution modulus, q, is dependent on the size of the particles. A lower value of q corresponds with a finer blend as the lower value will result in a higher packing density for a mixture with more fine material (Riding et al. 2019).

2.5 UHPC TEST METHODS

When it comes to testing the properties of UHPC, most of the test methods come from the American Society for Testing and Materials (ASTM) and the American Association of State Highway and Transportation Officials (AASHTO). These tests were based on test methods established for either conventional or fiber-reinforced concrete. There are some adjustments to the ASTM specifications due to the flowability, high strength, and durability of UHPC. These changes are provided in ASTM C1856 (2017) "Standard Practice for Fabricating and Testing Specimens of Ultra-High-Performance Concrete". This standard defines what adjustments are required to test UHPC using standard methods for testing conventional and fiber-reinforced concrete. ASTM C1856 (2017) is only applicable to UHPC with a compressive strength greater than 17,000 psi, a maximum aggregate size of 1/4 inches, and a flow between 8 and 10 inches. ASTM C1856 (2017) also specifies what size specimens should be used for each test. For a standard compression cylinder test, ASTM C1856 (2017) specifies the use of a 3 in. x 6 in. cylinder instead of the more common 6 in. x 12 in. specimen. For the flexural bending test ASTM C1609, ASTM C1856 specifies the 3 in. x 3 in. specimen cross-section based on the length of the steel fibers being less than 0.6 inch as shown in Table 2-3.

Table 2-3: Dimensions for Flexural Specimens Based on Fiber Length (ASTM C1856/C1856M 2017)

Maximum Fiber Length (l_f)	Nominal Prism Cross Section
< 15 mm [0.60 in.]	75 mm by 75 mm [3 in. by 3 in.]
15 mm to 20 mm [0.60 in. to 0.80 in.]	100 mm by 100 mm [4 in. by 4 in.]
20 mm to 25 mm [0.80 to 1.00 in.]	150 mm by 150 mm [6 in. by 6 in]
>25 mm [1.00 in.]	200 mm by 200 mm [8 in. by 8 in.]

2.5.1 COMPRESSIVE STRENGTH

The most common method for testing the compressive strength of concrete is by crushing cylindrical specimens in compression. ASTM C1856/C1856M (2017) specifies the use of ASTM C39/C39M (2021), which is the specification for testing the compressive strength of concrete cylinders, as the test method for determining the compressive strength of UHPC. The primary modifications for UHPC are the use of 3 in. x 6 in. cylinders, grinding the ends to ensure perpendicularity, and using a loading rate of 145 psi/sec (ASTM C1856/C1856M 2017).

2.5.2 TENSILE STRENGTH

A common method for determining the tensile strength of conventional concrete is the splitting tensile test. There are issues involved with using this test method with UHPC. One major issue comes from the loading state, which applies a vertical compressive stress that affects the post-cracking behavior (Graybeal 2006). This results in an increase in the load required for the steel fiber pull-out according to Graybeal (2006). However, Graybeal (2006) does state that the splitting tensile test can be used to compare the fiber pullout behavior. Two alternative test methods have emerged for evaluating the tensile performance of UHPC: flexural testing and uniaxial tension testing. Each has distinct advantages and limitations for UHPC that bear directly on their suitability for specification and quality control.

2.5.2.1 FLEXURAL TESTING (ASTM C1609)

The flexural test conducted in accordance with ASTM C1609/C1609M (2019) is a widely used method for evaluating the tensile performance of fiber-reinforced concrete. ASTM C1856/C1856M (2017) mandates using ASTM C1609 (2019) to determine the flexural strength of UHPC. Although it is not a direct tensile test, the flexural test can serve as a reliable proxy for evaluating the material's tensile capacity, post-cracking ductility, and overall toughness. This test uses a third-point loading test performed with a rectangular prism as the specimen. The specimen is loaded using a configuration similar to the one depicted in Figure 2-2. Riding et al. (2019) noted that the flexural test is simple to set up and implement for laboratories, which contributes to its widespread use.

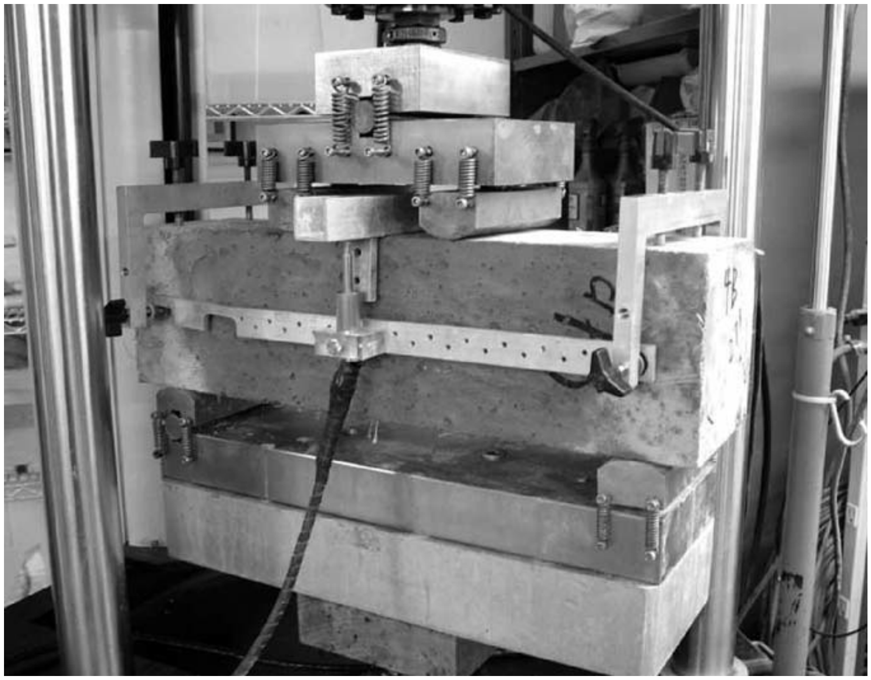

Figure 2-2: Flexural Bending Test Set-Up in Accordance With ASTM C1609/C1609M (2019)

To conduct testing in accordance with ASTM C1609, a servo-controlled testing machine capable of using the rate of midspan deflection to control the loading rate is required. The testing machine must receive a signal from two electronic deflection-measuring devices capable of a precision of 0.0005 inches, and the data acquisition system must sample at a frequency of at least 2.5 Hz. The support conditions for ASTM C1609 fall under two different specifications: the loading blocks must meet the requirements of (ASTM C78/C78M 2022), while the support rollers must meet the requirements of ASTM C1812, a specification detailing the support roller (ASTM C1812/C1812M 2015). For UHPC, the specimen cross-sectional size is determined by ASTM C1856. The specimen must be at least 2 inches longer than the desired span length. The molding and curing of specimens fall under the requirements of ASTM C192/C192M with modification per ASTM C1856, and testing must start within 15 minutes of the specimen being removed from the moist curing environment. The placement of the specimen during testing is such that the loading blocks and roller supports are on the molded sides of the specimen. During the test, the specimen is loaded at third points such that the supports and loading blocks result in three equal-length sections of the specimen.

The results of ASTM C1609 allow for determining the flexural strength and toughness of a given UHPC mixture (see Figure 2-3). The flexural strength is calculated according to Equation 2-3 (ASTM C1609/C1609M 2019). The toughness is calculated as the area under the load versus midspan deflection curve at a deflection of L/150, where L is the span length.

$$f = \frac{PL}{bd^2} \qquad \text{(Eq. 2-3)}$$

where f is the flexural strength corresponding to load P (psi), P is the applied load at any net deflection (lbf), L is the span length (in.), b is the average width of the specimen (in.), and d is the average depth of the specimen (in.).

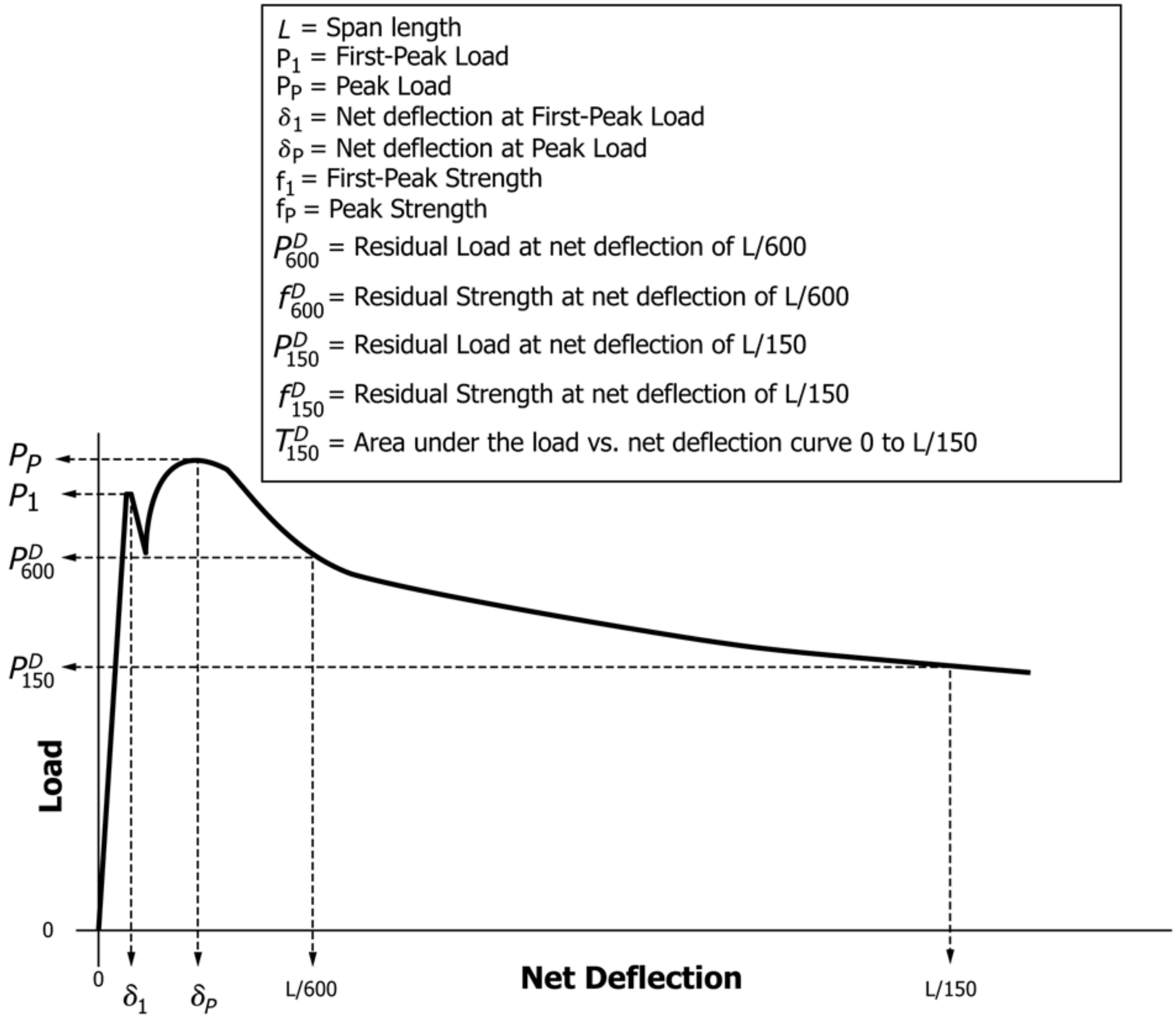

Figure 2-3: Example Test Results and Parameter Calculations for ASTM C1609/C1609M (2019)

The principal limitation of the flexural test is that the stress state in a bending beam is fundamentally different from uniaxial tension. Graybeal and Baby (2013) expressed concerns about using flexure-type tests to determine the tensile strength of UHPC because of "the assumptions and complex computations necessary to back-calculate the uniaxial behavior." The flexural stress reported by ASTM C1609 is computed assuming a linear elastic stress distribution, which ceases to be valid once cracking initiates. As a result, the measured flexural strength of a strain-hardening material is substantially higher than its uniaxial tensile strength (Maalej and Li 1994; Graybeal and Baby 2013). Translating flexural results into equivalent tensile properties requires an inverse or forward analysis, which is discussed in Section 2.6.

2.5.2.2 UNIAXIAL TENSION TESTING (AASHTO T 397)

To address the limitations of indirect test methods, Graybeal and Baby (2013) developed a uniaxial-tension test for UHPC. This was used to create AASHTO T 397 (2022) "Uniaxial Tensile Response of Ultra-High-Performance Concrete." This test method allows for the direct calculation of the pre- and post-cracking tensile strength. The test uses a prismatic specimen with transfer plates epoxy-bonded to each end, which are gripped in a universal testing machine (UTM). Displacement is measured over a defined gauge length, and the complete tensile stress-strain response is recorded, including the effective cracking stress, peak stress, localization stress, and localization strain (AASHTO T 397 2022). Figure 2-4 depicts a typical test setup to perform AASHTO T 397.

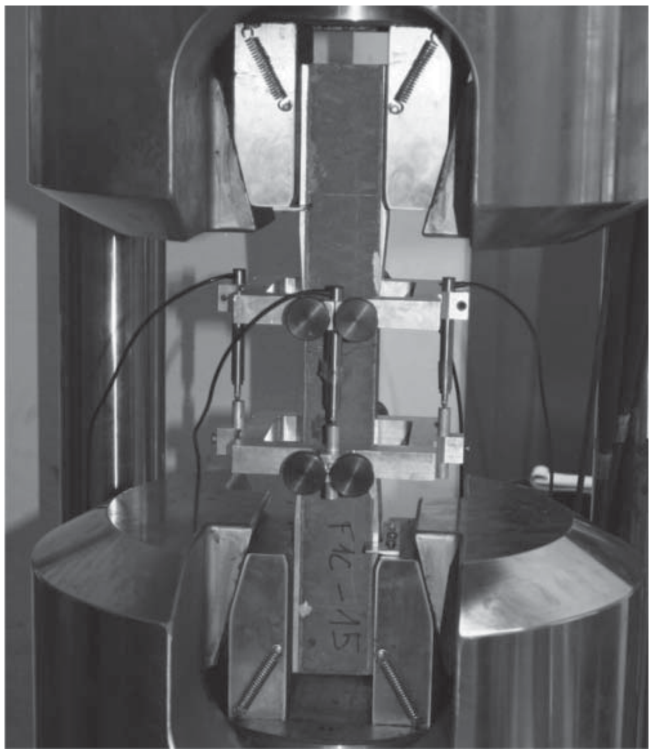

Figure 2-4: Typical Uniaxial Tension Test Set-Up (Graybeal and Baby 2013)

This test was recently released in 2022, so it is still being improved. One major issue regarding the test is that it suffers from a low success rate. Note 24 of AASHTO T 397 (2022) states that cracking or strain localization may be likely, so a large number of specimens may be required to produce three good test results. Riding et al. (2019) encountered issues with the aluminum transfer plates delaminating when specimens were being gripped in the testing machine. It is important to note that Riding et al. (2019) conducted their tests prior to AASHTO T 397 being officially released. Gali and Sritharan (2024) evaluated AASHTO T 397 and provided several recommendations and methods for improving the success rate of the test. Even with their recommendations, Gali and Sritharan (2024) give an estimated success rate of 50%, which is very low if the method is to be used for quality control or assurance purposes.

2.5.3 TOUGHNESS AND DUCTILITY

There is no specific test specification at this time to determine the toughness of UHPC. ASTM C1609 (2019), a flexural test, includes a toughness calculation. For ASTM C1609 (2019), the toughness is calculated as the area under the curve of the force versus midspan deflection at a deflection of *L*/150, with *L* being the span length of the specimen. Voss et al. (2022) calculated the toughness of UHPC using a uniaxial tension test by calculating the area under the curve until a strain of 0.005 mm/mm (in./in.).

Riding et al. (2019) observed that any tensile strength test method used for UHPC should provide an indication of the material's ductility or toughness, as a peak strength value alone is insufficient to characterize post-cracking behavior. Like toughness, ductility is a derived property rather than a directly measured quantity. Unlike toughness, which represents an energy measure, ductility is a measure of deformation and therefore depends heavily on the specific test being performed. The current lack of standardized specifications for calculating ductility in either fiber-reinforced concrete or UHPC compounds this difficulty, as results are not readily comparable across test methods.

2.5.4 FRESH STATE PROPERTIES

The primary fresh property test for UHPC is the flow test as shown in Figure 2-5. The flow test for UHPC is conducted in accordance with ASTM C1437 (2020) with the modifications specified in ASTM C1856/C1856M (2017). The testing procedure requires filling the specified mold in one lift without tamping, lifting the mold, and allowing the UHPC to flow for 2 minutes before measuring the flow along the maximum and corresponding perpendicular diameter (ASTM C1856/C1856M 2017). The acceptable flow range for UHPC is commonly reported as 7 to 10 inches (Graybeal 2014a; Mendonca et al. 2020). Flow below 7 inches indicates insufficient workability for placement, while flow above approximately 10 to 11 inches has been associated with fiber segregation in some studies (Mendonca et al. 2020; El-Tawil et al. 2018). Workability retention over time is an important consideration for field applications but is not addressed by a single standard test. Researchers have assessed workability retention by repeating the flow measurement at timed intervals after batching (Shafei and Karim 2021).

The temperature of the freshly mixed UHPC like conventional concrete is measured in accordance with ASTM C1064 (2023). Most specifications and field applications require that the UHPC temperature remain below 85 °F during batching (FDOT 2023; Mohr et al. 2025), and some below 80 °F (Graybeal 2014a).

Figure 2-5: Example of UHPC Flow Test (ACI 239R 2018)

2.6 CONVERSION FROM FLEXURAL TO TENSILE TEST RESULTS

The FHWA requires that UHPC used in structural applications exhibit a minimum effective post-cracking tensile strength of 750 psi and a localization strain of at least 0.0025 (Graybeal and El-Helou 2023). The direct-tension test conducted in accordance with AASHTO T 397 (2022) measures these properties directly and provides the complete tensile stress strain response, including the effective cracking stress, peak stress, localization stress, and localization strain. However, as documented earlier in Section 2.5, the direct-tension test presents significant practical challenges. Specimen preparation is demanding, the gripping and alignment procedure requires trained personnel, and failures outside the gauge length remain common even with careful execution.

The flexural test conducted in accordance with ASTM C1609/C1609M (2019) is a far more practical alternative. State DOTs and commercial testing laboratories can more easily perform flexural testing because specimen preparation is straightforward and the test, more reliable. The difficulty lies in converting flexural results into tensile properties that can be compared against the FHWA requirements. The stress state in a flexural beam is fundamentally different from that in a uniaxial tension specimen. The beam experiences a strain gradient through its depth, with the bottom fiber in maximum tension and the top fiber in compression. The flexural stress reported by ASTM C1609 is computed assuming a linear elastic stress distribution, which ceases to be valid once cracking initiates and the UHPC is in the post-cracking response region. As earlier mentioned, the measured flexural strength of a strain hardening material is substantially higher than its uniaxial tensile strength (Maalej and Li 1994; Graybeal and Baby 2013).

There are two analytical paths for relating flexural and direct-tension test results. The first is the *inverse analysis*, which begins with the measured flexural response and works backward to extract the uniaxial tensile behavior by using constitutive laws. The second is the *forward analysis*, which begins with known tensile properties and estimates the expected flexural response. Each path has distinct advantages and limitations, and these will be discussed in the following sections.

2.6.1 Inverse Analysis

The inverse analysis seeks to determine the tensile stress strain relationship from the measured flexural response. The general procedure involves converting the measured midspan deflection to a curvature at the critical section and then using sectional equilibrium to back-calculate the stress-strain relationship that would produce the observed moment curvature behavior.

Baby et al. (2013) proposed an inverse analysis method for UHPC that utilizes LVDTs mounted to the bottom face of the specimen to directly measure the bottom fiber strain. This allows the curvature to be calculated without assumptions about the curvature distribution along the beam. While this approach produces a more direct measurement, it requires additional instrumentation beyond what ASTM C1609/C1609M prescribes. Baby et al. (2013) validated their method against direct tensile tests on multiple types of commercially available UHPC, and the authors noted that bias or scatter can be induced when simplified constitutive laws are assumed for the analysis. Rigaud et al. (2012) developed a point-by-point approach that assumes a linear-curvature distribution in the shear spans and solves the tensile stress at each loading increment. This method processes the full load-deflection curve and does not pre-assume a constitutive shape, but it is sensitive to noise in the experimental data and requires smoothing of the output (Martínez 2017). The point-by-point method is also only valid up to crack localization, because the assumed curvature distribution becomes increasingly inaccurate once a dominant crack forms and the shear spans begin to unload.

López et al. (2016) proposed a simplified five-point inverse analysis method that requires only the deflection under the load and at midspan. This method has the advantage of a closed-form solution, making it practical for routine use without computational tools. It was developed using approximately 12 million theoretical concrete mixtures with varying properties (Martínez 2017) and relies on the assumption that a bilinear relationship during the ascending branch in tension is sufficient to describe UHPFRC behavior. The equations depend on the specimen geometry, specifically the ratio of span length (L) to specimen depth (h), and were calibrated for L/h values of 3 and 4.5. However, multiple researchers have reported the inaccuracy of its result with an issue possibility being due to the assumption of secant lines (Zhu et al. 2021).

Zhu et al. (2021) evaluated both the point-by-point method and the five-point inverse analysis on UHPC with treated steel fibers. They found that the five-point inverse analysis could not reproduce the tensile stress-strain relationship regardless of whether the fibers were aligned. The point-by-point method performed adequately for UHPC without fiber alignment but required a fiber orientation correction factor for UHPC with aligned fibers. The results from Zhu et al. (2021) raise concerns about the general applicability of inverse analysis methods to UHPC formulations that differ from those used to develop the methods.

The fundamental challenge shared by all inverse analysis methods is that the deflection to curvature conversion introduces modeling assumptions that cannot be fully analytically characterized. The curvature distribution along a cracked beam is not known a priori and changes continuously as cracking progresses. Any assumed distribution will deviate from the actual distribution at certain load levels (Baby et al. 2013; Martínez 2017). These deviations propagate through equilibrium calculations and affect the estimated tensile properties determined from the inverse analysis.

2.6.2 Forward Analysis

The forward analysis takes an opposite approach from the inverse analysis. Rather than extracting unknown tensile properties from a measured flexural curve, it begins with a known or assumed tensile constitutive law and estimates the flexural response that such a material would produce. If the estimated flexural results match the experimental results, the tensile properties used as input are validated. More importantly for practical specification purposes, the forward analysis allows the engineer to determine what flexural test result corresponds to a given set of tensile properties without ever needing to first perform the flexural test.

Maalej and Li (1994) established the theoretical framework for estimating the flexural strength of strain hardening cementitious composites from their uniaxial tensile properties. Their model assumed that plane sections remain plane during bending, so that strain varies linearly through the depth of the beam. For a known tensile constitutive law, the stress at any depth in the section can be determined from the strain at that depth. By enforcing force equilibrium across the section, the position of the neutral axis can be found, and the bending moment computed by integrating the stress times the moment arm across the section depth. Maalej and Li (1994) showed that for strain hardening composites, the flexural strength can far exceed the uniaxial tensile strength because the expanding zone of multiple cracks through the beam depth absorbs considerable energy and redistributes stress. For their 2 percent polyethylene engineered cementitious composite, the flexural strength was measured at five times the tensile first-cracking strength, and this ratio was estimated well by their model. They also demonstrated that the flexural strength to tensile strength ratio depends on the hardening ratio (the ratio of peak tensile stress to cracking stress) and the ultimate tensile strain capacity of the material.

Xia et al. (2018) applied sectional analysis to UHPC beams by using a constitutive model derived from the French design guideline, Association Française de Génie Civil (AFGC 2013). Their work covered both unreinforced and reinforced sections. For unreinforced prisms, they showed that an elastic-perfectly-plastic tension model gives conservative moment predictions within 5 percent across a range of section heights from 2.0 in. (51 mm) to 42 in. (1067 mm). They compared predicted load-displacement curves against experimental data for unreinforced prisms with varying fiber orientations and found satisfactory agreement, particularly for specimens with strong fiber alignment. Their analysis demonstrated the feasibility of predicting the flexural response of UHPC from assumed tensile properties using sectional analysis.

However, the work of both Maalej and Li (1994) and Xia et al. (2018) differ from what is needed for UHPC in this study. Maalej and Li (1994) used a bilinear tensile model (elastic followed by hardening to peak) that does not capture the softening and localization behavior characteristic of UHPC as measured by AASHTO T 397. Their material was a polyethylene fiber ECC with a tensile strain capacity exceeding that of typical strain-hardening UHPC (with localization strain ranging 0.002 to 0.005). Xia et al. (2018) derived their constitutive model from the French guideline using a stress-crack opening approach rather than from independently measured AASHTO T 397 direct-tension test data.

The limitations of both analysis paths highlight a gap in the state-of-the art. What remains to be investigated is a validated method to correlate ASTM C1609 flexural results to AASHTO T 397 direct tension results for UHPC, particularly non-proprietary UHPC made with regionally available materials.

2.7 MIXING OF UHPC

In the literature, there are several methods of mixing UHPC. These methods vary in how long each mixing stage is, what materials are added at a given stage, or even how many mixing stages there are. Mixing procedures are also different between laboratory- and field-mixed UHPC. Mendonca et al. (2020) summarized the various UHPC mixing methods. They generalized the process into three steps: “(1) mix the dry components, (2) add water and HRWR admixture, and (3) add fibers” (Mendonca et al. 2020). Some researchers, like Berry et al. (2017), divided the fine aggregate and silica fume from the remaining cementitious material to disperse the silica fume. Another consideration that Graybeal (2011) mentioned is that mixing UHPC requires an increased amount of mixing energy compared to conventional concrete. To provide this increased amount of energy, Graybeal (2011) discussed either increasing the mixing times with measures to control temperature or using a high-energy mixer. Looney et al. (2019) mentioned that a high-shear mixer is beneficial due to the energy requirements of mixing UHPC.

For mixing UHPC, Shafei and Karim (2021) added the fine aggregate and silica fume and mixed for 5 minutes. Next, they added the cement and mixed for a further 5 minutes before the water and HRWR admixture was added. The UHPC was then mixed until it became fluid, which was roughly 5 to 10 minutes. After the mixture became fluid, Shafei and Karim (2021) added the steel fibers and mixed until the fibers were dispersed, which was about 5 minutes. Once mixing was complete, they measured the flow and molded specimens (Shafei and Karim, 2021).

El-Tawil et al. (2018) noted that pan mixers with high energy and high-shear mixing energy have proved useful for mixing UHPC but have a number of limitations: they are not well suited for field construction because they require greater input energy than regular mixers, their volume is typically small, and they tend to cause the UHPC to overheat. Low-shear mixers such as rotating drum mixers can produce inconsistent mixing quality, including clumps of unmixed dry materials. El-Tawil et al. (2018) reported that these inconsistencies can be mitigated by using modified mixing procedures such as the half-batch method described by Tackett and Hale (2010) in which half the mixture is batched and mixed completely before the other half is added.

2.8 FIELD-SCALE PRODUCTION OF UHPC

Most published UHPC research has been conducted at laboratory scale. Field applications require volumes of 1 yd^3 or more, and the equipment available at most batch plants and job sites operates with fundamentally different mixing action and energy. Ready mixed concrete trucks and conventional batch plant mixers lack the high shearing action that laboratory planetary mixers provide, which means the dry constituents are not dispersed as thoroughly and the UHPC requires longer mixing times or modified batching sequences to achieve comparable results (El-Tawil et al. 2018; Giesler et al. 2016). This gap between laboratory success and field-scale viability has been a barrier to widespread adoption of non-proprietary UHPC.

The choice of mixing equipment has a direct effect on mixture quality. El-Tawil et al. (2018) noted that pan mixers with high-shear capacity produce consistent results but are limited in volume, require greater input energy, and tend to cause the UHPC to overheat. Rotating drum mixers and ready mixed concrete trucks, by contrast, offer the volume capacity needed for field applications but can produce clumps of unmixed dry materials if standard concrete batching procedures are followed (El-Tawil et al. 2018). Despite this concern, El-Tawil et al. (2023) demonstrated through a systematic comparison of lab-mixed and truck-mixed UHPC that high-quality mixtures are achievable with common mixing equipment, provided the batching sequence and HRWR admixture dosage are properly determined. Giesler et al. (2016) reached a similar conclusion after scaling production from small 3.0 ft^3 portable drum mixer batches to 1.0 yd^3 batches in a precast plant's batch mixer in New Mexico, finding that no modifications to existing precast plant facilities were necessary.

The most frequently reported challenge in field-scale UHPC production is cement balling or agglomeration. This occurs when cement grains contact moisture from the fine aggregate before being thoroughly dispersed with the other dry powders. The resulting agglomerations can be several inches in diameter and compromise the uniformity of the hardened product. Giesler et al. (2016) observed this problem when saturated sand was used instead of the oven-dried sand typical of bagged proprietary products. Kim et al. (2021), working on a 52' long, 35.42' wide pi-girder design bridge in Iowa, reported the same issue. This indicates that cement agglomeration is major issue because of the interaction between moist aggregate and cement during low-shear mixing. Several solutions have been reported. Giesler et al. (2016) found that pre-drying the fine aggregate eliminated the problem entirely. In a subsequent trial without drying, Giesler et al. (2016) resolved it by mixing all cementitious materials for one minute before introducing the sand and half the water, followed by ten minutes of mixing and then the remaining water and admixtures. El-Tawil et al. (2018) found that adjusting HRWR admixture dosage and staging was effective, noting that too low a dosage prevents the mixture from turning over while too high a dosage leads to fiber segregation.

Workability retention during transport and placement is another critical consideration that does not often arise in laboratory settings. In the laboratory, mixing and casting typically occur within minutes and in close proximity. Field applications, by contrast, involve transit from a batch plant to a job site and placement operations that can extend well beyond an hour. Without measures to control the loss of workability, the

UHPC can stiffen to the point where it no longer flows into formwork or around reinforcement. The use of hydration controlling admixtures (HCA) to extend working time has been reported as an effective strategy (Han and Han 2010; Scott et al. 2018); however, the published literature on non-proprietary UHPC workability retention under field conditions remains limited.

A related and practically significant challenge is the formation of what is commonly referred to as elephant skin. Because UHPC has a very low water content and minimal bleeding, the exposed surface is susceptible to rapid moisture loss through evaporation and self-desiccation when the material is placed or left idle. This produces a rough, hardened crust on the exposed surface while the material beneath remains plastic, as shown in Figure 2-6. Elephant skin formation hinders screeding and finishing in the fresh state and can negatively affect hardened properties by reducing load-bearing capacity and compromising structural integrity in multi-layer constructions (Yuan et al. 2023). It also traps air bubbles that cannot escape the placed UHPC (Yalçınkaya and Çopuroğlu 2021), as shown in Figure 2-7.

Figure 2-6: Surface Appearance of a Base UHPC Mixture, Depicting Elephant Skin Formation on the Exposed Surface (Chen et al. 2017)

Figure 2-7: Elephant Skin Formation Just After Slump-flow (Yalçınkaya and Çopuroğlu 2021)

Chen et al. (2017) evaluated several mitigation strategies and found that latex modification and immediately covering the exposed surface with a plastic sheet after finishing was the most effective measure, retaining surface aesthetics and mitigating surface cracking. Their finding that immediate surface coverage is the preferred mitigation approach is also supported by Yuan et al. (2023), who proposed curing in a high relative humidity (RH) environment. However, Yalçınkaya and Çopuroğlu (2021) found that even at 95% RH and 68°F (20°C), elephant skin still formed on the casting surface. At the same humidity but at a higher temperature of 95°F (35°C), no elephant skin was observed, a result attributed to vapor condensation on the casting surface. This finding is consistent with the observation by Yuan et al. (2023) that spraying water directly on the surface helped suppress elephant skin formation. It should be noted, however, that applying water to the surface of freshly placed, still-plastic UHPC introduces a practical concern: unlike post-set wet curing, which is standard practice, water applied immediately after placement has the potential to locally elevate the water-to-binder ratio at the surface, which could adversely affect the mechanical and durability properties of that surface layer.

Despite these challenges, field-scale studies collectively indicate that non-proprietary UHPC production at construction-relevant volumes is achievable. Giesler et al. (2016) produced UHPC with a water-cementitious materials ratio of 0.16 and a target compressive strength of 20 ksi using regionally available materials and existing plant equipment. El-Tawil et al. (2018) achieved 28-day compressive strengths exceeding 21.7 ksi and peak tensile strengths exceeding 1.2 ksi from mixtures sourced from multiple suppliers and concluded that field application of non-proprietary UHPC is feasible. The key to consistent field production appears to be careful attention to the batching sequence, sand moisture management, HRWR admixture dosage calibration through trial batches, and the use of hydration controlling admixtures to maintain adequate working times.

2.9 UHPC Specification Review in the U.S.

This section reviews the existing UHPC specifications and special provisions across the United States, with particular attention to the Southeastern Association of State Highway & Transportation Officials (SASHTO) region. The purpose is to identify commonalities and differences in how states address material requirements, acceptance testing, quality control, and construction practices for UHPC. This review supported the development of the draft ALDOT special provision that is covered in Appendix A.

2.9.1 SASHTO Region

Among the fifteen SASHTO member states (Alabama, Arkansas, Florida, Georgia, Hawaii, Kentucky, Louisiana, Mississippi, North Carolina, Puerto Rico, South Carolina, Tennessee, Texas, Virginia, and West Virginia), only Florida and Texas have published formal UHPC specifications. Alabama, Georgia, Louisiana, Tennessee, and Virginia have funded research that have in some cases let to proposed draft specification language.

a) Florida: FDOT maintains two developmental specifications for UHPC: Dev 349 for non-proprietary UHPC construction and quality control, and Dev 927 for prepackaged proprietary UHPC. The published Dev 927 requires a minimum flexural first-peak strength of 1,200 psi per ASTM C1609 and uses the Florida modified double-punch test (FM 5-626) for field QC of tensile strength. FDOT also requires a full-scale mockup demonstration at least 30 days before field placement. The specification addresses both proprietary and non-proprietary products and includes durability requirements for chloride content, chloride migration, and alkali-silica reactivity. Separately, a University of Florida research report (FDOT Project BDV31-977-130) recommended an expanded framework that classifies UHPC into two compressive strength classes (Class 17 at 17,400 psi and Class 21 at 21,000 psi at 28 days) and categorizes tensile performance into strain-hardening and enhanced-ductility classes based on AASHTO T 397 direct-tension testing.

b) Texas maintains Special Specification 4024 (updated in 2024). It requires a minimum compressive strength of 14,000 psi at 4 days and 18,000 psi at 28 days, shrinkage no greater than 800 microstrain, and freeze-thaw resistance having a RDM >95%. Texas does not include a tensile strength requirement in its specification; instead, it relies on requiring 2% steel fibers by volume and a fiber tensile strength exceeding 300 ksi. Quality control during construction consists of flow testing and temperature test on every batch and compressive strength cylinders (minimum three sets per production day). Texas requires a trial batch and a pre0pour meeting.

c) Georgia (GDOT Research Project 18-01) developed a non-proprietary UHPC using Georgia materials, targeting 14,000 psi at 3 days and 18,000 psi at 28 days. The Georgia work evaluated alternative sand sources across the state and found that only the masonry sand and river sand from southern Georgia met strength requirements. Georgia has deployed UHPC on the SR 211 Bridge over Beech Creek using precast deck panels with UHPC closure pours but has not yet published a standalone GDOT specification.

d) Tennessee (TDOT Research Report RES2024-04) developed two classes of non-proprietary UHPC: a high early strength (HES) UHPC requiring 4,000 psi at 8 hours and 12,000 psi at 28 days, and a traditional UHPC requiring 18,000 psi at 28 days. Both classes require a slump flow greater than 21 inches per ASTM C1856 and use 1% steel fibers by volume. Tennessee's draft special provision specifies Type I or Type IL cement, prohibits coarse aggregates and air-entraining admixtures, requires a high-shear mixer, limits ambient placement temperature to a maximum of 85 °F, and requires embedded thermocouples to ensure internal temperatures do not exceed 160 °F. The Tennessee draft also requires trial batches and QC compressive strength cylinders (4 x 8 in.) but does not include a tensile acceptance criterion.

e) Virginia has deployed UHPC beams on the Route 624 Bridge over Cat Point Creek, specifying 23 ksi compressive strength and a maximum w/cm of 0.20. VDOT's research (VCTIR 12-R1) recommended UHPC for closure pours and beams with optimized cross sections. In early 2025, VDOT's Northern Virginia District completed the first U.S. application of sprayable UHPC for abutment repair, performed by FIU's ABC-UTC team. Virginia does not have a standalone UHPC specification.

2.9.2 Specifications Outside the SASHTO Region

Beyond the SASHTO states, the most developed UHPC specifications belong to Iowa and California. Iowa DOT (SP-150289) requires a minimum compressive strength of 21 ksi at 28 days (non-heat-treated) and includes a pullout test for bar development per ASTM E488, which is unique among state specifications. Caltrans handles UHPC through a product authorization program rather than a prescriptive specification, requiring manufacturers to demonstrate compliance with published acceptance criteria before placement on the Authorized Material List. At 28 days, Caltrans requires a minimum compressive strength of 18 ksi, a minimum effective cracking strength of 0.8 ksi per AASHTO T 397, a crack localization strength no less than the effective cracking strength, and a minimum localization strain of 0.0025. Durability requirements include a chloride ion penetrability below 250 coulombs per ASTM C1202 and a minimum relative dynamic modulus of 95% after 300 freeze-thaw cycles per ASTM C666.

2.9.3 Summary of Key Specification Parameters

Table 2-4 summarizes the principal acceptance and quality control parameters across the specifications reviewed. Several patterns and points of divergence are worth noting. Compressive strength requirements are consistent in the 17,000 to 21,000 psi range at 28 days across nearly all specifications. The most significant divergence among states is in the treatment of tensile performance. California and Florida stands alone in requiring direct tension qualification testing through AASHTO T 397, while Florida also offers a modified double-punch test for field QC. Texas, Iowa, and Tennessee either omit tensile requirements entirely or address them indirectly through mandated fiber content or toughness indices. This gap is notable given that UHPC's post-cracking tensile capacity is arguably its most distinguishing structural property and a key parameter in the 2023 FHWA Structural Design Guide for UHPC.

All specifications that address flow require it to be measured per ASTM C1437 with modifications from ASTM C1856, with most targeting 7 to 10 inches. The Florida specification is the most prescriptive regarding mockup demonstrations, requiring a representative full-scale mockup at least 30 days in advance. Most states require a pre-pour meeting with the manufacturer's representative present on site during placement.

Table 2-4: Principal Acceptance Criteria for UHPC across Select States

	State DOT Specifications				Draft Specifications from Research	
Parameter	**Texas**	**Iowa**	**California**	**Florida**	**Tennessee (Mohr et al. 2025)**	**Florida (Riding et al. 2022)**
Minimum 28-day f'_c (psi)	18,000	21,000	18,000	17.400	18,000[a]	17,400 / 21,000
Early Strength	14,000 psi at 4d	12,000 psi at 4d	-	-	4,000 psi at 8h (HES)	14,000 psi / 16,000 psi at 7d
Tensile Req.	None (2% fiber minimum)	Toughness $I_{30} \geq 48$	AASHTO T 397 $f_{t,cr} \geq 0.8$ ksi $f_{t,loc} \geq f_{t,cr}$ $\epsilon_{t,loc} \geq 0.0025$	FM 5-625 (Double-punch test), $f_1 \geq 1200$ psi at 28d	None specified	AASHTO T 397 + DPT
Fiber Dosage (minimum amount)	2% by volume	-	2% by volume	-	1% by volume	-
Flow Range (in.)	8 to 10	7 to 10	8 to 10	8 to 10	> 21 (slump)	8 to 10
Max w/cm	-	-	0.25	0.25	0.18	0.25
Shrinkage (microstrain)	ASTM C157 ≤ 800	ASTM C157 ≤ 766	ASTM C157* ≤ 800	ASTM C157* ≤ 800	Not specified	≤ 800
Mockup Required	Yes	No	-	Yes	Yes	Yes
Pre-pour Meeting	Yes	Yes	-	Yes	Not specified	Yes
Durability Tests	Cl^- penetrability < 250 Coulombs, F-T (RDM) > 96% after 300 cycles	Cl^- penetrability < 250 Coulombs, F-T (RDM) > 96% after 600 cycles	Cl^- penetrability < 250 Coulombs, F-T (RDM) ≥ 95% after 300 cycles	F-T (RDM) ≥ 95% after 600 cycles	-	Cl- content, migration, ASR

Notes: * Modified per ASTM C1856
a = 4 x 8 in. cylinder
HES = High-early strength

CHAPTER 3
EXPERIMENTAL PLAN FOR LABORATORY WORK–PHASE 1

3.1 OVERVIEW

This chapter describes the experimental program designed for the laboratory to develop and characterize non-proprietary ultra-high-performance concrete (UHPC) using locally sourced Alabama materials. The primary objectives of this laboratory phase were to develop a non-proprietary UHPC mixture that satisfies the FHWA performance requirements for UHPC (Graybeal and El-Helou 2023) and to evaluate how key constituent materials influence the fresh and hardened properties of UHPC. The experimental plan for this phase is illustrated in Figure 3-1.

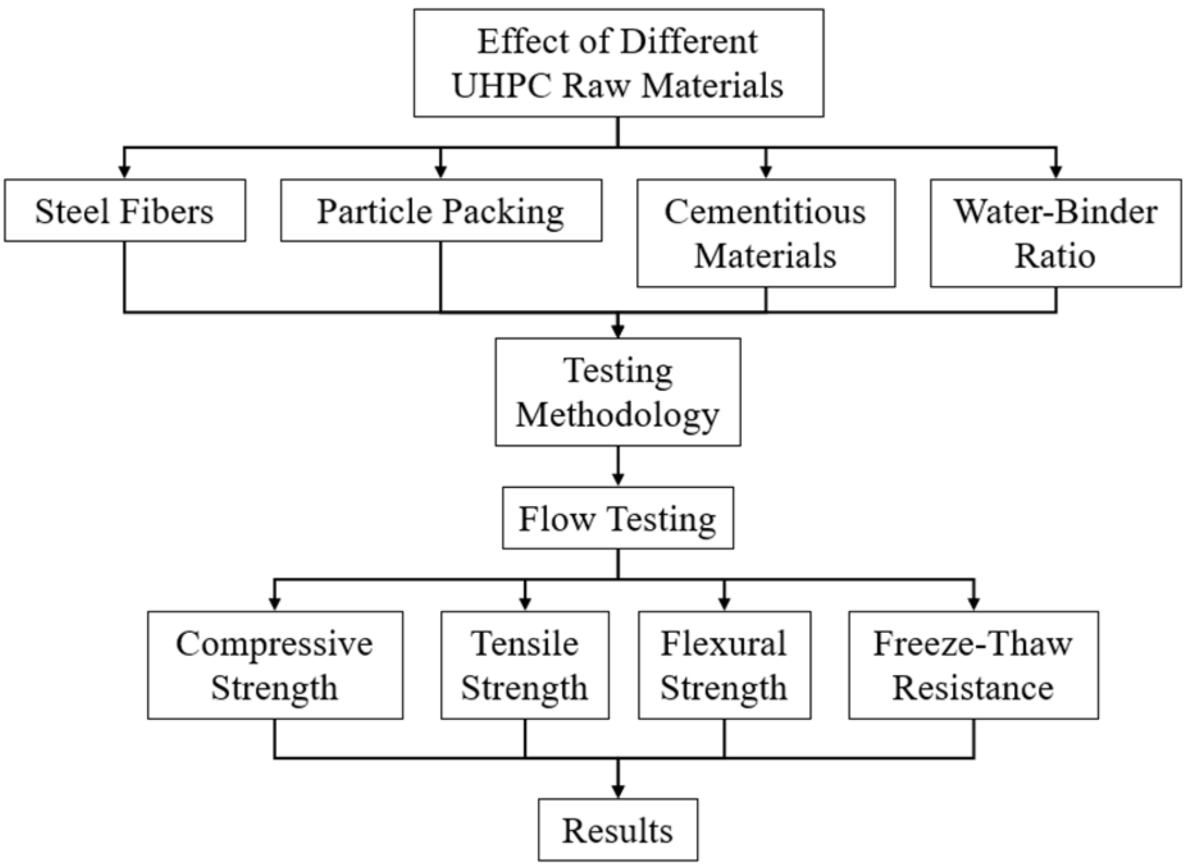

Figure 3-1: Experimental Plan

To characterize the behavior of UHPC made with materials that are available in the Alabama concrete industry, five constituent variables were systematically investigated: steel fiber dosage, fine aggregate gradation, cementitious blend type (binary versus ternary), silica fume dosage, and water-binder ratio. Each variable was selected to address a specific practical consideration relevant to the use of UHPC in Alabama transportation infrastructure. Steel fiber dosage was investigated first because steel fibers represent the single largest cost driver in UHPC, accounting for more than half of the total material cost (Graybeal 2013). Fine aggregate gradation was investigated to determine whether optimizing the aggregate particle packing provides any meaningful benefit over standard locally available river sand. Particle packing is a key principle in UHPC proportioning, and optimizing the fine aggregate gradation is one method by which packing density can be improved. However, aggregate blending introduces additional sourcing and batching complexity, raising the practical question of whether that effort yields any measurable benefit over standard, locally available river sand. The evaluation of binary versus ternary cementitious systems was motivated by the practical constraint that most ready mixed concrete plants are configured for only two cementitious materials, making the use of silica fume as a third component challenging and potentially very expensive. The silica fume dosage investigation then quantified the actual performance benefit of silica fume within the ternary system. Finally, the water-binder ratio was evaluated to determine its influence on both compressive and tensile strength.

All laboratory mixing was performed using a planetary high-shear mixer at a volume of 2 ft^3. The fabrication and testing of all specimens was conducted in accordance with ASTM C1856 (2017), the standard practice governing UHPC specimen production and testing. Note that no AASHTO standard exists for this topic, hence the use of ASTM C1856/C1856M. Each batch had its workability tested immediately after mixing, and tensile hardened state properties were tested at 28 and 91 days. The hardened state testing program included compressive strength, flexural strength, direct-tensile testing. Tests on freeze-thaw durability were performed per ASTM C1856/C1856M. Furthermore, additional assessment was performed on select batches as part of a parallel protocol development for direct-tension testing to improve the reliability of AASHTO T 397 (2022), which is separately discussed in Chapter 4.

3.2 Material and Mixture Proportions

3.2.1 Locally Sourced Materials

An emphasis was placed on using materials that are locally or regionally available to Alabama ready mixed concrete producers. The cementitious system consisted of a ternary blend of Type IL portland-limestone cement conforming to ASTM C595 (2025), slag cement, and densified silica fume. The Type IL cement and slag cement were sourced from suppliers serving the Alabama market. Densified silica fume was obtained from Elkem Materials through national distribution channels. Type IL cement was selected in part because it is widely available in the region and is increasingly the only type of cement available.

Two types of fine aggregate were used to evaluate the effect of gradation on UHPC performance. The primary fine aggregate was a natural river sand meeting the gradation requirements of AASHTO M 6 (2022), which is widely available throughout Alabama. Local masonry sand, the nearest locally available material to the AASHTO M 45 (2024) gradation requirements, was also evaluated. It should be noted that only natural river sand was investigated in this study because this is usually used for concrete application on ALDOT projects.

The steel fibers used throughout the study were smooth, straight fibers with a nominal length of 13 mm (0.51 in.), a diameter of 0.2 mm (0.008 in.), an aspect ratio of 65, and a minimum tensile strength of 400 ksi. During material sourcing, it was found that the 0.51-inch fiber length was commonly locally available and made in the United States, and this length was therefore used for all batches. The properties of the steel fibers are summarized in Table 3.1

Table 3-1: Steel Fiber Properties

Fiber Type	Fiber Length in. (mm)	Fiber Diameter in. (mm)	Fiber Strength ksi
Straight	0.51 (13)	0.008 (0.2)	444

Two chemical admixtures were incorporated. A high-range water-reducing admixture (HRWRA), MasterGlenium 7920, was used to achieve target workability at the low water-binder ratios required for UHPC. A hydration controlling admixture (HCA) was included to extend workability retention during mixing and placement, which is necessary given the extended production time associated with mixing UHPC.

3.2.2 MIXTURE PROPORTIONS

The complete mixture proportions for all batches produced in this study are presented in Table 3-2. The baseline mixture proportions were adapted from Abokifa and Moustafa (2021) and Floyd et al. (2024), with systematic modifications to evaluate the five material variables described in Sections 3.2.2.1 through 3.2.2.5. The baseline ternary binder system consisted of Type IL cement, slag cement, and silica fume. For all batches in which the fine aggregate gradation, binary versus ternary blend, silica fume dosage, or water-binder ratio was the variable of interest, the fiber dosage was fixed at 1.50% by volume unless otherwise noted. For all batches in which the steel fiber dosage was the variable of interest, the ternary binder system and water-binder ratio were held constant, and the fine aggregate content was adjusted for each batch to maintain a constant total mixture volume as the fiber volume changed. Additional HRWRA was added as necessary in all batches to maintain the target flow range.

3.2.2.1 STEEL FIBER DOSAGE

Steel fibers represent the largest single cost driver in UHPC, accounting for more than half of the total material cost at a typical dosage. Optimizing the fiber dosage is therefore the most effective means of reducing the overall cost of UHPC while maintaining the required post-cracking tensile performance. For this reason, the steel fiber dosage investigation was conducted first, before any other material variable was examined. Seven batches were produced covering fiber dosages of 0.00%, 0.50%, 1.00%, 1.25%, 1.50%, 1.75%, and 2.00% at a water-binder ratio of 0.19.

Table 3-2: Proportions for Mixtures Evaluated During the Laboratory Testing Phase

ID	Type IL Cement (lb/yd^3)	Slag Cement (lb/yd^3)	Silica Fume (lb/yd^3)	Water (lb/yd^3)	Fine Agg. (lb/yd^3)	HRWRA (fl oz/cwt)	HCA (fl oz/cwt)	Steel Fiber Vol. (%)
Effect of Steel Fiber Dosage								
FD 0.00	1180	590	177	370	1622	15.5	4	0.00
FD 0.50	1180	590	177	370	1553	15.0	4	0.50
FD 1.00	1180	590	177	370	1531	15.0	4	1.00
FD 1.25	1180	590	177	370	1519	17.0	5	1.25
FD 1.50	1180	590	177	370	1506	15.0	5	1.50
FD 1.75	1180	590	177	370	1494	15.5	5	1.75
FD 2.00	1180	590	177	370	1477	15.5	5	2.00
Effect of Fine Aggregate Gradation								
C33	1180	590	177	389	1522	10	5	1.50
Masonry	1180	590	177	389	1620	9	5	1.50
A-A	1180	590	177	389	1525	9	5	1.50
Effect of Cementitious Materials								
Ten. 1.5	1180	590	177	389	1522	10	5	1.50
Bin. 1.5	1180	798	0	396	1514	11.5	8	1.50
Bin. 2.0	1180	798	0	396	1484	12.5	9	2.00
Ten. 2.0	1180	590	177	370	1530	15	5	2.00
Effect of Silica Fume Dosage								
9% SF	1180	590	177	389	1522	10	5	1.50
12% SF	1180	525	232	388	1526	9	5	1.50
15% SF	1180	458	289	386	1526	9	5	1.50
Effect of Water-Binder Ratio								
w/b 0.18	1180	590	177	351	1623	12	5	1.50
w/b 0.20	1180	590	177	389	1522	10	5	1.50
w/b 0.22	1180	590	177	428	1427	8	5	1.50

Note: HRWRA = High-Range Water-Reducing Admixture
HCA = Hydration Controlling Admixture
A-A = Andreasen-Andersen

3.2.2.2 Fine Aggregate Gradation and Particle Packing

Particle packing is one of the factors that enables UHPC to achieve a very low water-binder ratio, which is reported to be fundamental to its exceptional mechanical and durability properties (Mendonca et al. 2020). Optimizing the fine aggregate gradation is one approach to improving overall particle packing, and this investigation was designed to determine whether such optimization provides a meaningful performance benefit over using standard locally available river sand.

Three batches were produced, each with a different combined fine aggregate gradation. The first used only natural river sand meeting AASHTO M 6 (2022) gradation limits. The second used local masonry sand, the nearest locally available material to the AASHTO M 45 (2024) gradation. The third used an optimized blend of 80% AASHTO M 6 (2022) river sand and 20% masonry sand, determined using the modified Andreasen and Andersen (A-A) particle packing equation (Funk and Dinger 2013) with a distribution modulus q = 0.23 per Yu et al. (2014). The gradation curves for each of the two fine aggregates without the blended gradation are presented in Figures 3-2 and 3-3. It can be seen in Figure 3-3 that the local masonry sand was finer than AASHTO M 45; however, this was reported to be typical masonry sand locally available in Alabama. Since this is a masonry sand available in Alabama and a finer fine aggregate might improve particle packing for UHPC, this masonry sand was used in this project. All other mixture variables were held constant across the three batches.

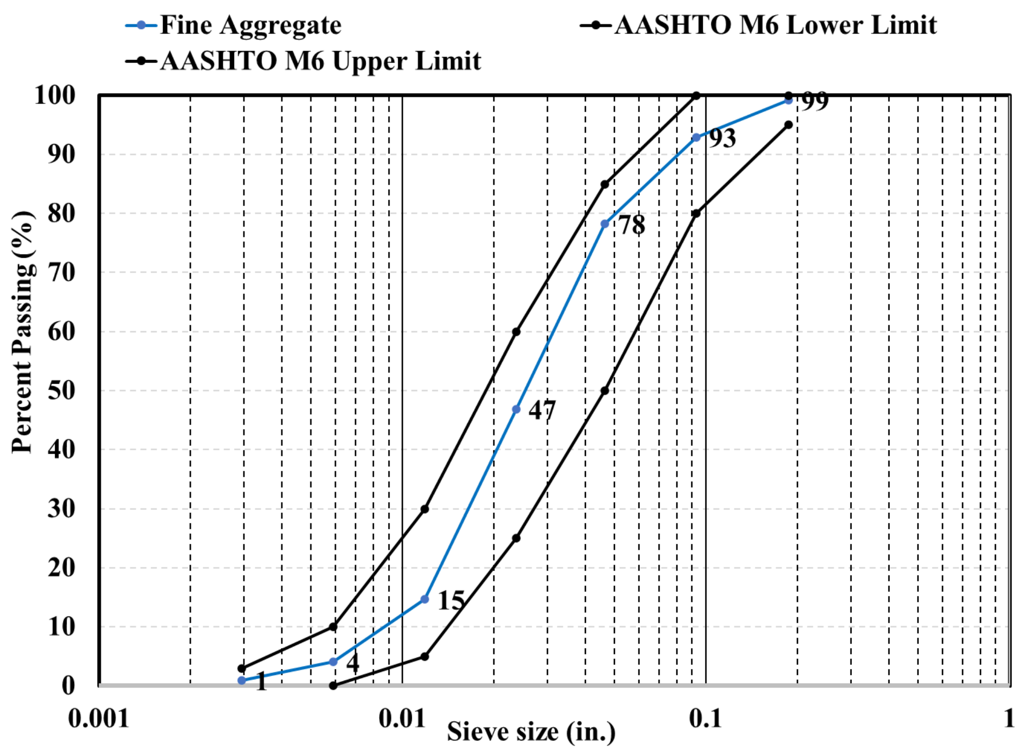

Figure 3-2: Fine Aggregate Gradation Meeting AASHTO M 6 (2022)

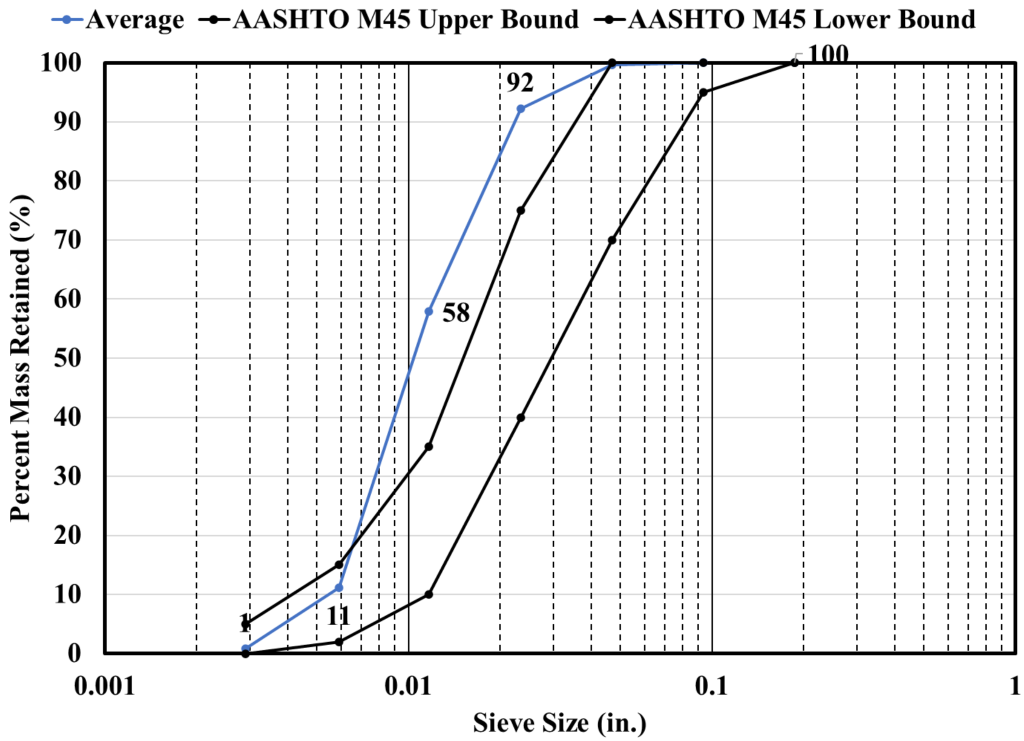

Figure 3-3: Local Masonry Sand Gradation

3.2.2.3 Binary versus Ternary Cementitious Blend

Most ready mixed concrete plants in Alabama are configured to handle two cementitious materials, typically portland cement and one supplementary cementitious material such as slag cement. Incorporating a third material such as silica fume requires either a temporary third silo or manual addition at the plant or job site, introducing logistical complexity and added cost. In addition, silica fume carries a significantly higher material cost than slag cement, estimated at approximately $350 per ton compared to $120 per ton for slag cement (Wille and Boisvert-Cotulio 2013). These practical and economic considerations motivated an investigation into whether a binary blend consisting solely of Type IL cement and slag cement, without silica fume, could produce UHPC meeting Graybeal and El-Helou (2023) performance requirements.

Two binary blend batches were produced at steel fiber dosages of 1.50% and 2.00%. These were selected to allow direct comparison against equivalent ternary blend batches at the same fiber dosages. All other mixture variables were held constant between the binary and ternary comparisons, with the slag cement increased to ensure total cementitious material volume.

3.2.2.4 Silica Fume Dosage

While the binary versus ternary investigation established whether silica fume is necessary within the cementitious system, the silica fume dosage investigation was designed to quantify the actual performance benefit associated with different amounts of silica fume within a ternary blend. Silica fume contributes to densifying the cementitious matrix through its pozzolanic reactivity and its particle packing effect at the finest scale of the mixture (Alkaysi et al. 2016; Khayat and Valipour 2018). Given its higher cost and the additional handling requirements at ready mixed concrete plants, there are economic and practical incentives to identify the minimum effective silica fume dosage.

Three batches were produced with silica fume contents of 9%, 12%, and 15% by mass of total binder, with the steel fiber dosage fixed at 1.50% for all three. To maintain a constant paste volume, the slag cement was reduced as the silica fume was increased across the adjusted batches. The water-binder ratio was held at 0.20 for all three batches.

3.2.2.5 Water-Binder Ratio

The water-binder ratio is one of the primary parameters governing the compressive strength of concrete. With UHPC having a minimum compressive strength of 17,500 psi, evaluating the water-binder ratio is an important component of the mixture development program. The investigation also examined how the water-binder ratio influences tensile strength and workability, as these properties are equally critical to the development of viable non-proprietary UHPC.

Three batches were produced at water-binder ratios of 0.18, 0.20, and 0.22, covering one value above and one below the baseline. The baseline of 0.20 was selected based on Russell and Graybeal (2013), who surveyed a broad range of published UHPC mixture proportions and found that a water-binder ratio of approximately 0.20 was common across many non-proprietary formulations. The ternary binder system and a steel fiber dosage of 1.50% were held constant across all three of these mixtures.

3.3 Batching and Mixing Procedure

All laboratory mixing was performed using a planetary high-shear mixer at the Auburn University Advanced Structural Engineering Laboratory (ASEL). The batching procedure was adapted from Shafei and Karim (2021) and held constant for all batches to ensure that any observed differences in performance were attributable to the material variables being investigated rather than inconsistencies in mixing. The established five-step mixing sequence was as follows:

1. Fine aggregate and silica fume were added to the mixer and mixed for 5 minutes.
2. Type IL cement and slag cement were added and mixing continued for an additional 5 minutes.
3. Eighty percent of the total mixing water, combined with the HCA, was introduced and mixed for 3 minutes.
4. The remaining 20% of the mixing water, along with the HRWRA, was added and mixing continued for 5 to 15 minutes until the mixture achieved the desired (i.e., fluid) consistency.
5. Once the mixture was fluid, steel fibers were added and mixed for an additional 5 minutes to ensure uniform fiber dispersion.

Following the completion of mixing, a flow test per ASTM C1856/C1856M (2017) was immediately performed. If the flow did not meet the 7-to-11-inch acceptance criterion, additional HRWRA was added and mixed for 3 minutes, followed by a 3-minute rest period and a 2-minute final remix before retesting. Only batches achieving the target flow range proceeded to specimen casting.

After completing the flow test, the UHPC was cast into steel molds. UHPC was introduced at one end of each mold and allowed to flow under its own weight to the opposite end. A rubber mallet was used to tap the sides of the molds (30 taps) to release any entrapped air. All specimens were cured in a moist curing room maintained at 73.5 ± 3.5 °F for the first 24 hours before demolding. Following demolding, specimens remained in the moist curing room until preparation for testing at the designated test ages.

For each batch, specimens were cast for three types of hardened property testing: fifteen 3 in. x 6 in. cylinders for compressive strength testing at five ages (1, 7, 28, 56, and 91 days, three per age); six 3 in. x 3 in. x 14 in. prisms for flexural strength testing (three at 28 days and three at 91 days); twelve 2 in. x 2 in. x 17 in. prisms for direct-tensile strength testing (six at 28 days and six at 91 days); and three 3 in. x 3 in. x 11.25 in. prisms for freeze-thaw durability testing on selected batches. The direct-tensile specimen count was initially six per batch but was increased to twelve following a low success rate observed in early testing. These specimens also served as part of a parallel protocol development effort aimed at improving the reliability of AASHTO T 397, which is discussed separately in Chapter 4.

3.4 Testing Program

3.4.1 Fresh Property Testing

The workability of each UHPC batch was assessed immediately after mixing using the flow test specified in ASTM C1856/C1856M (2017). A flow value between 7 and 11 inches was used for the acceptance criterion for all batches (ASTM C1856 2017; Mendonca et al. 2020), indicating sufficient fluidity for self-consolidating placement and proper fiber orientation. The flow test was the only fresh state property evaluated; air content and unit weight testing were not conducted as these are not relevant acceptance criteria for UHPC in the manner they are for conventional concrete.

3.4.2 Compressive Strength Testing

Compressive strength testing was conducted in accordance with ASTM C39/C39M (2021) with modifications specified in ASTM C1856/C1856M (2017). In place of the standard 6 in. x 12 in. cylinder, ASTM C1856/C1856M requires 3 in. x 6 in. cylinders for UHPC. Due to the high surface hardness of UHPC, the ends of the cylinders were ground to achieve perpendicularity with the specimen axis per AASHTO R 119M/R 119 (2024), as ASTM C1856/C1856M explicitly prohibits the use of capping compounds or unbonded neoprene pads. The tests were conducted using a 600,000-pound compression testing machine. The loading rate during testing was 145 ± 7 psi/second as specified. Three cylinders were tested at each of five ages (1, 7, 28, 56, and 91 days) to characterize the strength development of each mixture.

3.4.3 TENSILE STRENGTH TESTING

One of the objectives of this project is to determine how to test the tensile behavior of UHPC. This is important as a typical UHPC definition will include a tensile strength, like FHWA requiring a post-cracking tensile strength of 750 psi (Graybeal and El-Helou 2023). The two methods being assessed are the flexural strength test (ASTM C1609/C1609M, 2019) and uniaxial tensile strength test (AASHTO T 397, 2022). These are discussed further below.

3.4.3.1 FLEXURAL STRENGTH TESTING

The flexural strength of UHPC was determined using ASTM C1609/C1609M (2019) with modifications specified by ASTM C1856/C1856M (2017). The only modification made by ASTM C1856/C1856M (2017) is to the size of the specimen cross-section, being 3 in. x 3 in., due to fiber length being less than 0.6 in. (15 mm). Figure 3-4 shows this specimen geometry, which is 3 in. x 3 in. x 14 in. The general testing procedure of ASTM C1609/C1609M (2019) is first to ensure that the loading frame is properly aligned, meaning that the load frame will apply loads at the expected loading positions and that the loading frame is squared and properly seated. Figures 3-4 and 3-5 show the test setup used for testing, including LVDT placement. Important to note, as ASTM C1609/C1609M (2019) was used to conduct this test, the LVDTs used were mounted to measure the midspan deflection as shown in Figure 3-5.

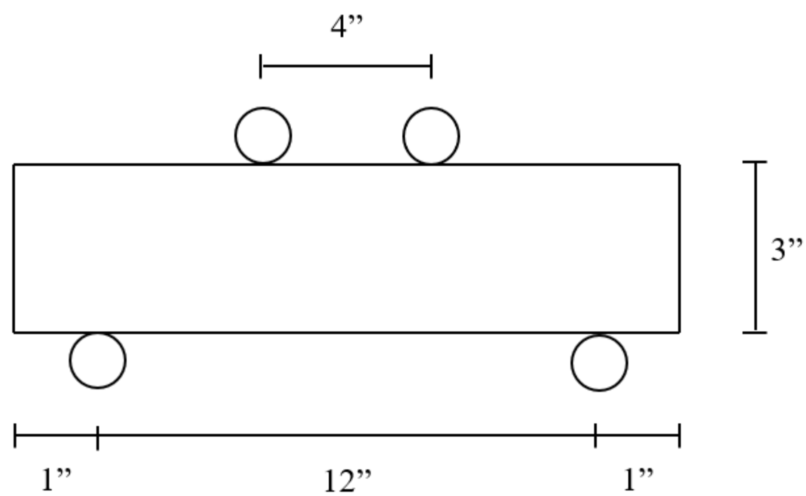

Elevation View

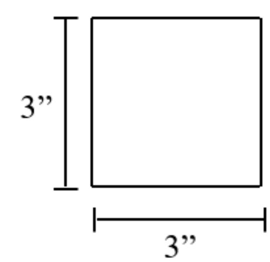

Cross Section

Figure 3-4: Flexural Test Geometry

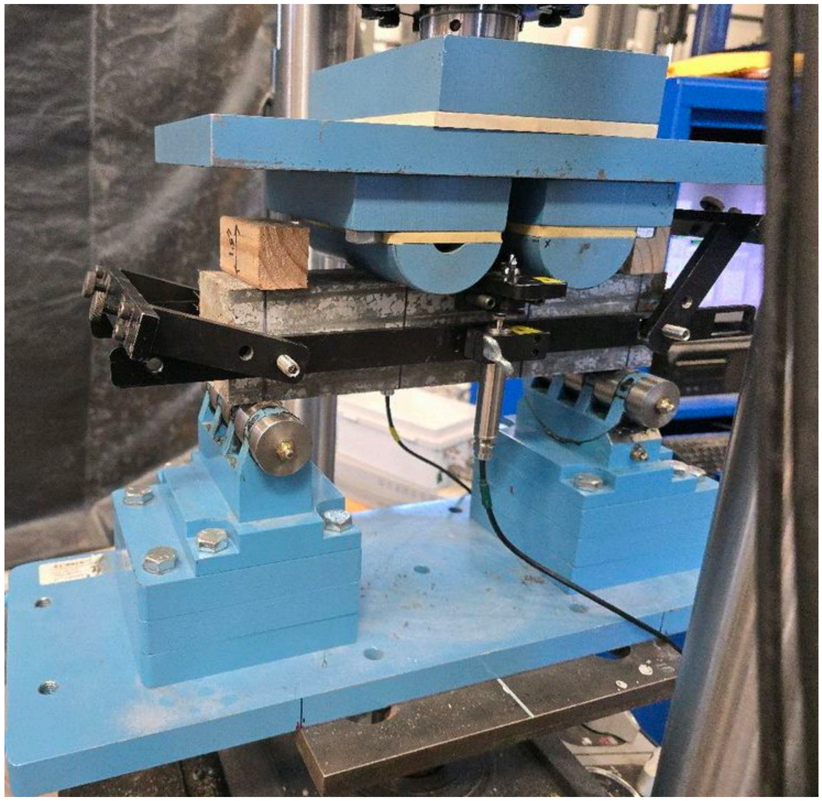

Figure 3-5: Typical Flexural Test Setup for UHPC Testing at ASEL

The rollers must be greased regularly to ensure that they have low friction so that they do not provide restraint that might affect the test results. Then, the specimens must be prepared and marked within 15 minutes of being removed from the moist-cure room. The midspan deflection controls the test loading rate, with acceptable displacement rate ranges that vary depending on the measured total displacement. These displacement rate ranges are shown below in Table 3-3. The increase in the loading rate must be less than 8 times the initial loading rate to consider the test acceptable, with the limit being 20 times for a sudden increase in loading rate. This means that a sudden crack during a test will not immediately result in the whole test needing to be discarded. A reduced initial loading rate must be used if the deflection rate cannot be controlled. Finally, the test is run until the net midspan deflection reaches a value of the span length (*L*) divided by 150. Throughout the test, the midspan deflection and the applied force must be measured at a rate of at least 2.5 Hz until the deflection reaches a value of 1/900th of the span length, at which point the measuring rate can be reduced to 2 Hz (ASTM C1609/C1609M 2019).

Table 3-3: ASTM C1609/C1609M (2019) Acceptable Displacement Rate Ranges

Beam size[A]	Up to net deflection of L/900	Beyond net deflection of L/900
100 by 100 by 350 mm [4 by 4 by 14 in.]	0.025 to 0.075 mm/min [0.001 to 0.003 in./min]	0.05 to 0.20 mm/min [0.002 to 0.008 in./min]
150 by 150 by 500 mm [6 by 6 by 20 in.]	0.035 to 0.10 mm/min [0.0015 to 0.004 in./min]	0.05 to 0.30 mm/min [0.002 to 0.012 in. min]

[A]The initial loading rate up to deflection of L/900 for other sizes and shapes of specimens shall be based on reaching the first-peak deflection 40 to 100 s after the start of the test. Beyond a net deflection of L/900, the rate of increase of net deflection shall not exceed 8 times the initial rate.

Once the flexural test is complete, the data needs to be processed. A successful test is one in which crack localization occurs within the constant moment region. An important criterion for determining whether the flexural test results vary significantly from what is normally associated with this type of test is to determine the acceptable variation between specimens using the coefficient of variation (COV). The COV defines the acceptable test-to-test difference in results when the same test method is conducted by the same operator in the same laboratory. In addition to the COV, the number of specimens affects how much variation is allowable between tests, with the precision statement in ASTM C670 (2015) defining was is acceptable. The acceptable range of variation between specimen results was calculated using the ASTM C1609/C1609M (2019) specified COVs by using the multiplier of 3.3 for three specimens as listed in ASTM C670 (2015). The procedure used was that the COV from ASTM C1609/C1609M (2019) was multiplied by 3.3 and 0.5, that value was then both added to and subtracted from one, and multiplied by the average of the tests to produce the upper and lower limits based on the COV. Equation 3-1 was used to calculate the COV limits.

$$Limits = Average \times (1 \pm 0.5 \times COV \times Factor_{Specimen}) \qquad \text{(Equation 3-1)}$$

where, *Limits* are the upper and lower acceptable limit of variation between specimens, *Average* is the average value of the result being calculated, *COV* is the coefficient of variation listed in the test standard for the result, and $Factor_{specimen}$ is the factor given by ASTM C670 (2015) that is based on the number of specimens being compared (e.g., .3 for three specimens).

As an example of how this will be used in this report, the COV limits will be calculated for the peak flexural stress, f_P. Calculating the average peak flexural stress of three specimens gave 2678 psi. The COV is 9.7% according to ASTM C1609/C1609M (2019) while the specimen factor is 3.3 for three specimens. Inputting these values into Equation 3-1 gives Equation 3-2, which simplifies to Equation 3-3.

$$Limits = 2678\,psi \times (1 \pm 0.5 \times 0.097 \times 3.3) \quad \text{(Equation 3-2)}$$

$$Limits = 2678\,psi \times (1 \pm 0.16) \quad \text{(Equation 3-3)}$$

Therefore, if the 28-day flexural peak stresses from flexural tests performed on various fine aggregate gradations are within 2,250 psi and 3,110 psi, they could be considered similar based on the precision of this test method. If this were to occur, then it can be concluded that there is no significant test-to-test variation in the results and that changes in fine aggregate gradations does not significantly affect the 28-day flexural peak stress of UHPC.

When comparing results, the focus of this study is on the variation between the stresses rather than the displacements or strains. This is due to the much larger variation allowed for the displacements in ASTM C1609/C1609M (2019), as the displacement at the peak flexural stress has a COV of 141%.

In addition, a forward analysis was used to establish the relationship between the direct-tension constitutive law and the expected flexural response, allowing the FHWA post-cracking tensile strength requirements to be expressed as equivalent flexural acceptance criteria rather than working backward from the flexural data alone.

3.4.3.2 Uniaxial Tensile Strength Testing (Direct-Tension Testing)

Direct-tension testing was performed in accordance with AASHTO T 397 (2022) to evaluate the uniaxial tensile response of the UHPC mixtures. The specimen geometry specified by AASHTO T 397 uses a 2 in. x 2 in. x 17 in. prism. Twelve specimens were cast per batch, with six designated for testing at 28 days and six at 91 days. Six specimens were made for testing at each age because of the low success rate reported in literature (Gali and Sritharan 2024). Prior to testing, aluminum transfer plates were bonded to the specimen ends using high strength, high modulus epoxy to facilitate uniform stress transfer through the wedge grips (see Figure 3-6). Three C clamps were applied at the top, middle, and tapered sections of each plate during curing of the epoxy to ensure consistent bond quality. The specimen preparation and plate installation procedures followed the requirements of AASHTO T 397.

Testing was conducted at ASEL using a 220-kip MTS universal testing machine equipped with hydraulic wedge grips. Four linear variable displacement transducers (LVDTs) were mounted on aluminum brackets attached to the specimen faces, establishing a gauge length of 4 inches (see Figure 3-7). Specimens were initially loaded in compression to 1 ksi to seat the grips, followed by tensile loading at a constant crosshead displacement rate of 0.006 in./min until the specimen load dropped to 50% of the peak tensile load. Data was collected at 10 Hz, capturing force and displacement readings from all four LVDTs. The strain was calculated as the average displacement from the four LVDTs divided by the gauge length, and the stress was calculated by dividing the recorded load by the measured cross-sectional area of the specimen. From the resulting stress strain response, the critical tensile parameters were determined in accordance with AASHTO T 397: the effective cracking stress ($f_{t,cr}$), peak stress ($f_{t,peak}$), localization stress ($f_{t,loc}$), and localization strain ($\varepsilon_{t,loc}$). These tensile parameters were obtained from individual test specimens and the mean calculated for each test. A successful test was defined as one in which crack localization occurred within the gauge length region. The test setup is shown in Figure 3-8.

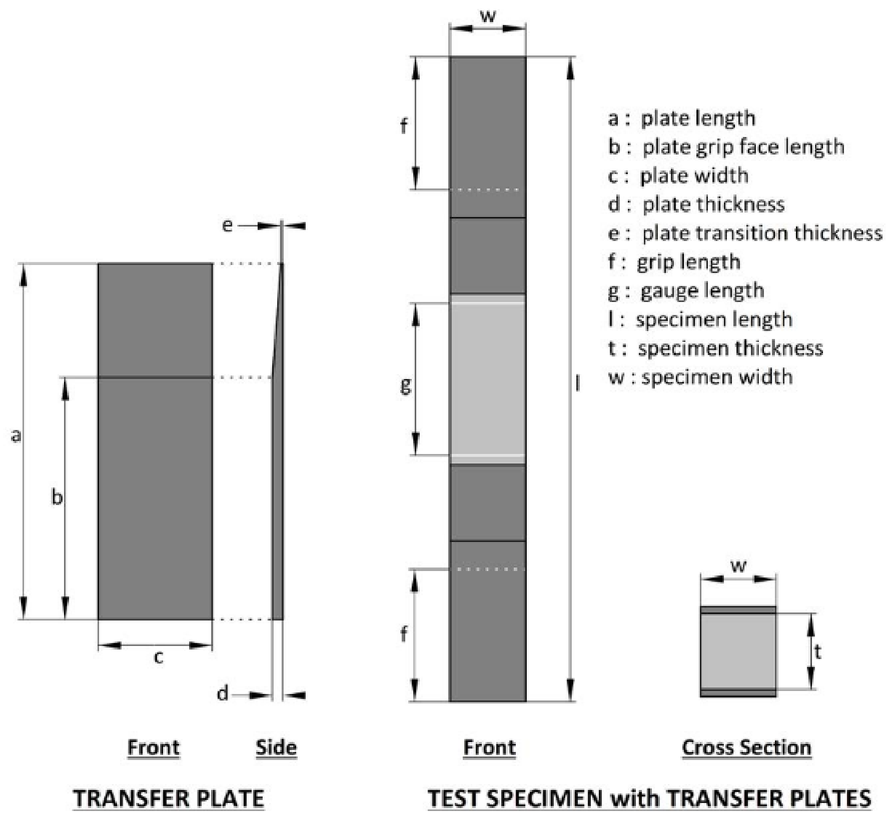

Dimensions a through e		
Dimension	mm	in.
a	160	6.25
b	108	4.25
c	50	2
d	5	0.188
e	1	0.04

Dimensions l, w, t, g, and f		
Dimension	mm	in.
l	432	17
w	50	2
t	50	2
g	102	4
f	89	3.5

Figure 3-6: Aluminum Plate and Specimen Dimension (AASHTO T 397 2022)

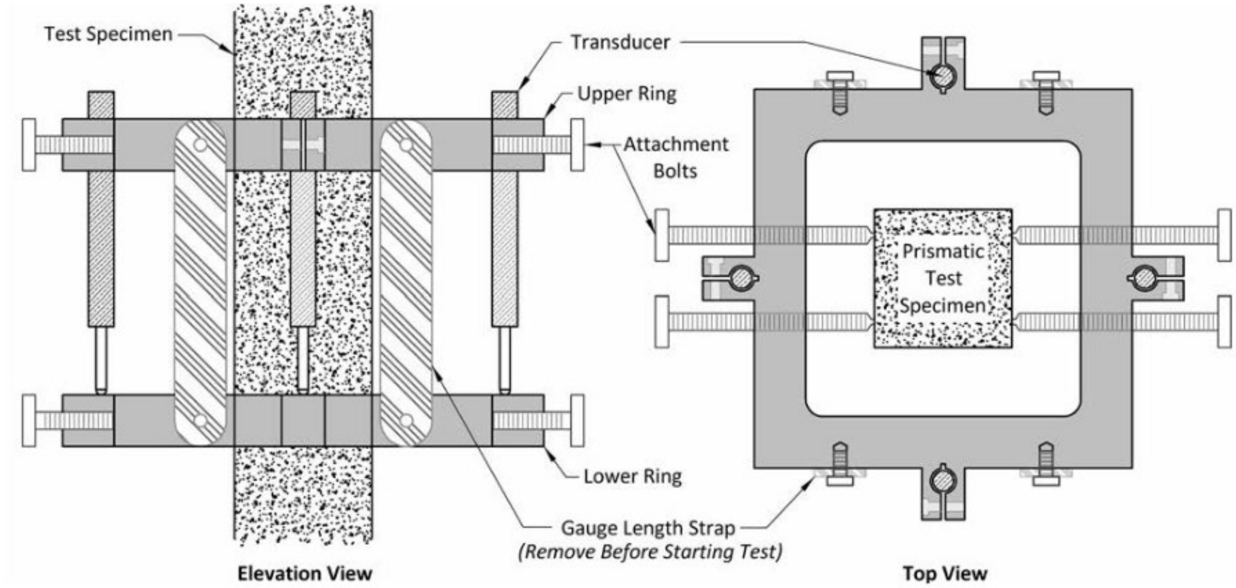

Figure 3-7: Uniaxial Tensile Test Setup (AASHTO T 397 2022)

Figure 3-8: Typical Uniaxial Tensile Test Setup for Auburn University UHPC Testing

3.5 FREEZE-THAW RESISTANCE

While not as severe as in many northern states, Alabama does experience freezing conditions, which can degrade conventional concrete that is at a high degree of saturation. As such, it is important to determine the freeze-thaw durability of UHPC because it does not contain any air-entraining admixtures. The freeze-thaw resistance was measured according to AASHTO T 161 (2022) with minor modifications from ASTM C1856/C1856M (2017). The modifications required by ASTM C1856/C1856M (2017) are to only utilize procedure A, and that a dynamic modulus of elasticity indicates specimen failure at a value that is 90% or lower compared to the initial value. All tests were performed in accordance with AASHTO T 161 (2022) which is equivalent to ASTM C666.

After being removed from the molds once initial curing was completed, the specimens were cured for 14 days in a lime-saturated bath. Testing with Procedure A means that the specimens experience freezing and thawing cycles fully submerged in water. The specimens are tested for 300 freeze-thaw cycles. After at most 36 freeze-thaw cycles, the transverse frequency is measured, and the dynamic modulus of elasticity is determined to assess the performance of the specimen. Additionally, the specimen test chamber is removed from the freeze-thaw machine and cleaned before being replaced and refilled with clean water.

CHAPTER 4

DIRECT-TENSION TESTING: PROTOCOL DEVELOPMENT AND RELIABILITY

4.1 Overview and Motivation

The FHWA requires that UHPC used in structural applications achieve a minimum post-cracking tensile strength (effective cracking stress, $f_{t,cr}$) of 750 psi and a minimum localization strain ($\varepsilon_{t,loc}$) of 0.0025 in./in. AASHTO T 397 (2022) is the only standardized test method that directly measures these values. This makes direct-tension testing the reference method for qualifying UHPC mixtures and verifying compliance with FHWA performance requirements. A typical UHPC tensile stress strain response with the key AASHTO T 397 parameters is shown in Figure 4-1. The effect of the steel fibers in UHPC can be better characterized based on the results from the direct-tension test than for example compression testing (Riding et al. 2019; Graybeal and Baby 2013).

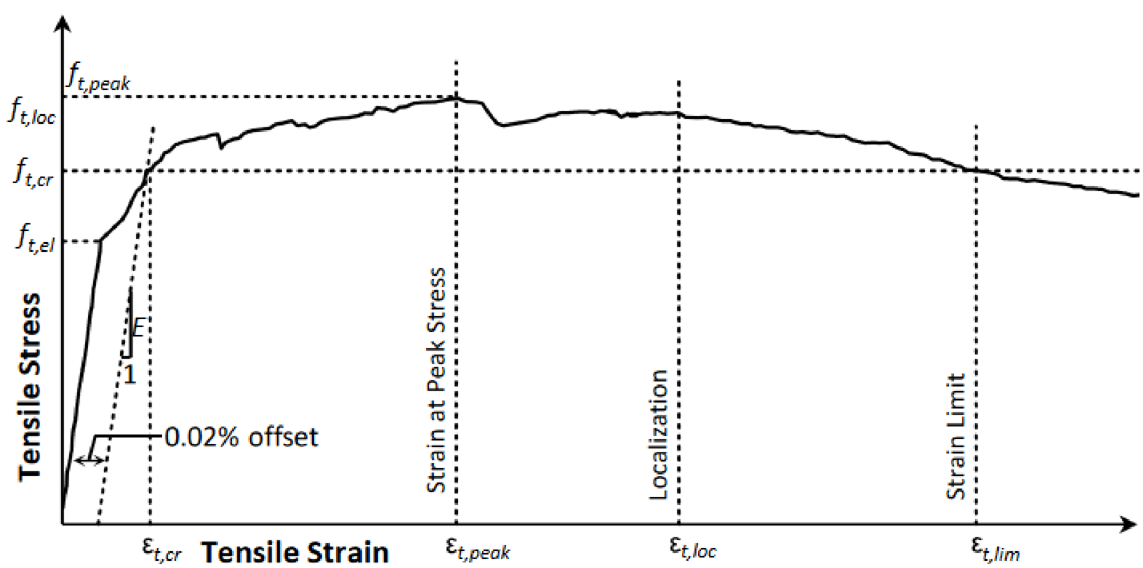

Figure 4-1: A Typical Stress-Strain Graph of UHPC (AASHTO T 397 2022)

Despite its importance, direct-tension testing of UHPC has been documented in the literature to have significant reliability problems. Reported success rates with 220-kip, wedge-grip machines have been well below what would be considered practical for quality control or quality assurance testing. These low success rates present a significant barrier to UHPC implementation. If the test required to qualify a mixture fails more often than it succeeds, the cost and effort of testing become impractical for agencies, engineers, and testing laboratories.

This chapter documents the challenges encountered during direct-tension testing in this study and the systematic test protocol refinements that were developed to improve the test success rate when following AASHTO T 397. The investigation was conducted across two phases of testing. Phase One tested specimens spanning fiber dosages from 0.00% to 2.00%, during which challenges were identified and initial adjustments were made. Phase Two tested specimens contained three silica fume contents (9%, 12%, and 15%) at a fixed fiber dosage of 1.50%, using the fully refined direct-tension test protocol. The same 220-kip, wedge-grip machine was used throughout both phases while using the same equipment required by AASHTO T 397. The material characterization results from both phases are presented separately in Chapter 5. This chapter focuses exclusively on the testing methodology and the changes in the test protocol to improve the reliability of AASHTO T 397.

4.2 CHALLENGES ENCOUNTERED AND PROTOCOL REFINEMENTS

The direct-tension test setup used in this study is described in Section 3.4.4. All testing was performed on 2 in. x 2 in. x 17 in. prismatic specimens using a 220-kip MTS universal testing machine equipped with hydraulic wedge grips. Four LVDTs were mounted on aluminum brackets to establish a 4-inch gauge length, and the crosshead displacement rate was 0.006 in./min. Consistent with the acceptance criterion of AASHTO T 397, a successful test was defined as one in which crack localization occurs within the gauge length region.

During Phase One testing, three primary issues were identified that substantially affected testing outcomes.

1) The first issue involved geometric tolerances of the formed specimens. During casting, the steel molds were tapped on the vertical sides with a rubber mallet to release entrapped air. This practice, though standard, introduced slight geometric deviations along the specimen sides. Even minor departures from perpendicularity caused misalignment at the grips during testing and resulted in localized crushing of the UHPC at the grip location. The consequence was failure either within the transfer plate region or at the tip of the transfer plate, both of which render the test invalid. To reduce this problem, tapping was limited to the lower sections of the mold where the geometry is more stable, and the mold screws were further tightened prior to casting. The use of vibrating tables was considered but avoided due to concerns about potential fiber settlement within the small cross section.
2) The second issue was crosshead misalignment. Direct-tension tests are sensitive to eccentric loading; therefore, crosshead rotational displacement during grip tightening induces bending stresses that cause failure outside the gauge length. The critical observation was that misalignment often occurred at the top grip during tightening. With the bottom grip closed, each time the top grip was tightened, the top crosshead rotated slightly, introducing an eccentric load. This was identified as the most common cause of invalid test results.
3) The third issue was excessive grip pressure. High pressures from the wedge grips caused aluminum plate delamination or crack initiation within the gripped region. Both outcomes rendered the test invalid and reduced the yield of usable test results per batch.

Upon identifying these issues, a systematic test protocol was developed to address each one. The refinements were implemented progressively over the course of the experimental program and are described below in the order they were developed.

4.2.1 SPECIMEN PREPARATION TO PREVENT PLATE DELAMINATION

The AASHTO T 397 specimen preparation protocol was found to be adequate for preventing plate delamination, provided that additional care was taken with surface preparation and epoxy application. The following procedure was established and used for all specimens in the refined protocol:

1) The formed surfaces of the UHPC specimen were smoothed using a steel file to remove any irregularities or fiber protrusion.
2) A paper towel was used to clean the formed surfaces.
3) An aluminum safe degreaser was sprayed onto the aluminum plates and the formed surfaces of the UHPC specimen, and both were subsequently cleaned with a dry paper towel.
4) A thin, uniform layer of epoxy (Sikadur Hi Mod 2) was applied to the cleaned formed surfaces of the UHPC specimen (as shown in Fig. 4-2a).
5) A similarly thin and uniform layer of epoxy was applied to the aluminum plates.
6) Each aluminum plate was carefully positioned and clamped at three locations (top, middle, and tapered section) to ensure uniform distribution of clamping pressure (as shown in Fig. 4-2b).
7) The epoxy was allowed to cure for 12 to 24 hours at laboratory temperatures to ensure adequate bond strength prior to testing.

a)
b)

Figure 4-2: Image Showing a) Thin Layer of Epoxy Applied to the Cleaned Surface and b) the Aluminum Plates Held in Place by Three C-Clamps at Each End (blue painters tape added for ease of cleanup)

4.2.2 GRIPPING AND ALIGNMENT SEQUENCE TO MINIMIZE ECCENTRICITY

The most significant improvement in test reliability came from the development of a systematic gripping and alignment sequence. This procedure was designed to prevent crosshead rotation during grip tightening, which had been identified as the dominant source of eccentric loading and invalid test results. The complete sequence was as follows:

1) Aligning the Deformation Measuring Device: To achieve precise perpendicular alignment of the parallel ring extensometer to the specimen, custom-cut wooden platforms were utilized as supports during installation as seen in Fig. 4-3.

Figure 4-3: Image Showing the Alignment of the Deformation Measuring Device

2) Positioning the Specimen in the Testing Machine: The specimen alignment within the bottom grip was facilitated by placing a wooden spacer block and metal disc beneath the specimen (see Fig. 4-4).

a) b)

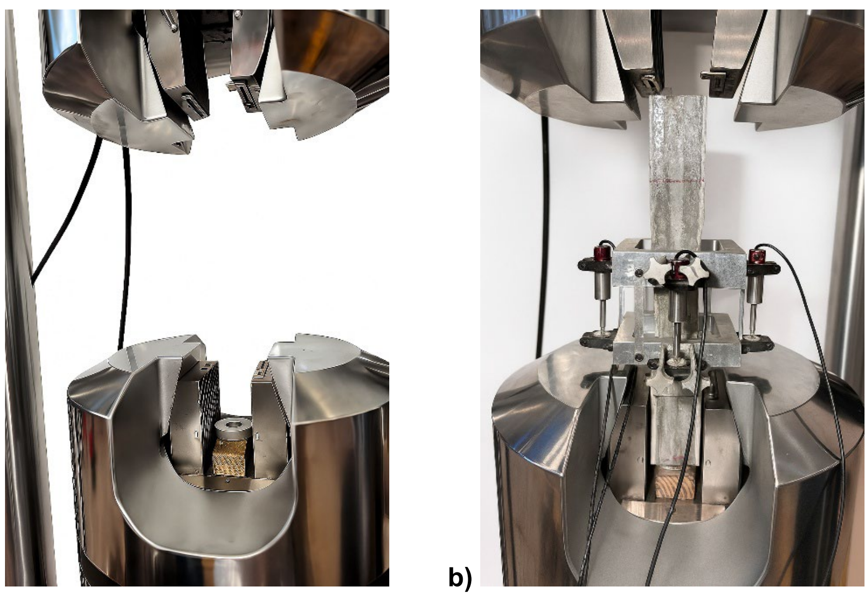

Figure 4-4: Images Showing a) Wooden Spacer Block and Metal Disc within the Bottom Grip and b) the Sample Sitting Directly on the Wooden Spacer Block and Metal Disc

3) Aligning the top crosshead and confirming alignment: With the top grip lowered and the machine in force-control mode, careful alignment of the top and bottom crossheads was

verified with a plumb line. Once aligned, the gauge length strap for the parallel ring extensometer was removed.

4) Initiating the gripping sequence that used the following steps:

   a. The gripping speed controller was set to its slowest rate by fully rotating the knob clockwise which reduces or increases the speed (see Fig. 4-5).

   b. Subsequently, the gripping speed controller knob was turned 360 degrees counterclockwise, establishing the final slow gripping speed. Note, this can be done at the start of the test and does not need to be altered thereafter.

   c. The grip pressure knobs were also turned counterclockwise to their slowest rate, to reduce the grip tightening speed to its slowest setting.

   d. The top wedge grip was partially closed, allowing slight vertical adjustment of the specimen (Note: once the grip valve is tightened clockwise, due to the grip pressure reduced to its lowest, it takes a few seconds for the grips to close).

   e. The bottom grip valve was then closed, pushing the specimen upwards and aligning it vertically. The gripping speed control remains untouched.

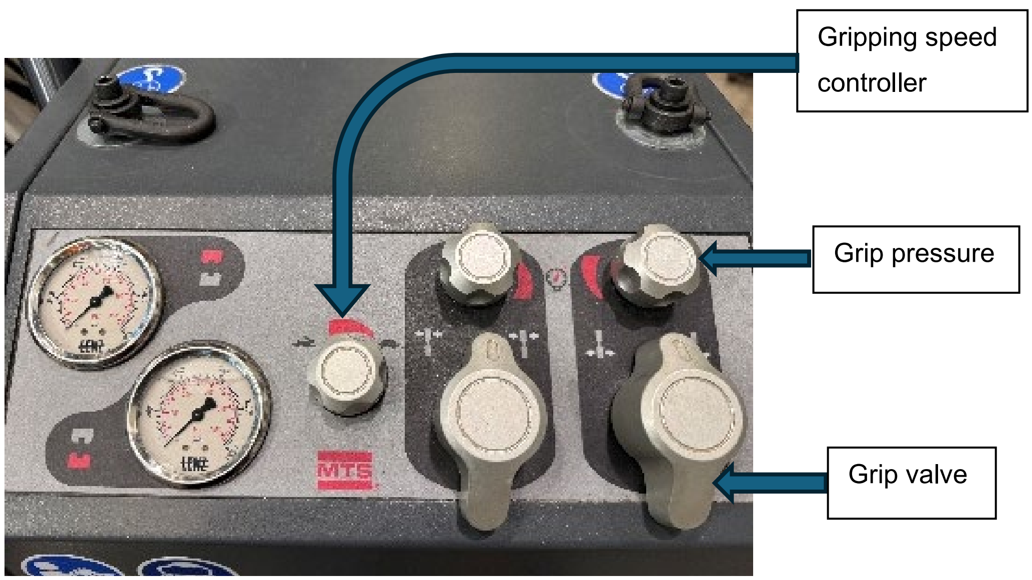

Figure 4-5: Grip Activation Control Panel

   f. Before completely tightening the top grip, alignment of the crossheads was confirmed again, and the bottom grip was slightly released to prevent rotation of the top crosshead. This rotation was found to be a major cause of eccentric loads which caused failure outside the gauge length.

   g. The top grip was then fully tightened.

   h. The metal disc between the bottom grip was removed (Note: a flat tool to push out the disc was found effective), and the recording from the LVDT initiated.

i. The bottom grip valve was then closed to complete the alignment sequence (see Fig. 4-5).
j. With both grips firmly secured, the grip pressure was incrementally increased to around 500 and 800 psi, ensuring sufficient pressure without inducing unwanted bending stress or crushing of the specimen (see Fig. 4-6).

Figure 4-6: Image Showing the Grips in an Aligned Position

After completion of the gripping and alignment sequence, the specimen was loaded to failure per the AASHTO T 397 loading protocol described in Section 3.4.3. With these refinements in place, failures occurred within the gauge length region at a substantially higher rate than in the earlier phases of testing. A photograph of an acceptable failure within the gauge length region is shown in Figure 4-7.

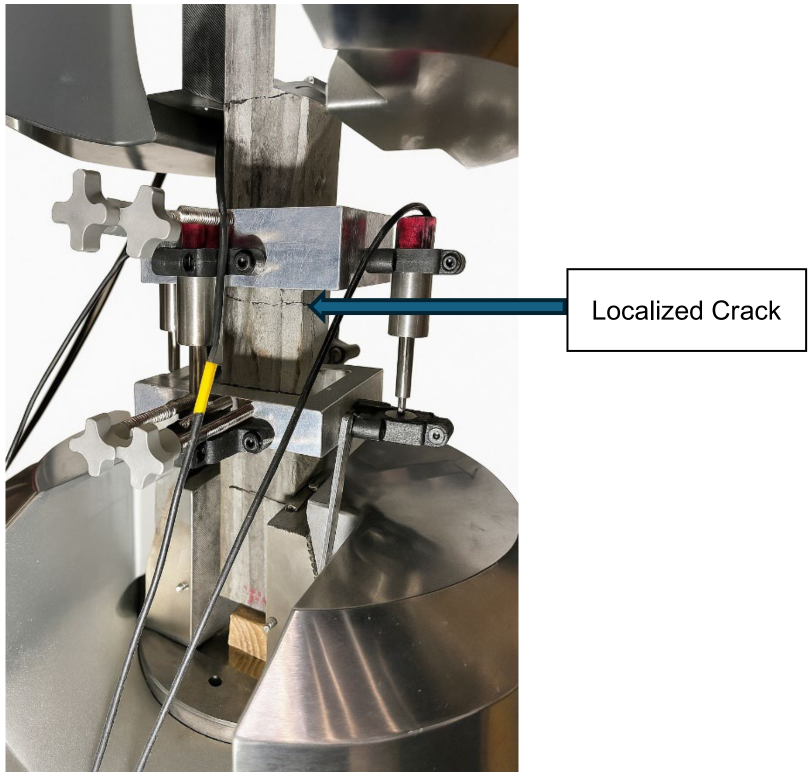

Figure 4-7: Image Showing an Acceptable Failure within the Gauge Length Region

4.3 RESULTS: FAILURE MODE AND SUCCESS RATES

The effectiveness of the protocol refinements was quantified by tracking success rates throughout the experimental program. Testing was categorized into three phases based on the level of protocol implementation, and the results are summarized in Table 4-1.

Table 4-1: Summary of Test Success Rates Across Refinement Phases

Testing Phase	Total Specimens Tested	Valid Specimens (Gauge Length Failures)	Success Rate (%)
Initial Phase	48	21	44
Intermediate Phase (Operator Alignment Trials)	68	33	49
Final Phase (Fully Implemented Protocol)	76	57	75

A total of 192 specimens were tested across the three phases. In the Initial Phase, the standard AASHTO T 397 procedure was followed without modification. The 44% success rate during this phase meant that achieving three valid tests per mixture required testing 6 to 8 specimens on average. During the

Intermediate Phase, operator alignment adjustments were introduced on a trial basis, producing a modest improvement to 49%. The full systematic protocol described in Section 4.2 was implemented in the Final Phase, producing a 75% success rate. At this rate, three valid tests per mixture could be achieved with approximately 4 to 5 specimens, representing a meaningful reduction in the number of specimens that needed to be fabricated, cured, and prepared per mixture. The bar chart in Figure 4-8 illustrates the progressive improvement across testing phases.

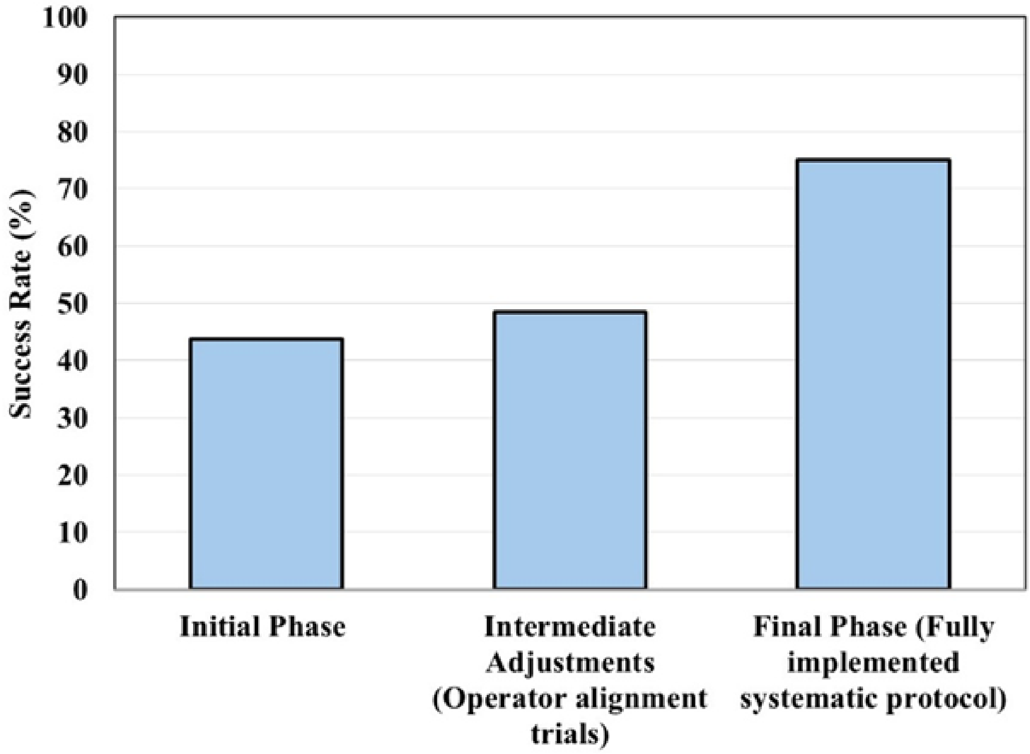

Figure 4-8: Graphical Representation Illustrating Incremental Improvements in Success Rates across Testing Refinement Phases

An important practical observation is that the protocol refinements did not require any capital equipment investment. The improvements were achieved using the same 220-kip, wedge-grip machine throughout the study. This is a significant consideration for ALDOT implementation, as it means testing laboratories that already own wedge-grip equipment can adopt the refined protocol without purchasing new machinery.

4.4 Reliability of Stress versus Strain Measurements

While evaluating the direct-tension results across both phases of testing, a consistent pattern emerged in the reliability of the measured tensile parameters. The stress-based parameters (effective cracking stress, peak stress, and localization stress) showed clear, repeatable trends that logically followed changes in mixture composition. As fiber content increased from 1.00% to 2.00%, the stress parameters increased in a predictable and consistent manner. Similarly, when silica fume content was varied at a fixed fiber dosage, the stress results showed modest but discernible differences between mixtures.

The strain-based parameters (effective cracking strain, peak strain, and localization strain) did not show the same consistency. Across all fiber dosages and silica fume contents, the strain values exhibited high variability with no discernible relationship to the mixture variables. The scatter was substantial even within a single mixture group, where replicate specimens from the same batch produced markedly different strain values while their stress values were in reasonable agreement.

This observation is consistent with findings reported elsewhere. Gali and Sritharan reported standard deviations for strain parameters ranging from 23% to 38% of mean values in their evaluation of AASHTO T 397 (Gali and Sritharan 2024). ASTM C1609 (2019) documents that the coefficient of variation of displacement at peak load in flexural testing of fiber reinforced concrete may exceed 100%, whereas the coefficient of variation of flexural stress is only 9.7%. The underlying cause is that strain measurements are highly sensitive to out of plane alignment, slip or imperfections at the gripping interface, and localized defects in the specimen, all of which have a much larger effect on strain than on stress.

The implication of this finding is direct. For material optimization, specification, and quality control of UHPC, only stress-based performance metrics should be used. Specifically, the effective cracking stress and localization stress are the appropriate parameters for evaluating compliance with FHWA requirements and for establishing acceptance criteria. Strain based criteria should not be included in specifications or used for quality control purposes, as the variability of strain measurements under current testing conditions does not support their use as reliable acceptance parameters. This recommendation is carried forward into the implementation recommendations for ALDOT in Chapter 7.

4.5 Recommended Direct-Tension Testing Protocol

Based on the findings documented in this chapter, the following protocol is recommended for direct-tension testing of UHPC per AASHTO T 397 using a wedge-grip machine.

The specimen preparation procedures specified in AASHTO T 397 are adequate for preventing plate delamination, provided that both the UHPC surfaces and the aluminum plates are thoroughly cleaned, a thin and uniform epoxy layer is applied to both surfaces, clamping is applied at three locations on each plate, and specimens are within the permissible geometric tolerances of the standard. The detailed specimen preparation procedure is provided in Section 4.2.1.

Two modifications to the standard AASHTO T 397 procedure are recommended. First, crosshead alignment should always be verified after the specimen is positioned in the machine and prior to applying any load. The standard recommends checking alignment before installing the specimen, but the experience in this study demonstrated that alignment must be reconfirmed after specimen positioning because crosshead rotation can occur during grip closure. Second, the gripping procedure should follow the controlled sequence described in Section 4.2.2, with particular attention to preventing crosshead rotation during top grip tightening and maintaining grip pressure between 500 and 800 psi. The complete gripping and alignment sequence is summarized in Table 4.2 for reference by testing personnel.

Table 4-2: Recommended Direct-Tension Test Protocol Summary

Step	Action
Specimen Preparation	File surfaces, clean with degreaser, apply thin epoxy, and then clamp
Extensometer	Mount LVDT with the bracket
Specimen Positioning	Place on wooden spacer and metal disc within the bottom grip
Grip Speed	Set to slowest rate, and increase by one revolution (full CW, then 360° CCW)
Alignment Check	Verify crosshead alignment before and after partial gripping
Gripping Sequence	Close top grip, remove disc, initiate data collection, and then, close bottom grip
Grip Pressure	Increase incrementally to 500-800 psi
Loading	1 ksi compression pre-load, then apply 0.006 in./min. tension load

The complete setup sequence, including crosshead alignment verification and controlled gripping, adds approximately 5 to 10 minutes per specimen compared to the time required under the standard AASHTO T 397 procedure. The expected success rate with the refined protocol is approximately 75%, compared to 36% to 50% reported in the literature for standard implementation of AASHTO T 397 with wedge-grip machines.

For specification and acceptance purposes, stress-based criteria (effective cracking stress and localization stress) should be used. Strain-based criteria are not recommended, as documented in Section 4.4. The material characterization results obtained using this protocol are presented in Chapter 5, and the testing and quality control recommendations for ALDOT implementation are covered in Chapter 7.

CHAPTER 5
MATERIAL CHARACTERIZATION RESULTS

This chapter includes the results and discussion of the results from the experimental plan covered in Chapters 3 and 4. The fresh concrete properties and the relative strength differences of each UHPC are presented and discussed.

5.1 FRESH PROPERTY RESULTS

All batches that proceeded to specimen casting achieved the 7- to 11-inch flow acceptance range. Within the fiber dosage series, increasing the steel fiber content generally required a higher HRWRA dosage to maintain flow within the target range. This is expected, as steel fibers increase the internal friction of the fresh mixture and resist the flow of the cementitious paste between particles.

The binary blend batches (Type IL cement and slag cement without silica fume) exhibited a notably faster loss of workability compared to the equivalent ternary blend batches at the same fiber dosage. Although both binary batches achieved the target flow range during testing, the working time before the mixture stiffened was observably shorter. In the laboratory, this was managed by extending the Step 4 mixing duration beyond the standard 5 minute minimum. For field-scale production, where the UHPC must maintain adequate flow during transport and placement, this reduced working window is a potential practical constraint that should be considered and addressed with additional chemical admixtures. This observation is one of the reasons a ternary blend is recommended over a binary blend, as discussed further in Section 5.4.

For the silica fume dosage series, higher silica fume contents required less HRWRA to achieve the target flow. This suggests that silica fume, at the particle sizes used in this study, contributes a lubricating effect within the fresh paste, likely through improved particle packing at the finest particle scale of the mixture.

For the water-binder ratio series, lower water-binder ratios reduced flow and required more HRWRA.

5.2 EFFECT OF STEEL FIBER DOSAGE

Seven batches were produced at steel fiber dosages of 0.00%, 0.50%, 1.00%, 1.25%, 1.50%, 1.75%, and 2.00% by volume to quantify the influence of fiber content on the mechanical properties of UHPC. For all seven batches, the ternary binder system (Type IL cement, slag cement, and silica fume) and the water-binder ratio of 0.19 were held constant. The fine aggregate content was adjusted for each batch to maintain a constant total mixture volume (fixed yield) as the fiber volume changed.

5.2.1 COMPRESSIVE STRENGTH RESULTS

Compressive strength results for the fiber dosage series are presented in Figure 5-1. Three cylinders were tested at each of five ages corresponding to 1, 7, 28, 56, and 91 days for each fiber dosage. From the result, it shows that the compressive strength of the UHPC was not significantly affected by changes in the steel fiber dosage. Across the range of 0.00% to 2.00% fiber, the 28-day compressive strengths ranged from approximately 15,500 to 17,500 psi, with most strengths falling between 16,000 and 17,500 psi. By 91 days, all seven dosages achieved and exceeded the FHWA minimum compressive strength requirement of 17,500 psi, with values ranging from approximately 17,500 to 18,800 psi. The 0.00% fiber batch, which serves as the matrix only control, achieved a 28-day compressive strength of approximately 15,500 psi and a 91-day strength of approximately 17,500 psi. In addition, across 0.50% to 2.00%, there is no clear trend of an increase or decrease in strength with fiber dosage, confirming that the compressive performance is governed by the cementitious matrix rather than the steel fiber dosage.

The 0.00% batch exhibited an anomalous 56-day result that was slightly lower than its 28-day value, which is likely attributable to a specimen or testing irregularity rather than an actual loss of strength. This isolated anomaly does not affect the overall conclusion. Steel fibers do not significantly alter the compressive load carrying capacity of the matrix.

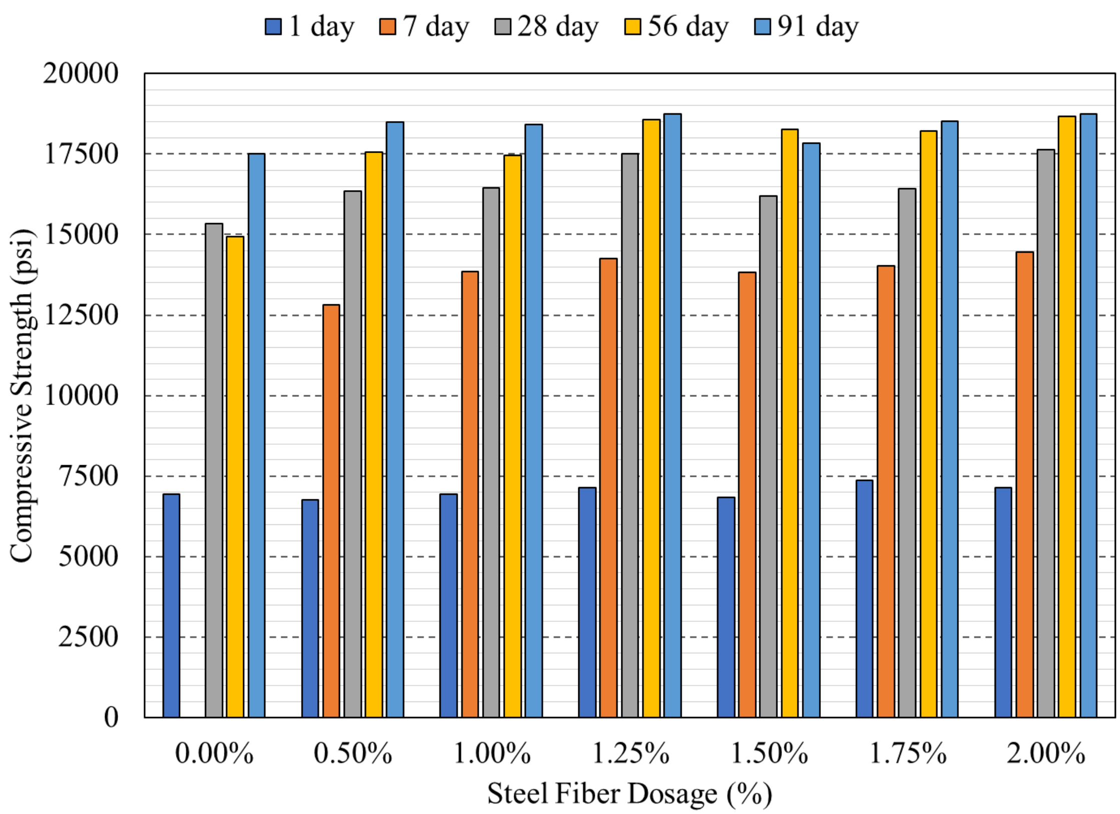

Figure 5-1: Compressive Strength Development across Fiber Dosages at all Test Ages

5.2.2 Flexural Strength Results

Flexural strength results for the fiber dosage series are presented in Figures 5-2 and 5-3. Steel fiber dosage had a significant effect on the flexural performance of the UHPC, and this effect is visible across the full range of dosages tested.

The 0.00% fiber specimens failed immediately upon matrix cracking with no post-cracking capacity whatsoever. The 0.50% fiber specimens exhibited deflection softening behavior at both 28 and 91 days, with load carrying capacity decreasing sharply after cracking. This response indicates that 0.50% fiber is insufficient to sustain load redistribution across a cracked section.

Beginning at 1.00% fiber, the flexural response transitioned to deflection hardening behavior, where the peak flexural stress exceeded the first-peak stress (f_1). This transition is significant because deflection hardening indicates that the fibers are effectively bridging cracks and redistributing stress across the section, which is a defining characteristic of well-performing UHPC. At 28 days, the peak flexural stresses (f_P) increased progressively from approximately 2,270 psi at 1.00% to approximately 2,670 psi at 1.25%, 2,865 psi at 1.50%, 2,915 psi at 1.75%, and 3,300 psi at 2.00%. The 2.00% dosage produced the highest peak flexural stress of any batch in the study.

The 91-day flexural results revealed a similar trend, with strength gains observed across all dosages relative to the 28-day values. At 91 days, the 1.50% dosage reached approximately 2,985 psi and the 2.00% dosage approximately 3,200 psi. The 91-day data for the 1.00% and 1.25% dosages were not available.

The COV bounds plotted on Figures 5-2 and 5-3 provide an additional layer of interpretation. Each figure shows the upper and lower COV limits marked at two stress states, f_1 and f_P, indicating the range of expected batch-to-batch variability at each point. This was obtained by taking the average of the batches at a stress state and calculating the COV as discussed in section 3.4.3.1. Dosages whose stresses fall within these limits are performing within normal variability, while dosages that fall outside represent a departure that cannot be attributed to scatter alone.

At the first-peak stress (f_1), all fiber dosages fall within the COV limits at both 28 and 91 days. This is consistent with what would be expected physically. The cementitious matrix composition is essentially the same across all batches, so the stress at which the matrix first cracks is governed by the matrix rather than the fiber content. At this point in the response, the fibers have not yet been engaged in any meaningful redistribution.

At the peak stress (f_P) at 28 days, the intermediate dosages from 1.00% through 1.75% all fall within the COV limits at f_P, indicating that while peak stress does increase progressively across that range, those differences remain within the variability one would expect across batches of the same mix. The two dosages that fall outside the COV limits are 0.50%, which falls below the lower bound, and 2.00%, which exceeds the upper bound. At 91 days, the same pattern holds for the dosages that were tested, with 0.50% and 2.00% again falling outside the COV limits while the intermediate dosages remain within them.

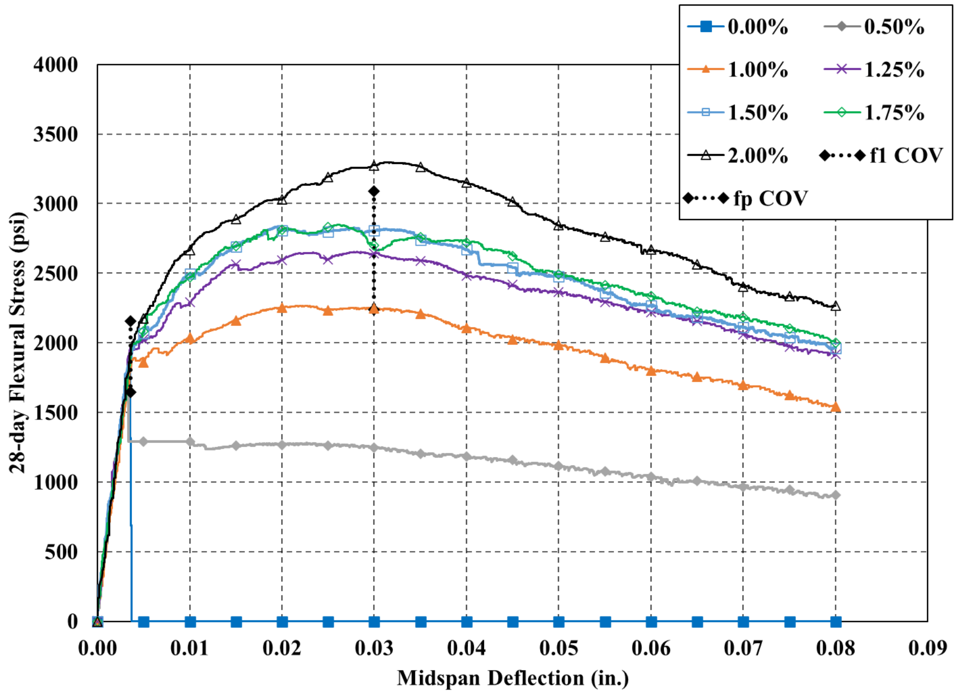

Figure 5-2: 28-day Flexural Stress versus Midspan Deflection for all Fiber Dosages

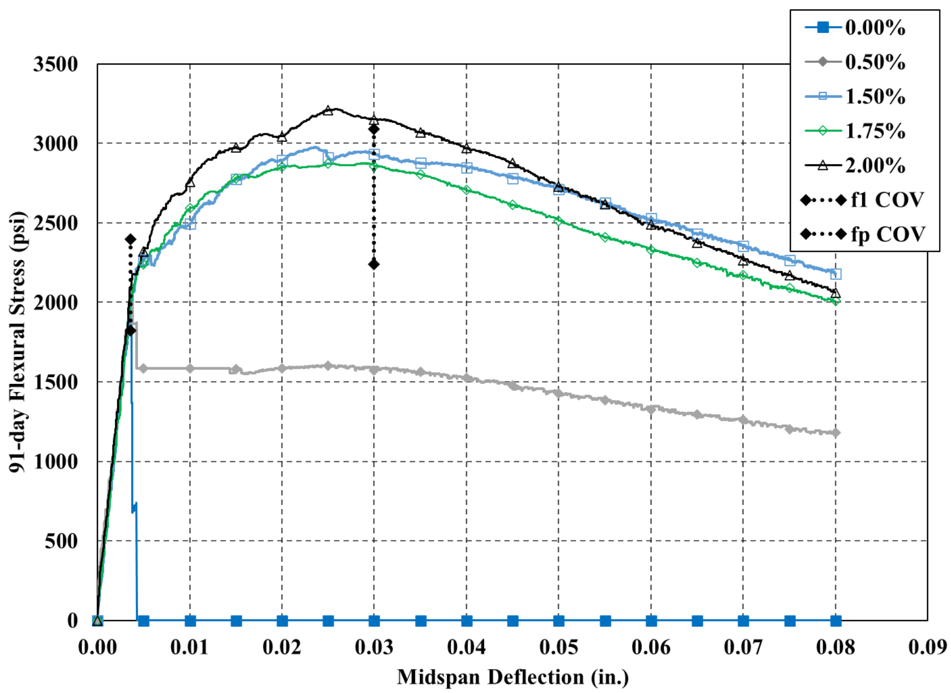

Figure 5-3: 91-day Flexural Stress versus Midspan Deflection for Different Fiber Dosages

5.2.3 Direct-Tension Results

Direct-tension results for the fiber dosage series are presented in Figures 5-4 and 5-5. The direct-tension results reinforced the same trend observed in flexural testing, that steel fiber dosage is the dominant factor for tensile performance. At 28 days, the 0.50% dosage reached a peak stress of approximately 600 psi, which falls below the FHWA minimum effective cracking strength of 750 psi. All dosages at or above 1.00% exceeded the 750 psi threshold. The effective cracking stress increased consistently with an increase in steel fiber dosage, from approximately 900 psi at 1.00% to approximately 1,010 psi at 1.25%, 1,030 psi at 1.50%, 1,170 psi at 1.75%, and 1,330 psi at 2.00%.

At 91 days, the order remained the same: 2.00% was highest at approximately 1,360 psi, followed by 1.75% at approximately 1,340 psi, 1.50% at approximately 1,160 psi, and 1.25% at approximately 1,030 psi. All dosages from 1.00% and above remained well above the FHWA threshold at both test ages.

It should be noted that the 0.50% and 2.00% dosages had fewer than three valid test results at 28 days due to the DTT reliability issues documented in Chapter 4.

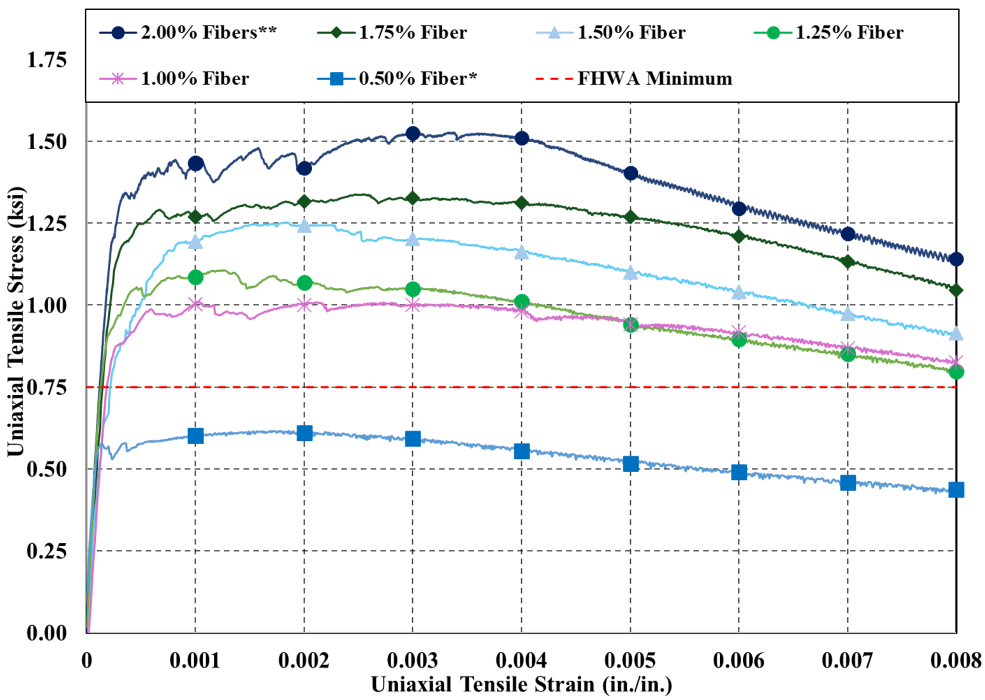

Figure 5-4: 28-day Mean Tensile Stress-Strain Response for Each Fiber Dosage.

Note: "*" Denote how many specimens are missing to meet the minimum number of three specimens.

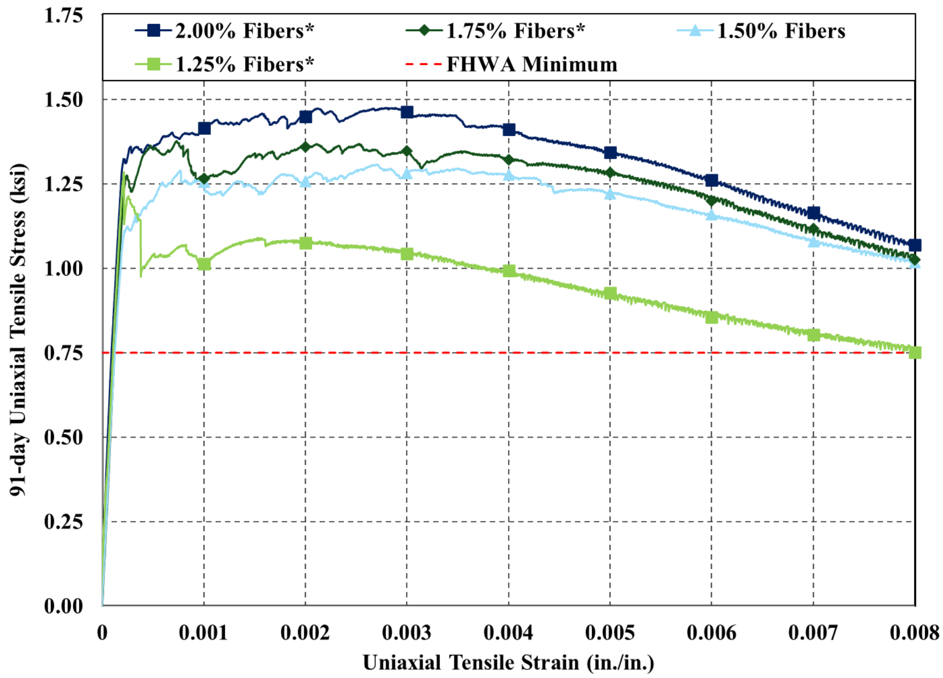

Figure 5-5: 91-day Mean Tensile Stress-Strain Response for Select Fiber Dosages.

Note: "*" Denote how many specimens are missing to meet the minimum number of three specimens.

5.2.4 Discussion of Results

The results from the fiber dosage investigation led to a clear set of observations. Steel fiber content has no significant effect on the compressive strength of UHPC because the compressive strength is governed by the properties of the cementitious matrix. In contrast, steel fiber dosage is a dominant factor controlling both the flexural and direct-tension performance. The transition from deflection softening to deflection hardening in flexural testing occurs between 0.50% and 1.00% steel fiber dosage for the UHPC tested. In direct tension, the FHWA 750 psi threshold is exceeded at dosages of 1.00% and above.

However, the 1.00% dosage provides only a narrow margin above the 750 psi threshold, with an effective cracking stress of 900 psi at 28 days. This leaves limited room for the natural variability inherent in field-produced UHPC. A fiber dosage of 1.50% provides a substantially more comfortable margin, with effective cracking stress at 28 days of approximately 1,030 psi in direct-tension and approximately 2,865 psi in peak flexural testing. Increasing the dosage to 1.75% and 2.00% produced further gains; however, steel fiber dosage above 1.5% might be unnecessary when considering economy and workability requirements.

5.3 Effect of Fine Aggregate Gradation

Three batches were produced to evaluate the effect of fine aggregate gradation on UHPC performance: one using natural river sand meeting AASHTO M 6 (2022) gradation limits, one using local masonry sand (the nearest locally available material to the AASHTO M 45 gradation), and one using an optimized blend of both the AASHTO M 6 river sand and the masonry sand. This blend was obtained using the modified Andreasen and Andersen curve (Funk and Dinger 2013). Using a value of 0.23 for *q* in Equation 2.2, the most optimal blend of the AASHTO M 6-compliant fine aggregate and the local masonry sand was 80% AASHTO M 6-compliant fine aggregate and 20% local masonry sand. This value for *q* came from Yu et al. (2014). Figure 5-6 shows the optimized fine aggregate gradation and how it compares to the modified Andreasen Anderson equation (Funk and Dinger 2013). The equation is covered in Chapter 2 as Equation 2.2. All three batches had the same ternary binder system, a water-binder ratio of 0.20, and a fiber dosage of 1.50%.

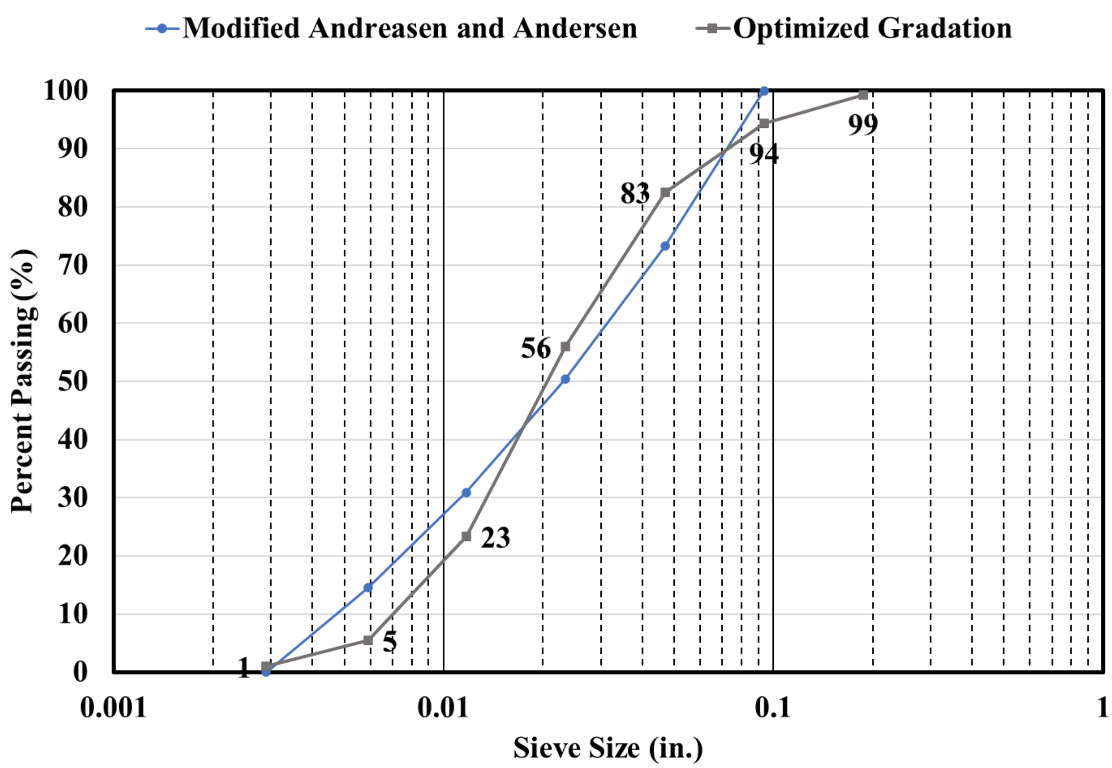

Figure 5-6: Optimized Fine Aggregate Gradation

5.3.1 Compressive Strength Results

Compressive strength results for the fine aggregate gradation series are presented in Figure 5-7. All three gradations produced compressive strengths that were within the acceptable range of test-to-test variation defined by AASHTO T 22 (2022). The 28-day compressive strengths for all three gradations fell between approximately 16,000 and 17,000 psi. The masonry sand exhibited marginally higher 56- and 91-day compressive strengths. This slight increase can be attributed to the more densely packed nature the fine masonry sand provides. However, it is also important to note that the differences were within the allowable coefficient of variation for three specimens as calculated per in AASHTO T 22M/T 22 (2022). Therefore, changes in fine aggregate gradation do not significantly affect the compressive strength of the UHPC developed in this study.

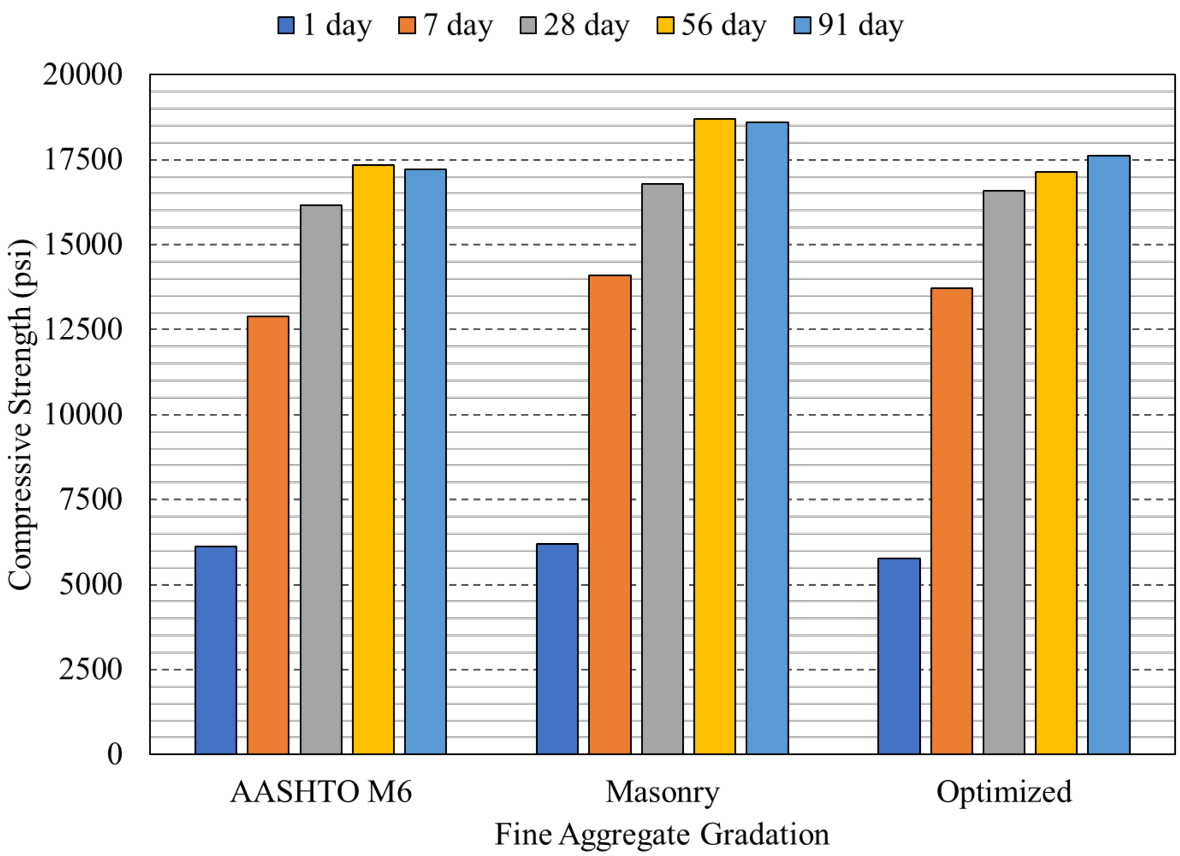

Figure 5-7: Compressive Strength Development for Three Fine Aggregate Gradations

5.3.2 FLEXURAL STRENGTH RESULTS

Flexural strength results for the fine aggregate gradation series are presented in Figures 5-8 and 5-9. These figures show that there is no clear trend in the results, as the results vary between the 28-day and 91-day tests for the AASHTO M 6 and optimized fine aggregates. As was the case for the compression test results, the highest values belong to the masonry sand, but similar to the compressive results, the range of COV is within an acceptable range per AASHTO T 22 (2022). The COV limits for the first-peak flexural stress and peak flexural stress are shown in the figures. At 28 day, the upper and lower COV for f_1 and f_P are 1724 2262 and 2250, 3106 psi. At 91 day, the upper and lower COV for f_1 and f_P are 1654, 2172 and 2436, 3364 psi. If the fine aggregate gradation did significantly affect the flexural strength, then it was expected that the optimized fine aggregate gradation would have the highest strength, followed by the AASHTO M 6-compliant fine aggregate, with the lowest strength belonging to the masonry sand, due to the masonry sand being the furthest from the best particle packing curve. In conclusion, the fine aggregate gradation does not significantly impact the flexural strength of the UHPC evaluated in this study.

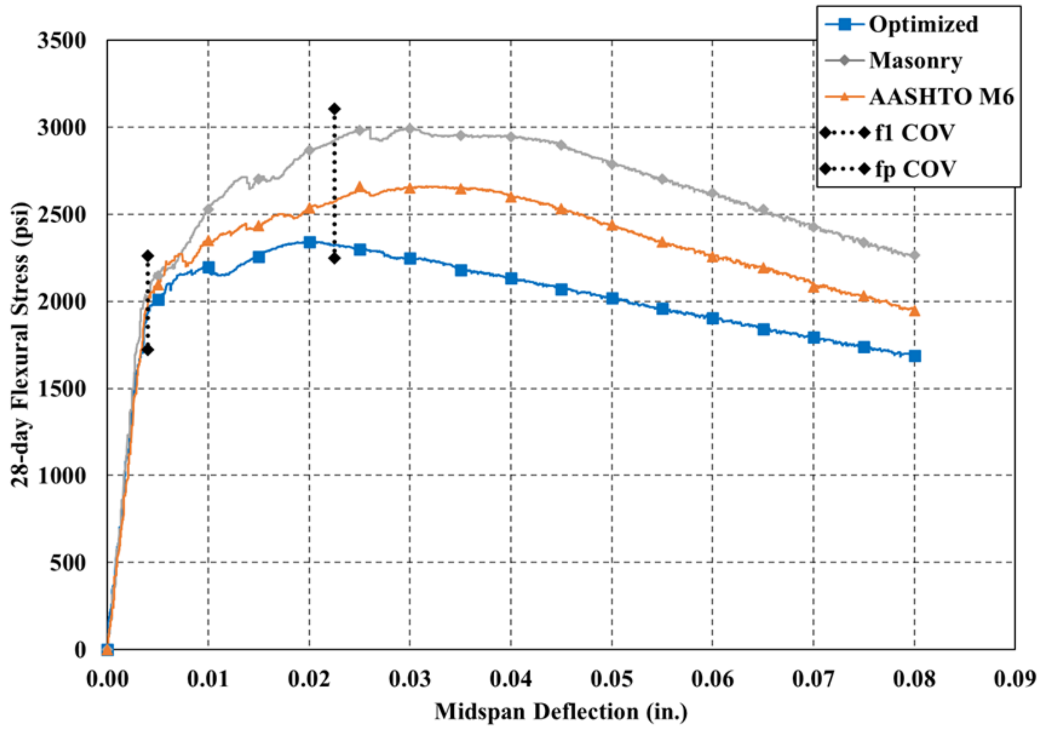

Figure 5-8: Flexural Strength Results for the Fine Aggregate Gradation at 28 Days.

(COV variation based on midpoint data - AASHTO M 6 midpoint)

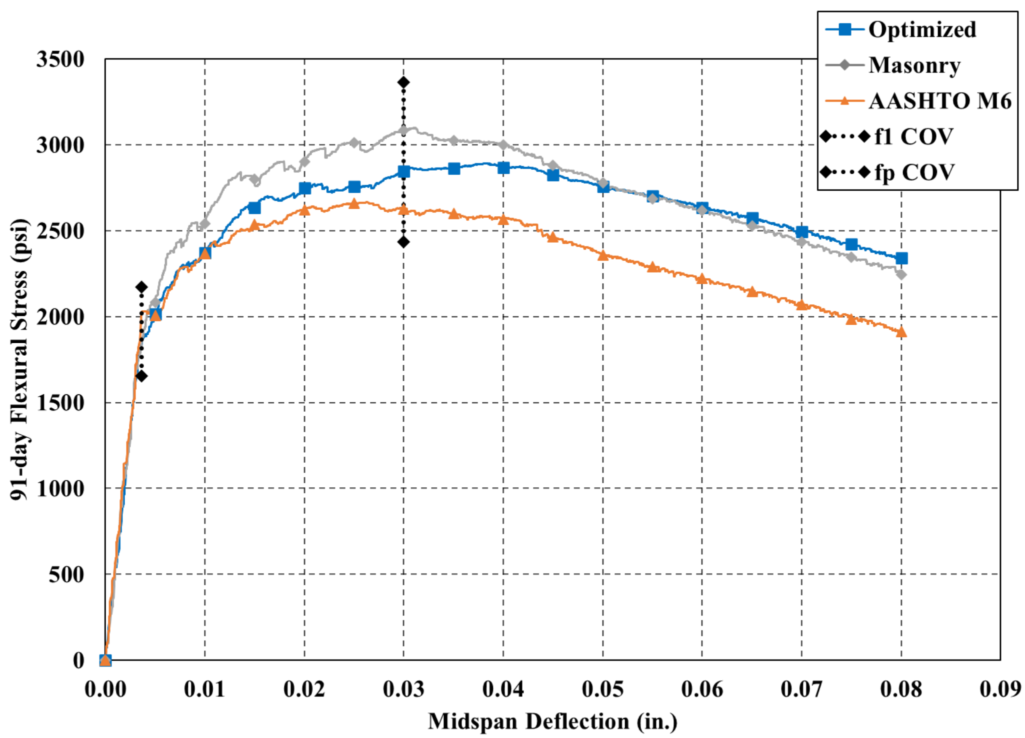

Figure 5-9: Flexural Strength Results for the Fine Aggregate Gradation at 91 Days

(COV variation based on midpoint data - Optimized midpoint)

5.3.3 Direct-Tension Results

Direct-tension results for the fine aggregate gradation series are presented in Figures 5-10 and 5-11. These show that the three fine aggregate gradations have similar results under uniaxial tension. Similarly to the flexural results, there is no clear trend where a change in the fine aggregate gradation increases or decreases the uniaxial tensile strength of UHPC. Because AASHTO T 397 (2022) does not define the acceptable test-to-test COV, the lack of a clear trend in the results clearly indicates that the fine aggregate gradation does not significantly affect the uniaxial tensile strength of the UHPC evaluated in this study.

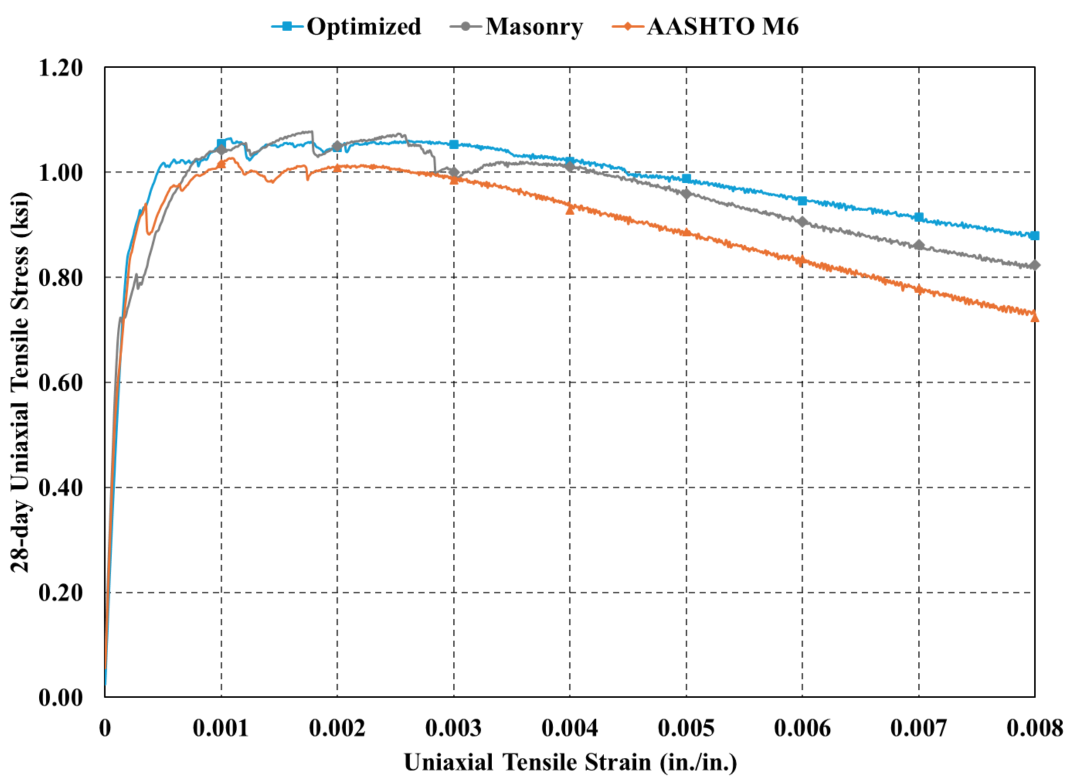

Figure 5-10: Tensile Stress-Strain Results for the Fine Aggregate Gradation at 28 Days

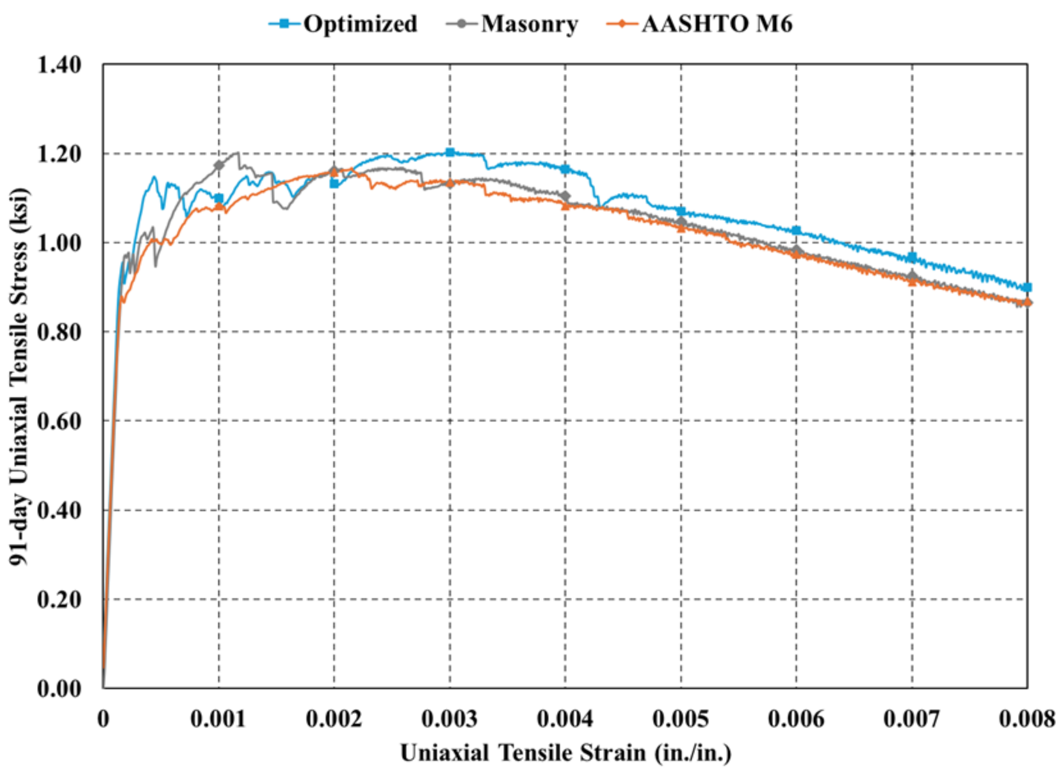

Figure 5-11: Tensile Stress-Strain Results for the Fine Aggregate Gradation at 91 Days

5.3.4 DISCUSSION OF RESULTS

The fine aggregate gradation investigation produced a consistent observation across all three test methods. There is no significant difference in compressive, flexural, or tensile strength among the three gradations evaluated. This result has substantial practical value for ALDOT implementation. Standard AASHTO M 6 compliant natural river sand, which is available throughout Alabama, is adequate for producing non-proprietary UHPC that meets FHWA performance requirements. There is no need to source specialized fine aggregates, manufacture optimized blends, or maintain inventory of multiple sand types. This simplifies production logistics and reduces the material sourcing burden on ready mixed concrete producers.

5.4 EFFECT OF CEMENTITIOUS BLEND (BINARY VERSUS TERNARY)

Two binary blend (Type IL cement and slag cement, without silica fume) batches were produced at steel fiber dosages of 1.50% and 2.00% and compared against equivalent ternary blend batches at the same dosages. During mixing and placement, the binary UHPC mixtures had issues with rapid loss of workability. After roughly 50 minutes of mixing, the UHPC mixture had no flow unless it was agitated. This led to difficulties in placing viable UHPC, as workability was lost shortly after mixing was completed. Even if the flow test showed an acceptable flow, several batches were discarded due to having lost all flow over the course of less than 10 minutes while molding specimens.

5.4.1 COMPRESSIVE STRENGTH RESULTS

Compressive strength results for the binary versus ternary comparison are presented in Figure 5-12. At both fiber dosages, the binary and ternary blends produced comparable compressive strengths. At 28 days, the ternary blend achieved strengths of 17,500 psi, while the binary blends reached approximately 16,200 to 16,800 psi. At 91 days, most mixtures converged to a similar compressive strength of approximately 18,800 psi. The binary 1.5% blend exhibited a lower 91-day strength compared to other mixtures and its 56-day result. This is due to poor specimens being available as a result of the rapid loss of workability during the placement of UHPC. Despite this difference, the averaged results across all four mixtures fell within the allowable coefficient of variation per AASHTO T 22 (2022), and there is no evidence that removing silica fume from the binder system produces a consistent reduction in compressive strength.

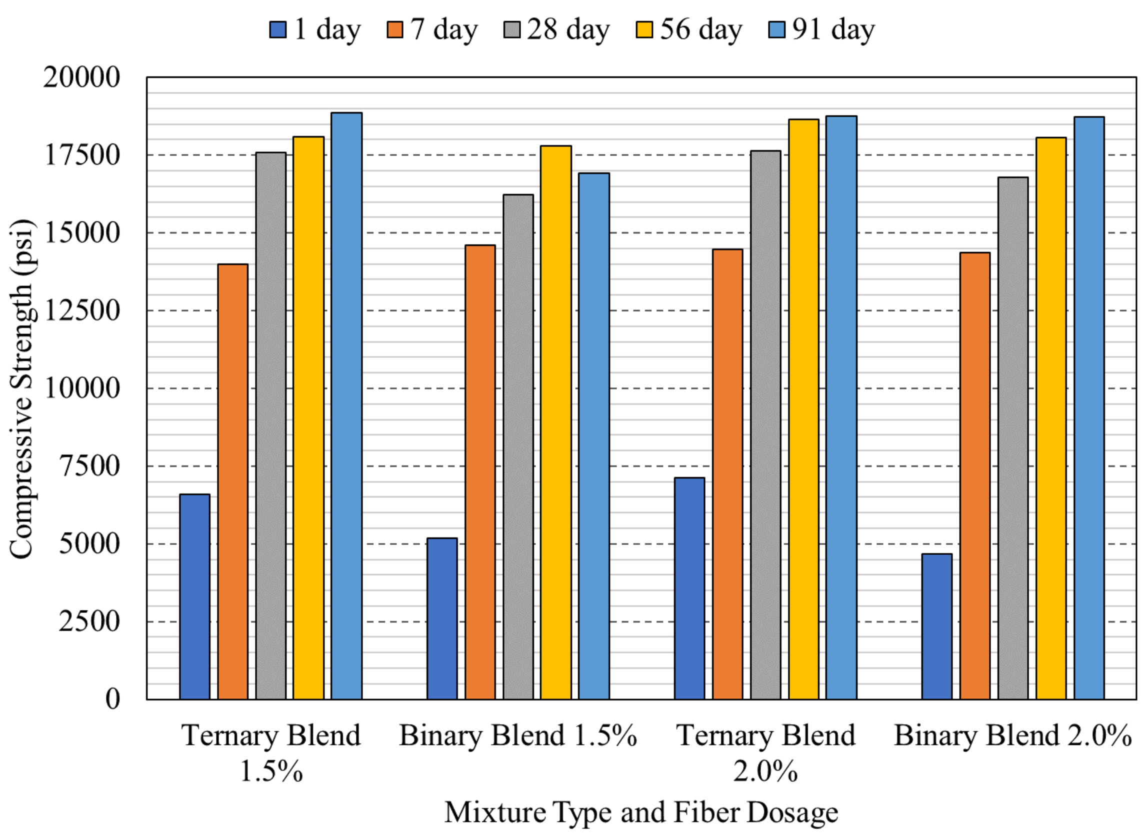

Figure 5-12: Compressive Strength Development for Binary and Ternary Blends

5.4.2 FLEXURAL STRENGTH RESULTS

Flexural strength results for the binary versus ternary comparison are presented in Figures 5-13 and 5.14. At 28 days, the flexural results were comparable between binary and ternary blends at both fiber dosages. The 2.00% fiber mixtures (both binary and ternary) reached peak flexural stresses of approximately 3,100 to 3,300 psi, while the 1.50% fiber mixtures reached approximately 2,400 to 2,550 psi. The differences between binary and ternary at the same fiber dosage fall within the ASTM C1609 coefficient of variation for repeated tests. At 91 days, the ternary 2.00% blend differed from the binary 2.00% blend more noticeably, reaching approximately 3,230 psi compared to approximately 2,700 psi for the binary blend. The 1.50% blend remained comparable at 91 days at approximately 2,500 to 2,600 psi.

The results indicate that the dominant influence on flexural strength is the fiber dosage, not the type of cementitious material blend. The difference between 1.50% and 2.00% fiber is substantially larger than the difference between binary and ternary blend at the same fiber dosage.

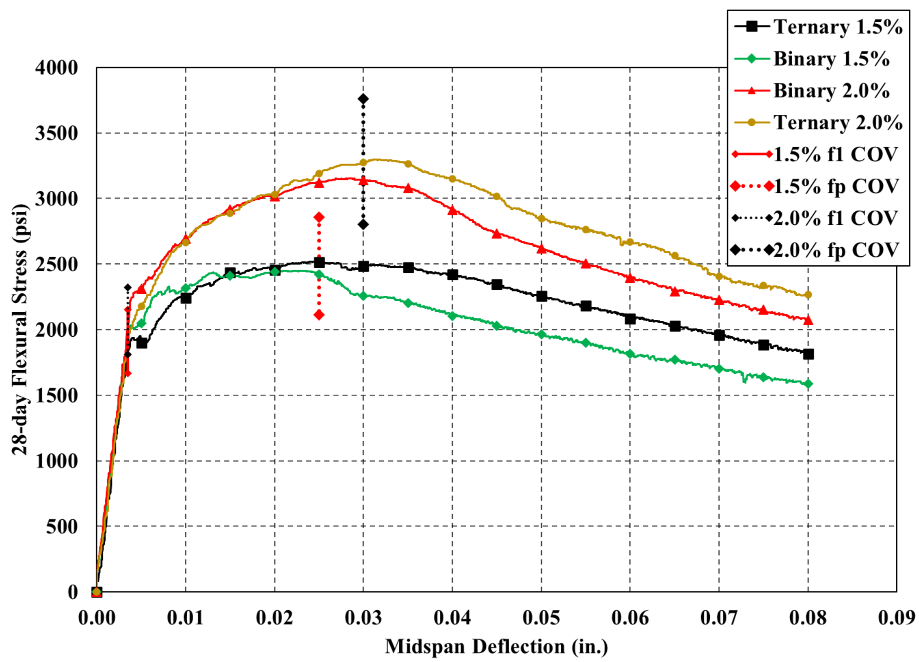

Figure 5-13: Flexural Strength Results for Binary and Ternary Blends at 28 Days

(COV variation based on average)

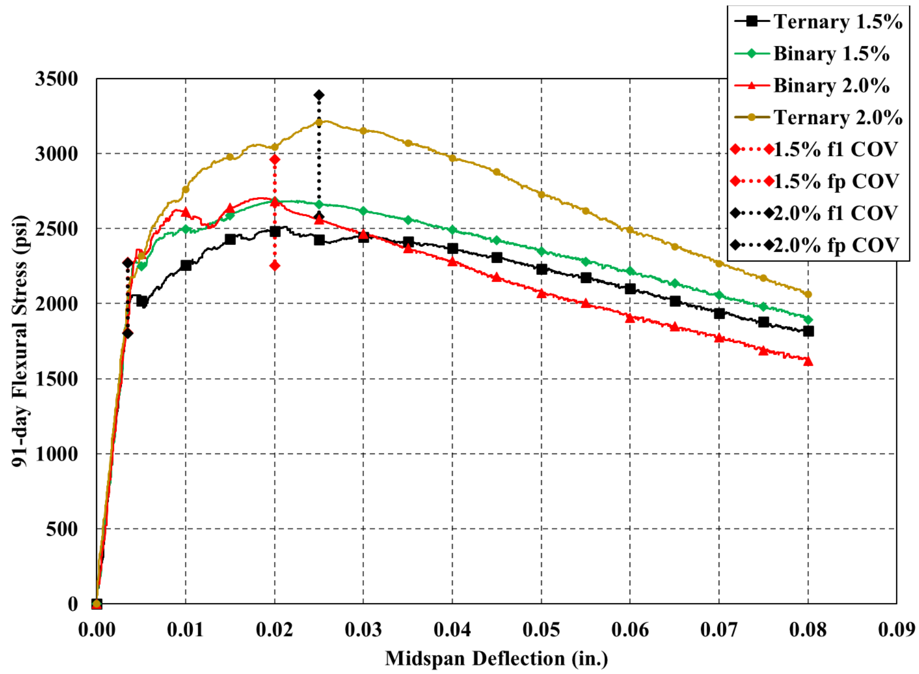

Figure 5-14: Flexural Strength Results for Binary and Ternary Blends at 91 Days

(COV variation based on average for the binary mixture)

5.4.3 DIRECT-TENSION RESULTS

Direct-tension results for the binary versus ternary comparison are presented in Figures 5-15 and 5-16. From Figures 5-15 and 5-16, it can be seen that the uniaxial tensile strength of the binary blends is fairly similar to that of the ternary 1.5% blend. The ternary 2.0% blend was not included due to only having 28-day results for the batch. As there is no clear trend between binary and ternary blends, it can be concluded that the binary blends do not significantly affect the uniaxial tensile strength of UHPC when compared to the ternary blend for the materials tested.

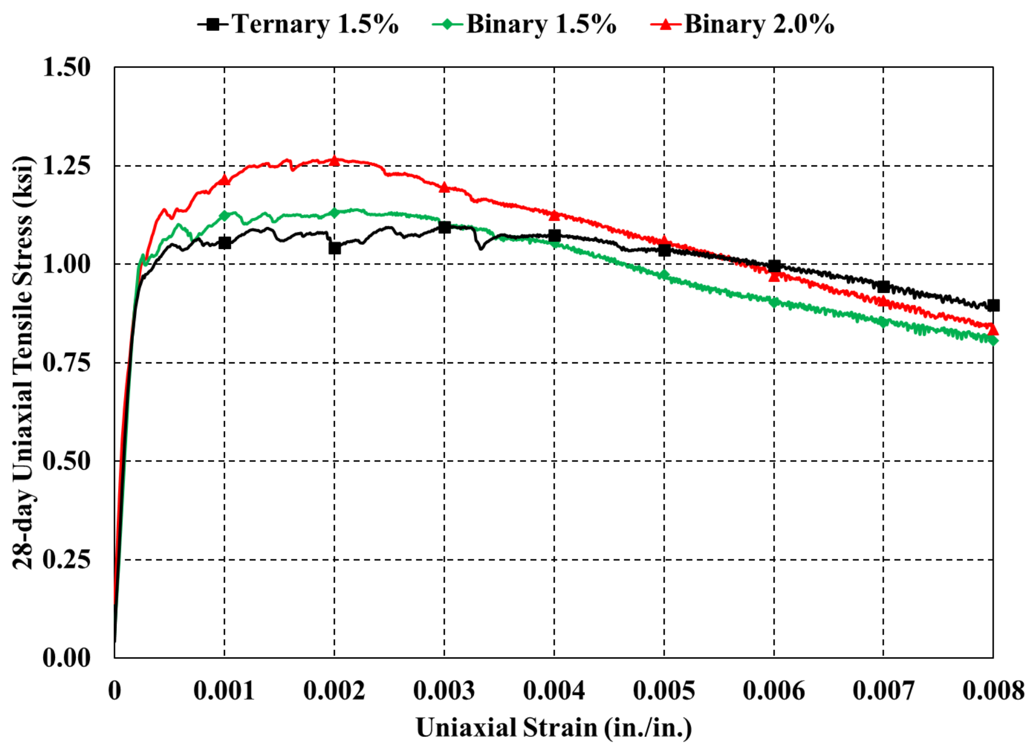

Figure 5-15: Tensile Stress-Strain Results for Binary and Ternary Blends at 28 Days

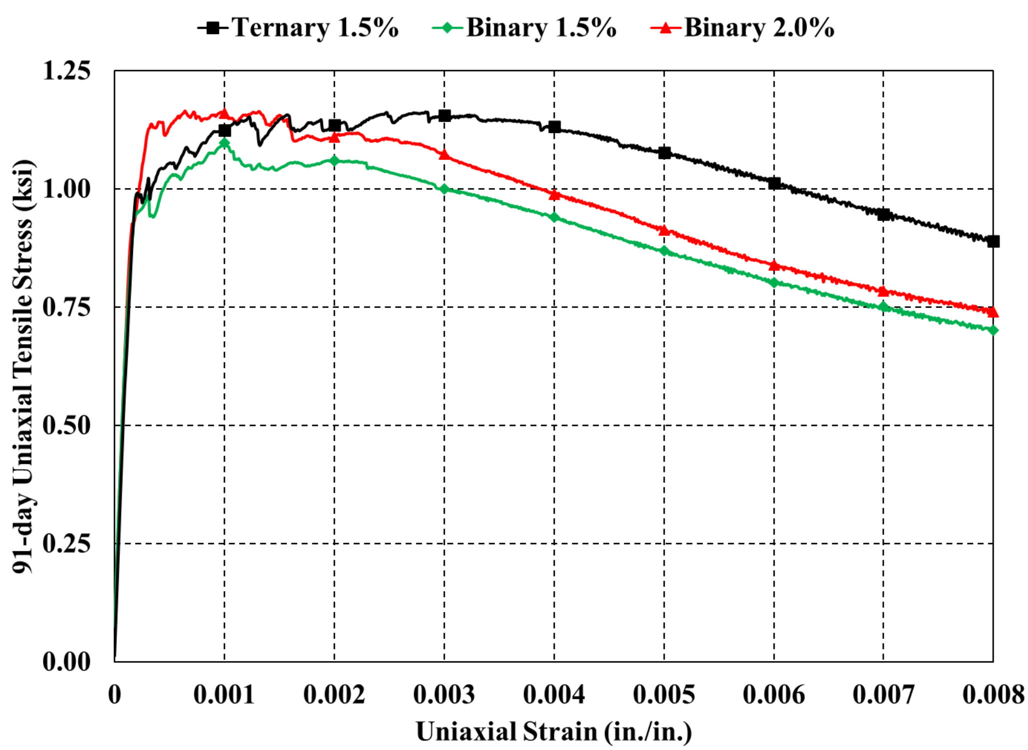

Figure 5-16: Tensile Stress-Strain Results for Binary and Ternary Blends at 91 Days

5.4.4 DISCUSSION OF RESULTS

The strength properties of binary and ternary blends are broadly comparable across compressive, flexural, and tensile testing. Based on strength results alone, a binary blend would be an acceptable option. However, the workability behavior of the binary blend is the decisive factor. As documented in Section 5.1, the binary batches exhibited rapid loss of workability within minutes of completing the flow test. Several batches were discarded because the material stiffened during specimen casting. In a field production environment, where UHPC must maintain adequate workability during transport from the batching plant and through the full placement operation, this shortened working window presents a constructability challenge.

The ternary blend, which includes silica fume, provides substantially better workability retention. While adding silica fume introduces logistical complexity at the ready mixed concrete plant (requiring a third silo or manual addition), this is a one-time setup cost that is far less consequential than the risk of material lacking sufficient workability at the job site. For these reasons, a ternary blend is recommended for ALDOT implementation in non-proprietary UHPC. The question of how much silica fume is needed within the ternary system is addressed in the following section, Section 5.5.

5.5 EFFECT OF SILICA FUME DOSAGE

Three batches were produced with silica fume contents of 9%, 12%, and 15% by mass of total binder. The steel fiber dosage was held constant at 1.50% for all three batches. To maintain a constant paste volume, the slag cement content was reduced as the silica fume content was increased.

5.5.1 COMPRESSIVE STRENGTH RESULTS

Compressive strength results for the silica fume dosage series are presented in Figure 5-17. The results shown in Figure 5-17 does not appear to have a clear trend regarding how the silica fume dosage affects the compressive strength. The results from each age tested are fairly similar, except for the 56-day results for the 12% silica fume dosage. Even with one visual outlier and considering acceptable test-to-test variation, these results are fairly similar.

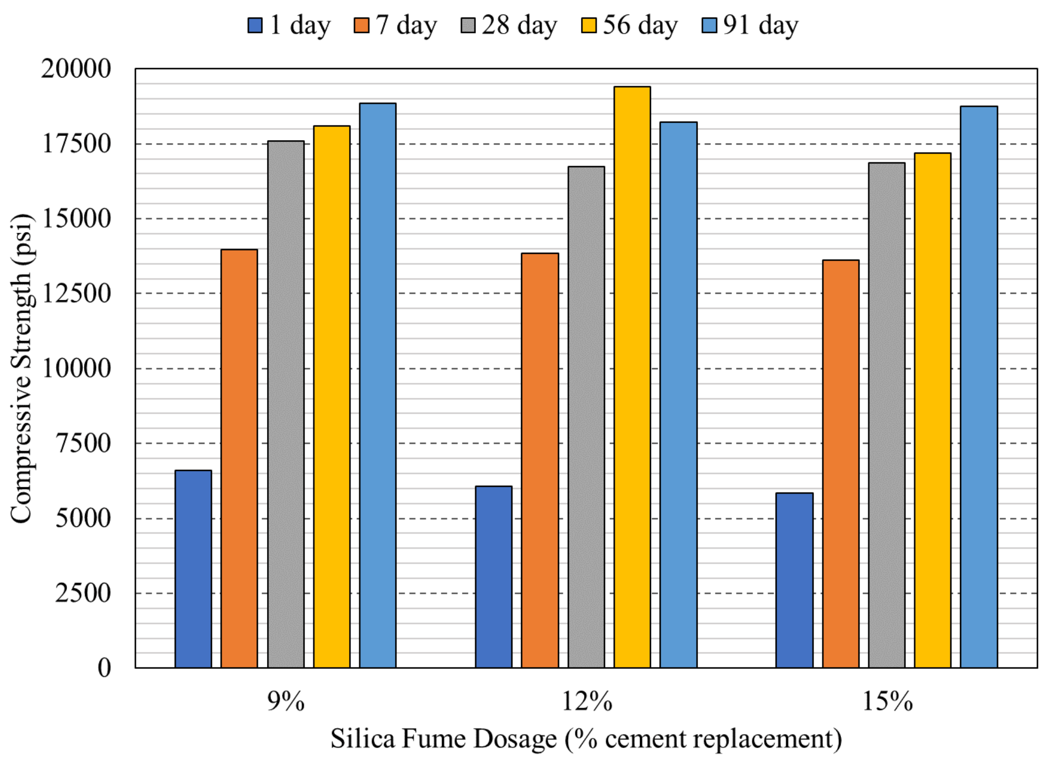

Figure 5-17: Compressive Strength Development at Three Silica Fume Dosages

5.5.2 FLEXURAL STRENGTH RESULTS

Flexural strength results for the silica fume dosage series are presented in Figures 5-18 and 5-19. The results in these two figures show that the silica fume dosage does not have a clear trend, as all three results are quite similar. The COV limit shown in Figures 5-18 and 5-19 reinforces the lack of a trend since all three silica fume dosages fall within the allowable variation of ASTM C1609/C1609M (2019). The lack of a trend and the results falling within the COV limits indicate that the flexural strength of UHPC is not significantly affected by the silica fume dosage when the silica fume replaces slag cement.

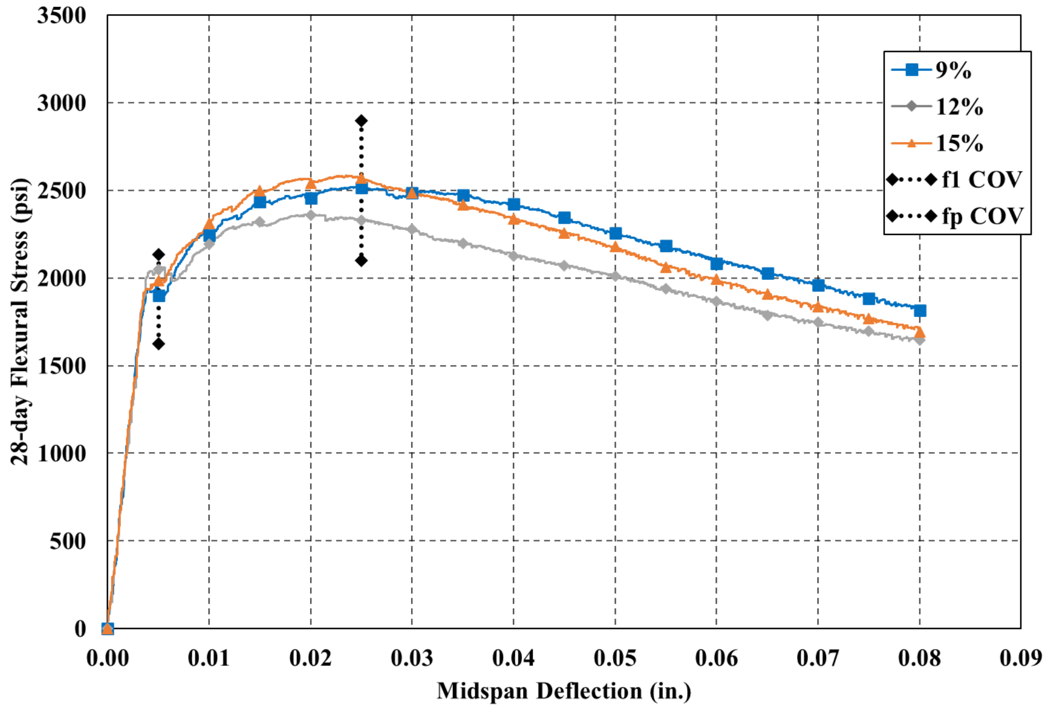

Figure 5-18: Flexural Strength Results for Three Silica Fume Dosages at 28 Days

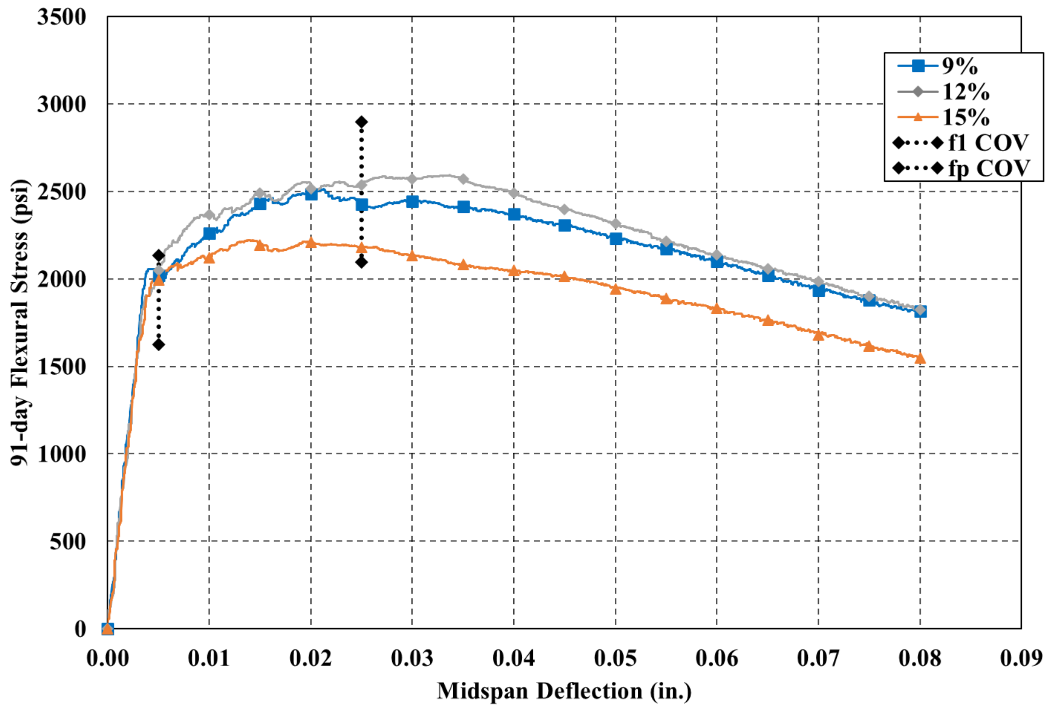

Figure 5-19: Flexural Strength Results for Three Silica Fume Dosages at 91 Days

5.5.3 Direct-Tension Results

Direct-tension results for the silica fume dosage series are presented in Figures 5-20 and 5-21. At 28 days, the 9% silica fume dosage produced the highest effective cracking stress at approximately 1,000 psi, followed by 12% at approximately 900 psi and 15% at approximately 800 psi. This initial ordering might suggest a trend of decreasing tensile strength with increasing silica fume, but the 91-day results do not support this interpretation. At 91 days, all dosages converged between 900 to 970 psi. All three dosages easily exceeded the FHWA 750 psi threshold at both test ages.

The silica fume dosage is not a significant factor in the tensile performance of the UHPC when varied within the range considered in this study.

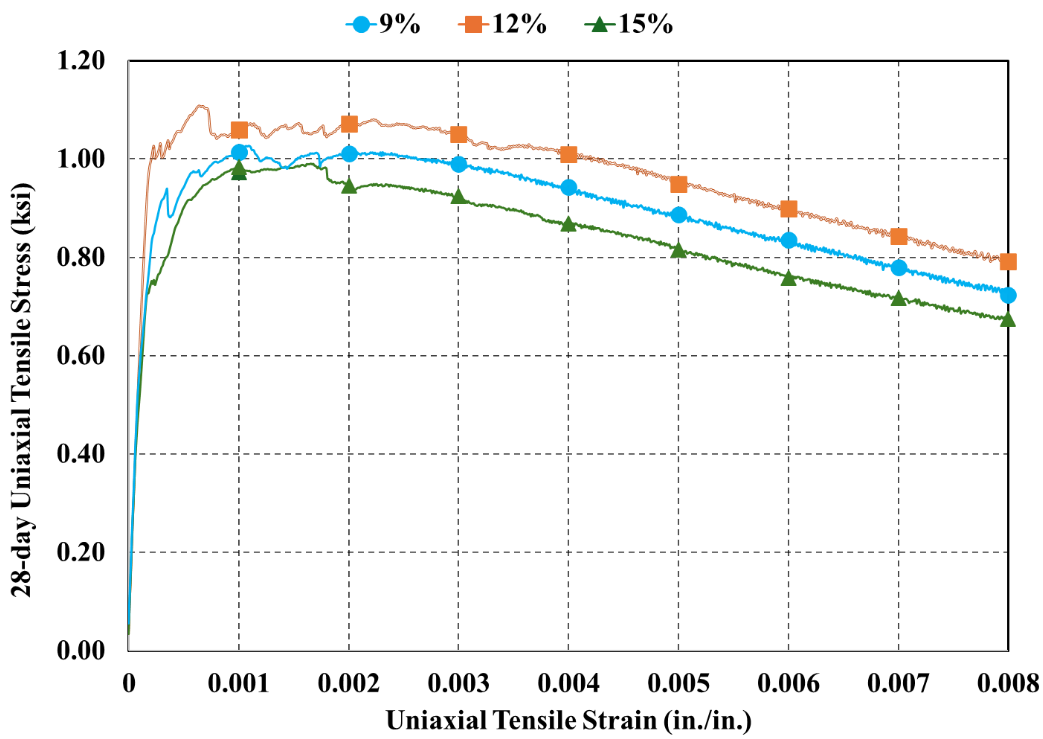

Figure 5-20: Tensile Stress-Strain Results for Silica Fume Dosage at 28 Days

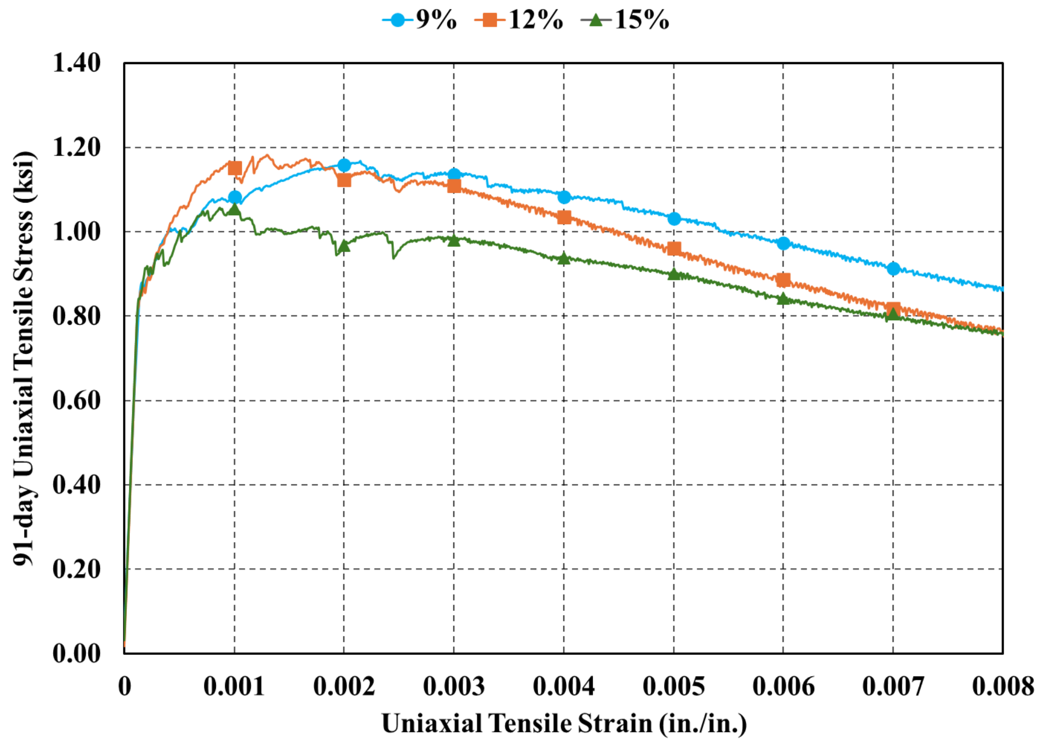

Figure 5-21: Tensile Stress-Strain Results for Silica Fume Dosage at 91 Days

5.5.4 Discussion of Results

Replacing slag cement with increasing amounts of silica fume from 9% to 15% of total binder content does not produce a significant change in compressive, flexural, or tensile strength. This finding, combined with the workability observation from Section 5.1 that higher silica fume dosages require less HRWRA, means that the selection of silica fume dosage can be based on practical and economic considerations rather than performance requirements.

Silica fume is approximately three times more expensive than slag cement per ton (Wille and Boisvert-Cotulio 2013), and incorporating it requires a third silo or manual addition at the ready mixed concrete plant. Given that 9% silica fume produces the same mechanical performance as 12% or 15%, a dosage of 9% is would meet the non-proprietary UHPC's need in Alabama. This reduces the silica fume cost per cubic yard of UHPC and minimizes the quantity of material that must be handled through the additional silo. The slight reduction in HRWRA demand at higher silica fume dosages does not justify the increased material cost.

5.6 Effect of Water-Binder Ratio

Three batches were produced at water-binder ratios of 0.18, 0.20, and 0.22, using the ternary binder system and a steel fiber dosage of 1.50% for all three. The test results will be presented and discussed in the following sections.

5.6.1 Compressive Strength Results

Compressive strength results for the water-binder ratio series are presented in Figure 5-22. A commonly known method for increasing the compressive strength of concrete is to reduce the water-binder ratio and this also applies to UHPC. Figure 5-22 shows that lower water-binder ratios result in an increase in compressive strength. At 28 days, both the 0.18 and 0.20 water-binder ratios meet the 17,500 psi required strength, and the 0.22 water-binder ratio achieving 17,500 psi at 91 days. This trend confirms that a reduction in water-binder ratio improves the compressive strength of UHPC.

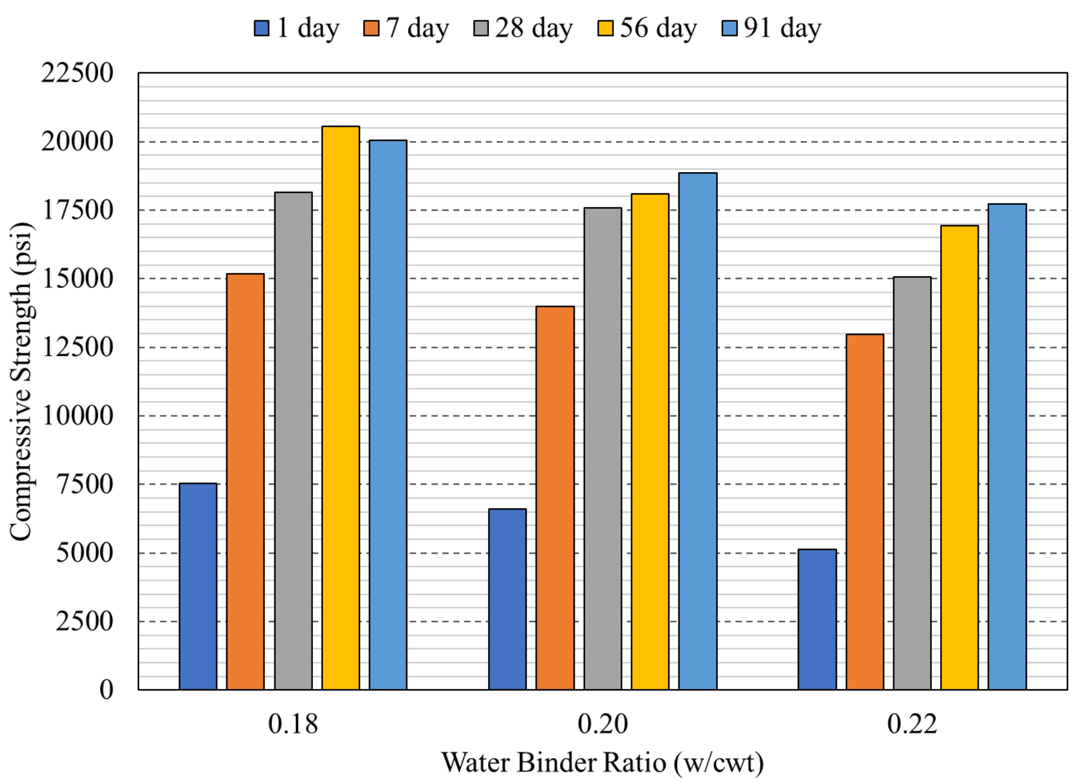

Figure 5-22: Compressive Strength Development at Water-Binder Dosages

5.6.2 Flexural Strength Results

Flexural strength results for the water-binder ratio series are presented in Figures 5-23 and 5-24. From Figures 5-23 and 5-24, there is no clear trend in the flexural results. For both 28-day and 91-day results, the lowest water-binder ratio tested is the strongest. However, the 0.20 and 0.22 water-binder ratio blends have very similar flexural results at both ages. The average flexural results are within the acceptable variation calculated using the COV of ASTM C1609/C1609M (2019) for three specimens. Therefore, there does not appear to be a significant impact on flexural strength by increasing or decreasing the water-binder ratio, for the range of ratios tested.

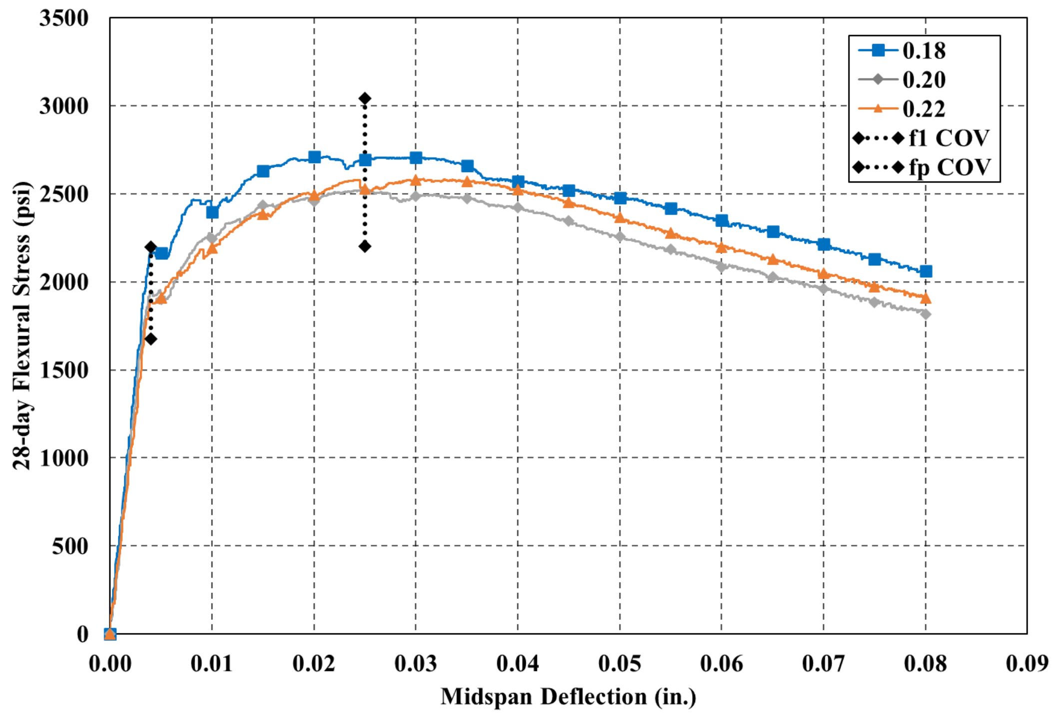

Figure 5-23: Flexural Strength Results for Water-Binder at 28 Days

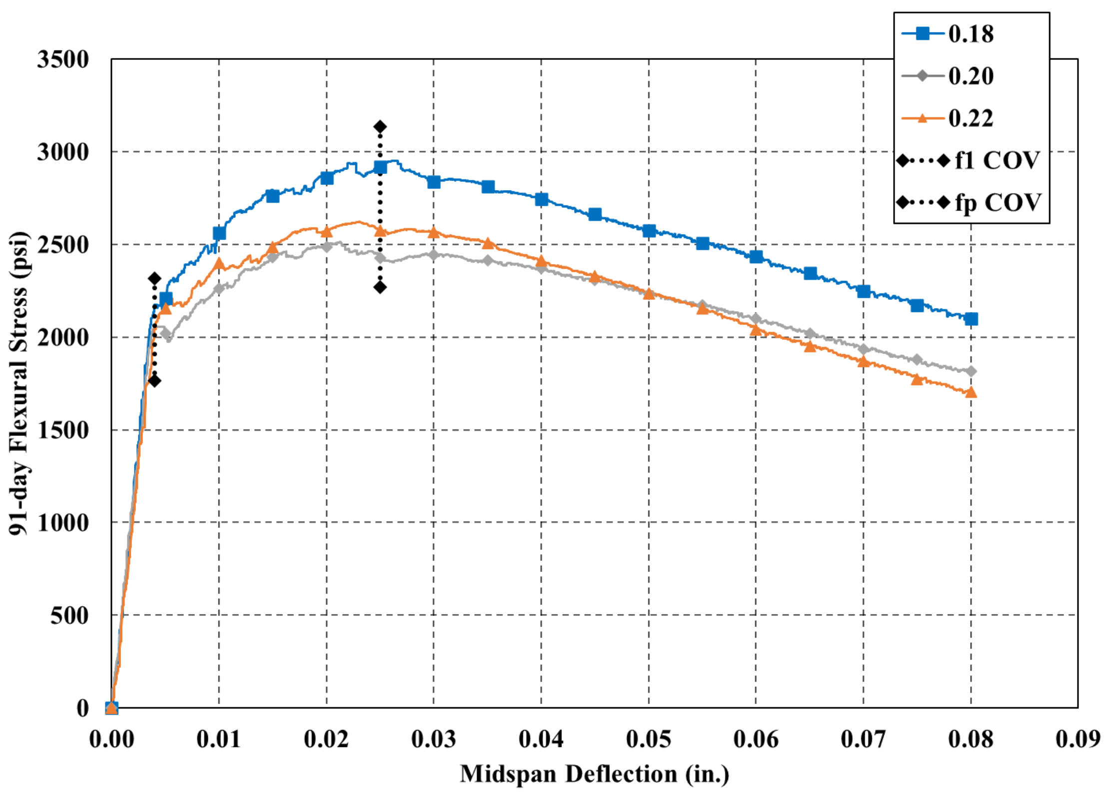

Figure 5-24: Flexural Strength Results for Water-Binder at 91 Days

5.6.3 DIRECT-TENSION RESULTS

Direct-tension results for the water-binder ratio series are presented in Figures 5-25 and 5-26. Like the flexural results, Figures 5-25 and 5-26 show that the 0.18 water-binder ratio has the greatest uniaxial tensile strength. The 0.20 and 0.22 water-binder ratio blends also show similar results, like the flexural test. For comparison note that there is no precision and bias statement currently available for AASHTO T 397 (2022). From these uniaxial tensile results for the tested ratios, the 0.18 water-binder ratio results in the highest peak stress at 28 and 91 days. At the effective cracking strength, all dosages range between 1,000 to 1,250 psi.

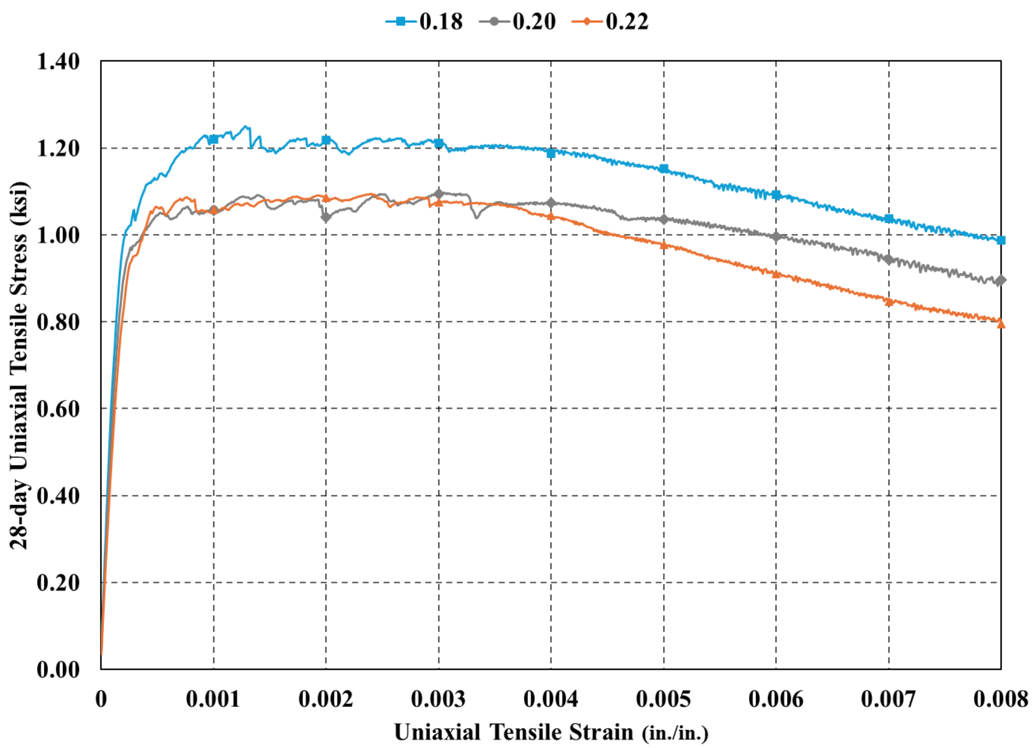

Figure 5-25: Tensile Stress-Strain Results for Water-Binder Ratios at 28 Days

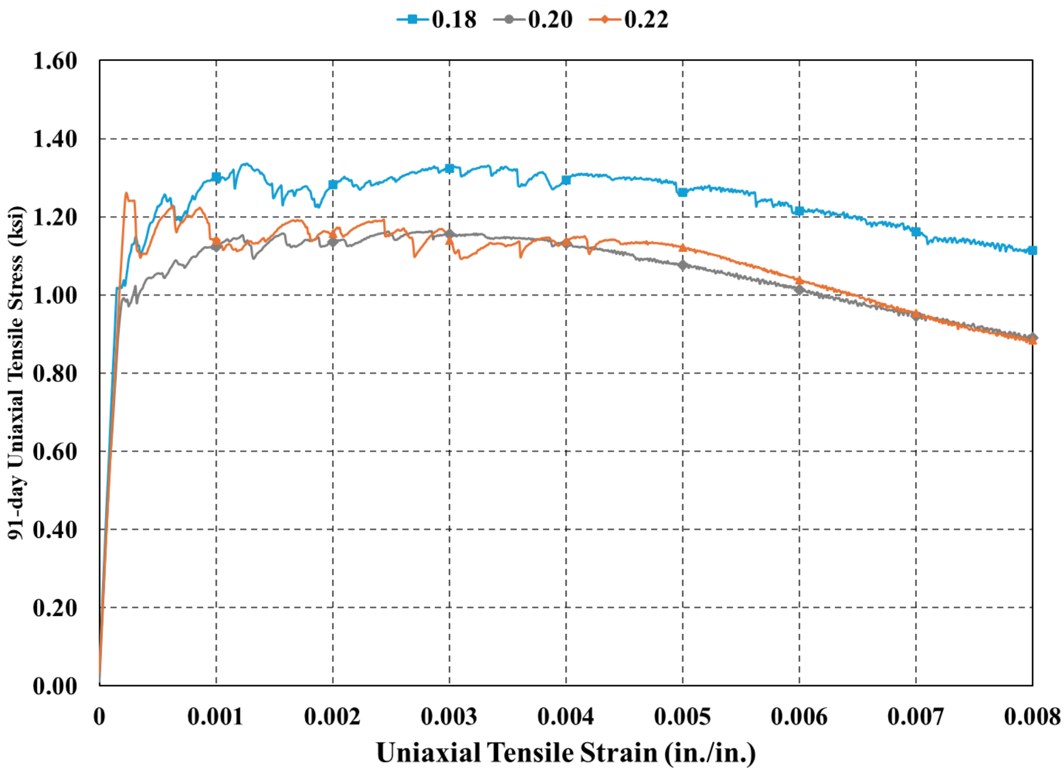

Figure 5-26: Tensile Stress-Strain Results for Water-Binder Ratios at 91 Days

5.6.4 Discussion of Results

The water-binder ratio is the primary lever for controlling compressive strength in UHPC. The relationship follows the same well-established principle from conventional concrete: lower water content relative to cementitious materials produces a denser matrix with higher compressive capacity. The influence on tensile and flexural properties is less pronounced, with only the 0.18 ratio producing a measurable increase, and even then, the differences are moderate.

A minimum water-binder ratio of 0.20 is recommended for ALDOT implementation. At this ratio, the UHPC exceeds the FHWA compressive strength requirement of 17,500 psi, and the tensile performance exceeds the 750 psi threshold by a reasonable margin. The 0.18 ratio provides higher strength across all strength types, and the 0.22 ratio does not meet the 17,500 psi compressive strength requirement at 28 or 56 days.

5.7 Test Variability

5.7.1 Sensitivity of Strain Measurements

A recurring theme across the direct-tension testing program is the inherent variability of results associated with the test. This is particularly evident when examining the relationship between fiber dosage and key tensile response parameters.

Figures 5-27a and 5-27b show the effect of fiber dosage on effective cracking stress and strain, respectively. As shown in Figure 5-27a, increasing fiber content consistently increases the effective cracking stress, peaking at approximately 2.0% fiber dosage. This aligns with the trend previously covered in Figure 5-4, where an increase in fiber dosage improves the tensile strength of UHPC. However, Figure 5-27b reveals that the corresponding effective cracking strain does not follow a comparably systematic trend. Instead, substantial scatter was observed, with peak values not corresponding to the optimum fiber dosage identified from the effective cracking stress response.

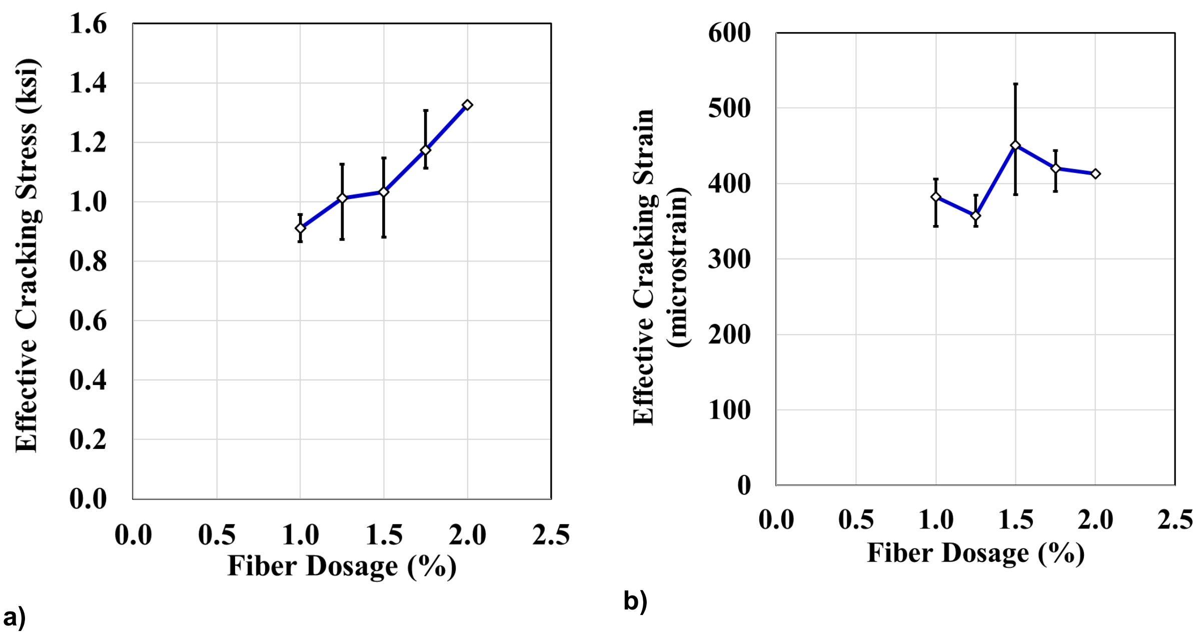

Figure 5-27: The Effect of Fiber Dosage on the Effective Cracking Stress and Strain of UHPC

Similar patterns are seen in Figures 5-28a and 5-28b, which plot the peak stress and peak strain against fiber dosage. The peak stress (Figure 5-28a) rises in tandem with fiber content, indicating improved post-cracking load capacity up to 2.0%, after which a marginal decline occurs, with reasons likely due to workability issues or simply the optimum content as discussed for phase one. In contrast, the peak strains in Figure 5-28b have high variability, with no discernible dose-response relationship.

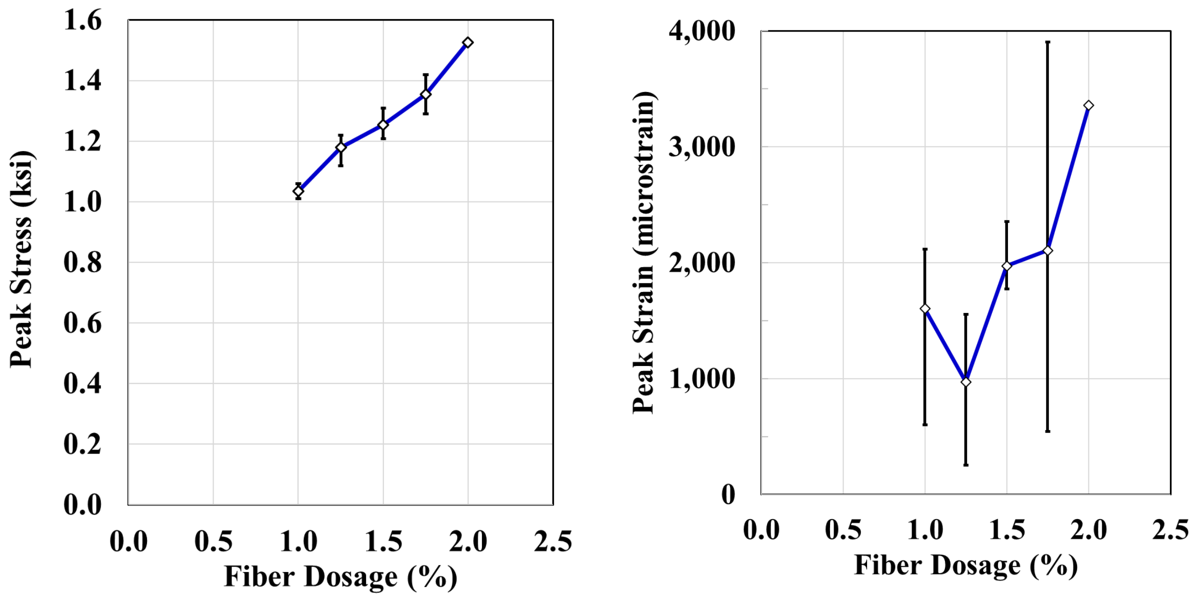

a) b)

Figure 5-28: The Effect of Fiber Dosage on the Peak Stress and Strain of UHPC

The same response can be seen in Figures 5-29a and 5-29b, where localization stress increases with fiber dosage, again supporting the beneficial effects of fiber inclusion, while localization strain displays marked inconsistency and high variability, emphasizing the unreliable nature of the strain results collected with this test method. It is worth noting that 0.0% and 0.5% steel fiber dosage post-cracking response was not added here as they did not meet the minimum FHWA requirement.

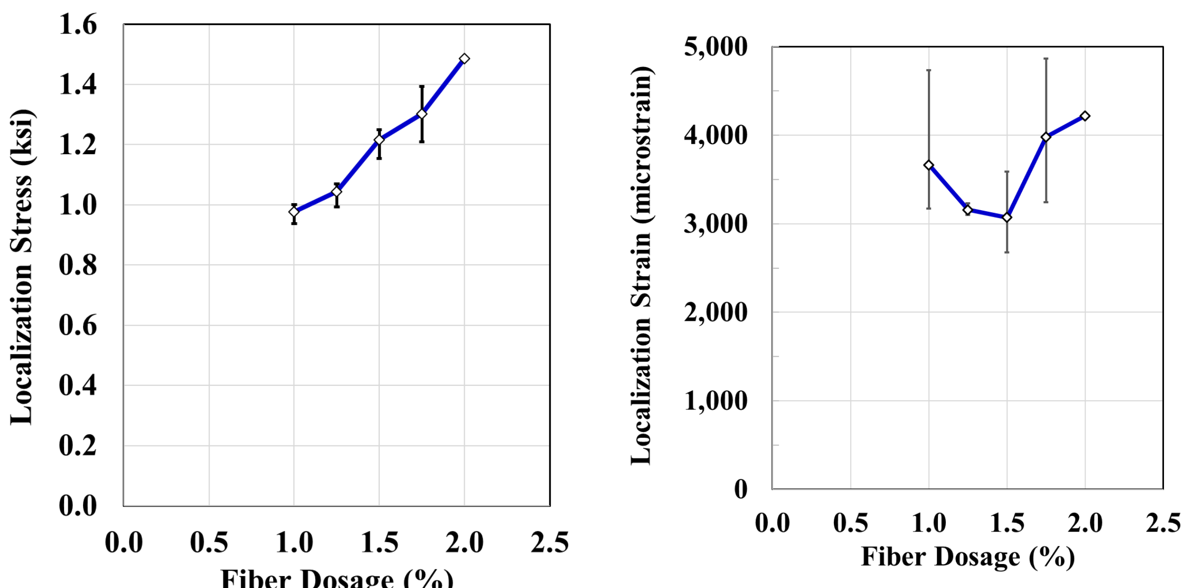

a) b)

Figure 5-29: Trend Showing the Effect Of Fiber Dosage on the Localization Stress And Strain

5.7.2 Implications of Observed Variability

The consistent stress response across fiber dosages provides strong evidence that UHPC's mechanical enhancement via steel fiber addition is real and measurable and can also be reliably captured through direct-tension testing in accordance with AASHTO T 397. However, the lack of a corresponding trend in strain-based parameters indicates that strain-based results from the direct-tension test, as currently implemented, are highly variable and not suited for implementation in ALDOT specifications.

This interpretation is supported by both recent multi-laboratory studies and established testing precedents. Gali and Sritharan (2024), reported standard deviations for strain parameters ranging from 23-38% of mean values in their evaluation of AASHTO T 397. ASTM C1609 (2024) documents that deflection at peak load in flexural testing of fiber-reinforced concrete may exhibit coefficients of variation above 100%, whereas the COV of flexural stress is only 9.7%. The high variability indicates that, while stress values are relatively insensitive to small alignment issues or localized defects, strain measurements are significantly impacted by out-of-plane alignment, slip, or even small imperfections at the gripping interface. Accordingly, for material optimization, specification, and quality control, stress-based performance metrics (effective cracking and localization stress) should be used, whereas strain-based criteria should not be used.

5.8 Flexural to Direct-Tension Comparison (Forward Analysis of Flexural Response)

5.8.1 Methodology

The forward analysis approach used in this section follows the closed-form sectional equilibrium framework established by Maalej and Li (1994). The application of sectional analysis to UHPC has been validated by Xia et al. (2018), who also confirmed that a linear elastic compression assumption introduces negligible error for UHPC flexural members. The constitutive tensile model is a four-stage piecewise linear representation of the AASHTO T 397 test output, defined by the effective cracking stress, peak stress, localization stress, and the continued softening response beyond localization. The procedure takes the measured tensile properties from AASHTO T 397 as input and uses constitutive laws to compute the flexural stress versus midspan deflection curve that the material would produce in the ASTM C1609 four-point bending test. The beam geometry matches the tested specimens: 3 in. x 3 in. x 14 in. prisms with a 12 in. span loaded at the third points.

The tensile behavior is represented by a four-stage piecewise linear stress-strain model, shown in Figure 5-30. The first stage is linear elastic from zero strain to the effective cracking strain. The second stage is linear strain hardening from the effective cracking stress to the peak tensile stress. The third stage is linear softening from the peak tensile stress to the localization point, defined by the localization stress. The fourth stage represents continued softening beyond localization, the role of which in the analysis is discussed below. The effective cracking stress, $f_{t,cr}$, used as the stage 1 endpoint in the idealized model, is the effective cracking strength determined by the 0.02% strain offset method per AASHTO T 397. In the representative stress-strain response shown in Figure 5-30(a), $f_{t,el}$ denotes the elastic proportional limit of the raw test data. This value lies below $f_{t,cr}$ because the raw response exhibits some nonlinearity between $f_{t,el}$ and $f_{t,cr}$ as microcracking initiates. The idealized model simplifies this transition by extending the linear elastic stage up to $f_{t,cr}$, so $f_{t,el}$ does not enter the idealization directly. Figure 5-30(b) shows the resulting four-stage idealized model.

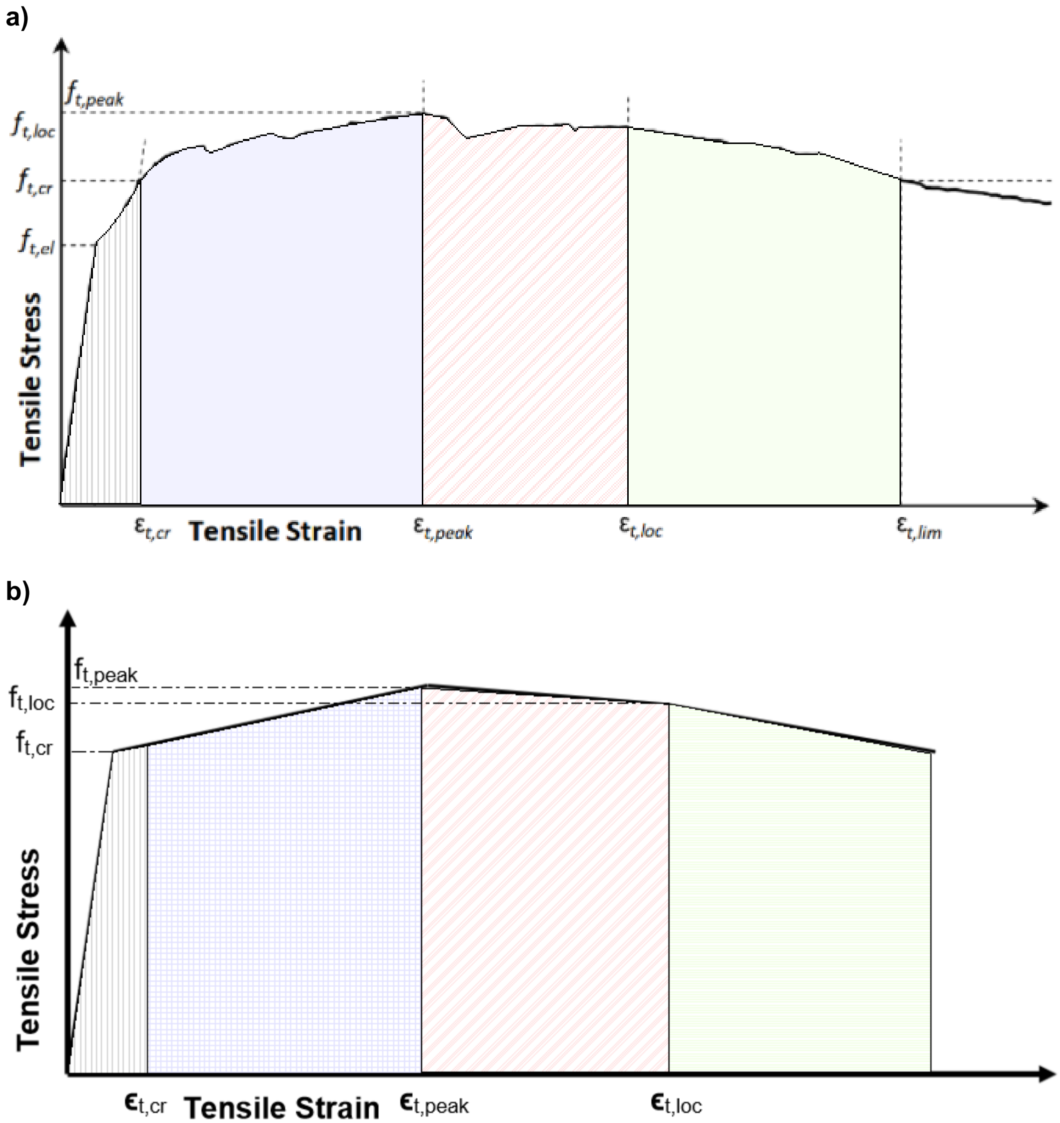

Figure 5-30: Representative UHPC Tensile Response: (A) Raw Test Data with Idealized Four-Stage Model Overlay. (B) Idealized Four-Stage Piecewise Linear Stress-Strain Model

In compression, the material is assumed to behave linearly elastically. This assumption is justified because the compressive strains that develop in a UHPC flexural member remain well below the compressive capacity of the material throughout the loading range of interest. Given the high compressive strength of UHPC, the strain at the extreme tension fiber reaches the localization strain before the compression zone approaches its capacity, and the linear-elastic assumption introduces negligible error (Xia et al. 2018).

The section analysis follows the assumption that plane sections remain plane. The resulting strain and stress distributions across the beam cross section are illustrated in Figure 5-31. For a given curvature Φ, the strain at any depth, y measured from the top fiber is defined by (Equation 5-1).

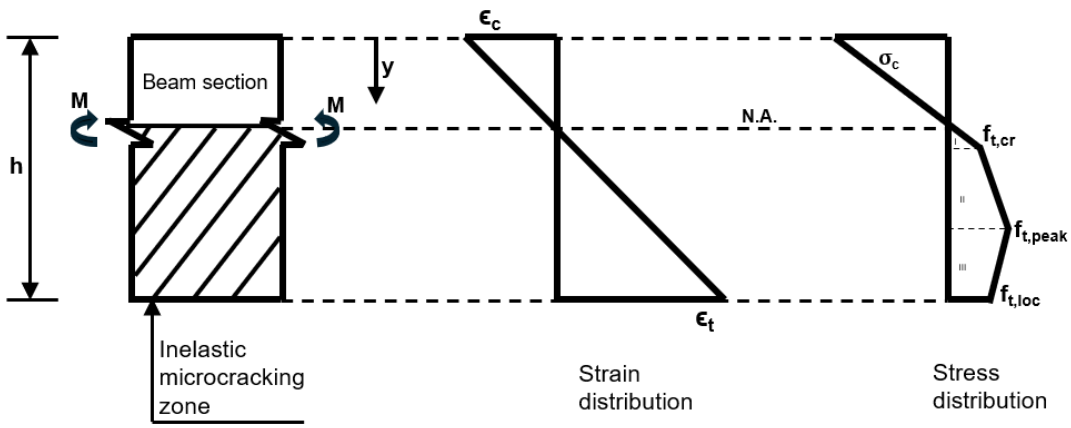

Figure 5-31: Strain and Stress Distribution along Beam Depth (Maalej and Li 1994)

$$\epsilon(y) = \epsilon_c + \Phi * y \qquad \text{Equation 5-1}$$

where, ϵ_c is the strain at the top (compression) fiber. The stress at each depth is then obtained from the four-stage constitutive model. The neutral-axis depth, y_n, serves as the single unknown, which is iteratively adjusted using a root-finding algorithm at each curvature increment until the net axial force across the section equals zero (Equation 5-2):

$$\int_0^h \sigma(\epsilon_c + \Phi * y) * b * dy = 0 \qquad \text{Equation 5-2}$$

where h is the total depth of the section, σ is the stress at a given depth obtained from the four-stage constitutive model for the corresponding strain, and b is the width of the section. Once the equilibrium condition is satisfied, the neutral axis position is known, and the bending moment is computed by integrating the stress times the moment arm about the neutral axis across the section depth (Equation 5-3)

$$M = \int_0^h \sigma(\epsilon_c + \Phi * y) * (y - y_n) * b * dy \qquad \text{Equation 5-3}$$

The equivalent flexural stress (σ_{fl}) is then obtained from the standard elastic bending formula, consistent with ASTM C1609 (Equation 5-4):

$$\sigma_{fl} = 6M/(bh^2) \qquad \text{Equation 5-4}$$

where σ_{fl} is the equivalent flexural stress, M is the bending moment calculated from Equation 5-3, b is the width of the section, and h is the depth of the section. This procedure is repeated at successive curvature increments from zero through the curvature at which the extreme tension fiber strain reaches the localization strain and into the early post-localization softening regime. Once localization strain is reached at the extreme fiber, deformation transitions from distributed microcracking to a single dominant crack, and the plane-sections assumption on which the sectional model is built progressively loses validity. The estimated response past the localization point is therefore presented for completeness but is not treated as a reliable characterization of the post-localization behavior.

To convert the moment-curvature relationship to a flexural stress versus midspan deflection curve, the curvature-to-displacement transformation developed by Martínez (2017) for four-point bending was used. The transformation accounts for both the flexural and shear contributions to the total midspan deflection. Two curvature distribution hypotheses are considered: a linear hypothesis that is accurate from the onset of loading through approximately 70 percent of peak load, and a logarithmic hypothesis that provides better accuracy near the peak load, where cracking concentrates curvature within the constant moment region. In the forward direction, the linear formula produces the smaller, and more accurate, deflection estimate at low curvatures, while the logarithmic formula takes over near peak as the curvature distribution becomes increasingly nonlinear. The estimated deflection at each curvature increment (shown in equations 5-5 to 5-7) is taken as:

$$\delta\mathrm{linear} = \left(\frac{23L^2}{216}\right) * \Phi + \frac{12PL}{25Ebh} \qquad \text{Equation 5-5}$$

$$\delta\mathrm{logarithmic} = \left(\frac{5L^2}{72}\right) * \Phi + \frac{P}{6Eb} * \left(\frac{L}{h}\right)^3 + \frac{12PL}{25Ebh} \qquad \text{Equation 5-6}$$

$$\delta = \min\left(\delta\mathrm{linear}, \delta\mathrm{logarithmic}\right) \qquad \text{Equation 5-7}$$

where, L is the span length, Φ is the curvature at the given increment, E is the elastic modulus, b is the width of the section, h is the depth of the section, and P = 6M/L from the statics of third-point loading. In both expressions, the first term accounts for deflection due to bending and the final term accounts for shear deflection. The logarithmic formulation includes an additional bending term that captures the concentration of curvature at high-load levels. The shear correction warrants inclusion for the tested specimen geometry: at a span-to-depth ratio of 4, shear deformations contribute a meaningful fraction of the total midspan deflection and omitting them would introduce measurable error in the estimated response.

The input parameters for each batch were obtained directly from the AASHTO T 397 test results: the elastic modulus E, determined from the stress-strain response between compressive and tensile stresses of 1.5 ksi in accordance with AASHTO T 397, the effective cracking stress and its corresponding strain, the peak tensile stress and its corresponding strain, and the localization stress and its corresponding strain. The complete forward analysis, including the sectional equilibrium, moment calculation, and displacement transformation, was implemented in MATLAB. The MATLAB code is provided in Appendix B.

5.8.2 UHPC Mixtures Analyzed

The forward analysis was applied to the UHPC mixtures that had a minimum average data point at both the flexural strength testing and direct-tension testing. These batches span five mixture variables of steel fiber dosage (1.00, 1.25, 1.50, 1.75, and 2.00 percent by volume), silica fume content (9, 12, and 15 percent of total binder), binder type (ternary blend with 1.5 percent fiber, binary blend with 1.5 percent fiber, and the binary blend with 2.0 percent fiber), water to binder ratio (0.18, 0.20, and 0.22), and fine aggregate source (A-A, C144, and C33). Only batches with a minimum of two valid specimens from both the direct-tension and flexural tests were included, so as not to skew the comparison. Each included batch had paired direct-tension and flexural datasets, providing the input and validation data for the forward analysis. Figure 5-32 shows the estimation result of this analysis. As seen in Figure 5-32, the displacement estimates are more variable, which is consistent with the findings reported in Section 5.7. Section 5.7 established that strain-based and displacement-based results exhibit high variability and are not suited for specification limits, whereas stress-based metrics are reliable and consistent. For this reason, stress-based comparison is the basis for establishing the correlation to the flexural stress response.

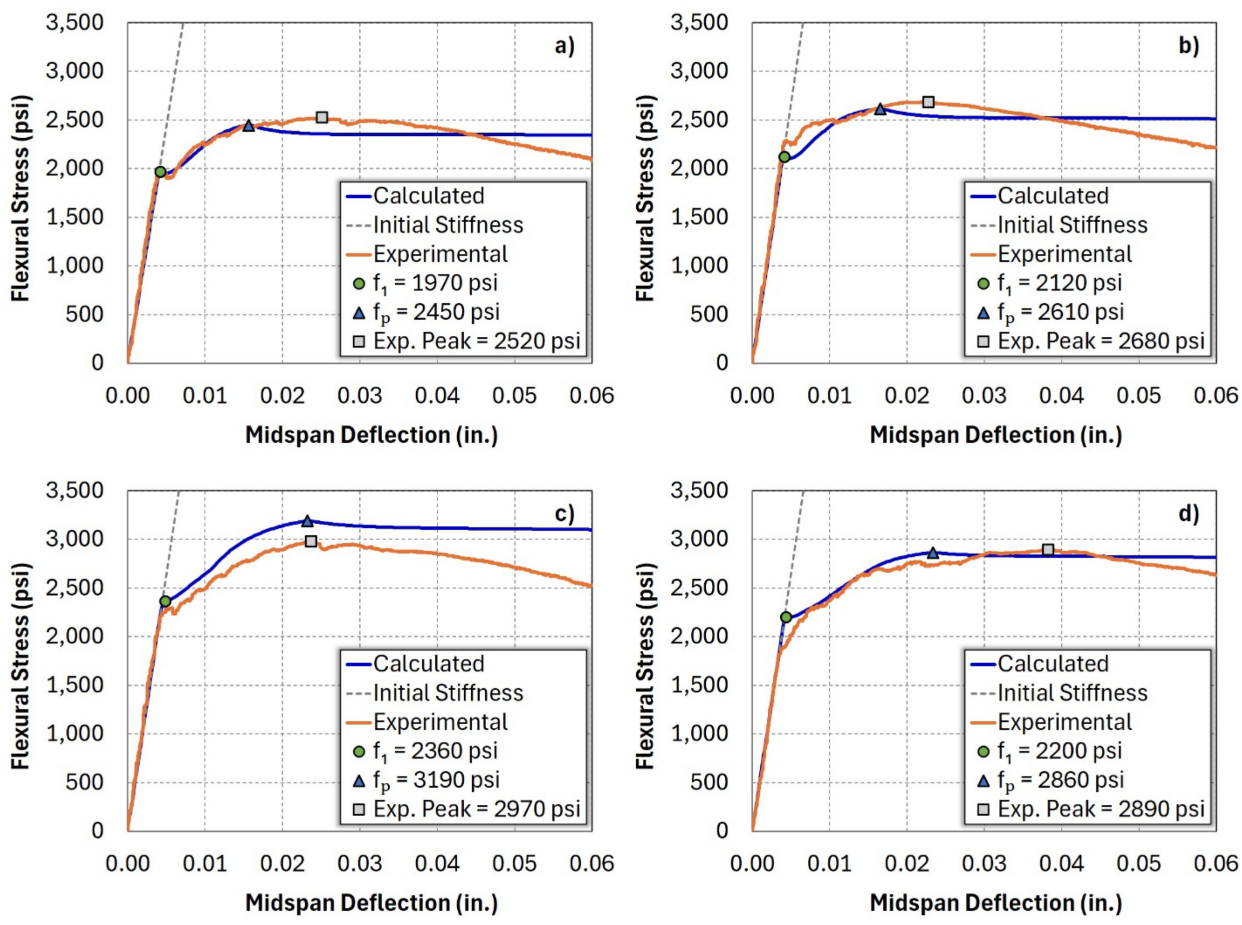

Figure 5-32: Sample Estimation of Flexural Response from Direct-Tensile Test Results:
a) 9% SF at 28 days, b) Bin. 1.5 at 91 days, c) FD 1.50 at 91 days, and d) A-A at 91 days

5.8.3 COMPARISON OF CALCULATED AND EXPERIMENTAL FLEXURAL TEST RESULTS

Table 5-1 contains the experimental and calculated values of the elastic limit flexural stress, referred to as the first-peak load (f_1) per ASTM C1609, and the peak flexural stress (f_P) for the batches meeting the inclusion criteria described above.

Table 5-1: Experimental Versus Calculated Flexural Test Results

	UHPC Mixture	Measured f_1 (psi)	Estimated f_1 (psi)	Measured f_P (psi)	Estimated f_P (psi)
28-day Results	FD 1.00	1870	1910	2270	2440
	FD 1.25	1950	2275	2670	2700
	FD 1.50	1990	1940	2865	2760
	FD 1.75	2005	2185	2920	3120
	9% SF	1970	1970	2520	2450
	12% SF	1970	2090	2360	2710
	15% SF	1910	1880	2585	2350
	Ten. 1.5	1870	2260	2545	2750
	Bin 1.5	2010	1950	2490	2730
	Bin 2.0	2275	2100	3180	3020
	w/b 0.18	2120	2290	2730	3070
	w/b 0.22	1850	1890	2590	2660
	A-A	1870	1860	2350	2560
	Masonry	2080	1960	3020	2540
	C33, w/b 0.20	2045	1890	2675	2460
91-day Results	FD 1.50*	2080	2360	2980	3190
	FD 1.75	2200	2580	2915	3520
	FD 2.00	2330	2680	3230	3600
	Ten. 1.5	1970	2230	2520	2860
	Bin 1.5	2230	2120	2680	2610
	Bin 2.0	2320	2240	2740	2970
	w/b 0.18	2140	2430	2960	3220
	w/b 0.22	2080	2170	2630	2960
	9% SF	1980	2190	2680	2800
	12% SF	2020	2240	2650	2770
	15% SF	1990	2250	2320	2550
	A-A	1855	2200	2900	2860
	Masonry	1960	2130	3110	2850
	C33, w/b 0.20	1980	2190	2680	2800

The estimated versus measured first-peak flexural stress (f_1) for all batches are plotted in Figure 5-33. Figure 5-34 plots the corresponding comparison for the peak flexural stress (f_P). The solid diagonal line represents the line of equality, and the other diagonal lines represent ±20% error.

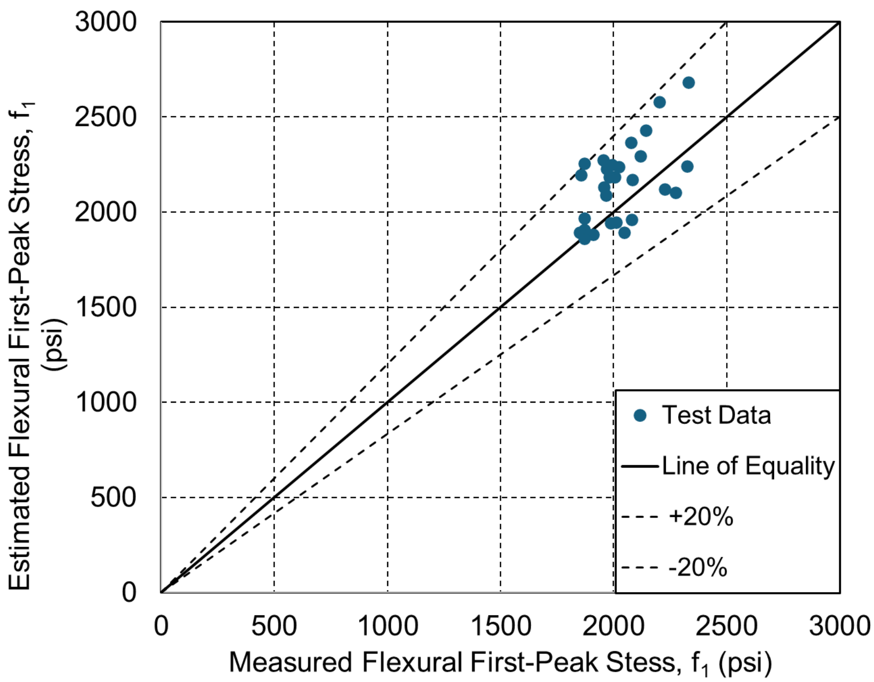

Figure 5-33: Estimated versus Measured First-Peak Flexural Stress (f_1)

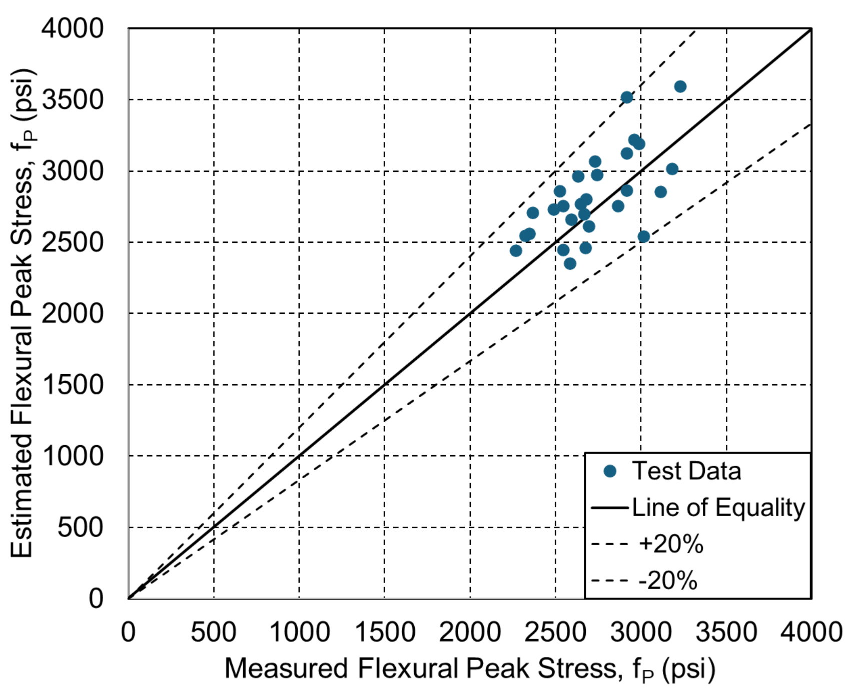

Figure 5-34: Estimated versus Measured Peak Flexural Stress (f_P)

The first-peak stress estimates generally fall within the ±20% error region, though some scatter is present, particularly for batches where the direct-tension cracking stress was higher relative to the flexural first peak. The peak flexural stress estimates show similar agreement, with most results falling within or near the ±20% error region across both ages and all mixture variables.

5.8.4 PARAMETRIC STUDY FOR ESTABLISHING A FLEXURAL STRENGTH SPECIFICATION VALUE

Having established in Section 5.8.3 that the forward-analysis procedure produces reasonably accurate estimates of flexural stress from direct-tension test results, the analysis was used to determine the flexural response corresponding to the FHWA minimum tensile strength requirements. The objective was to translate the tensile strength acceptance criteria into an equivalent flexural strength value that can be specified for quality assurance testing because flexural testing is easier to perform and more reliable than direct-tension testing.

Two levels of effective cracking stress were considered: 750 psi, which is the FHWA minimum for UHPC (Graybeal and El-Helou 2023), and 850 psi, which is a higher threshold proposed in this study to provide improved performance obtained with non-proprietary UHPC made from Alabama materials. For each cracking stress level, the analysis was run at elastic modulus values of 4,000, 5,000, and 6,000 ksi to bound the range of material stiffness observed across the UHPC mixtures tested. The remaining input parameters were obtained as the average ratios found from the experimental data: the peak tensile stress was taken as 1.18 times the cracking stress, the localization stress as 1.11 times the cracking stress, and the localization strain as 0.0025 in./in. The cracking strain was computed as $f_{t,cr}$ / E_c, and the peak strain was taken as the midpoint between the cracking strain and the localization strain. Table 5-2 details this result.

Table 5-2: Estimated Flexural Response Based on Different $f_{t,cr}$ Tensile Result

	Direct-Tension Test Results							Estimated Flexural	
$f_{t,cr}$ (psi)	E_c (ksi)	$f_{t,cr}$ (psi)	$f_{t,pk}$ (psi)	$f_{t,loc}$ (psi)	$\varepsilon_{t,cr}$ (in./in.)	$\varepsilon_{t,pk}$ (in./in.)	$\varepsilon_{t,loc}$ (in./in.)	f_1 (psi)	f_P (psi)
750	4000	750	885	833	0.00018	0.0013	0.0025	1250	1975
	5000	750	885	833	0.00015	0.0013	0.0025	1200	2010
	6000	750	885	833	0.00012	0.0013	0.0025	1150	2050
850	4000	850	1003	944	0.00021	0.0014	0.0025	1450	2225
	5000	850	1003	944	0.00017	0.0013	0.0025	1448	2250
	6000	850	1003	944	0.00014	0.0013	0.0025	1300	2295

For a cracking stress of 750 psi, the calculated peak flexural stress ranges from 1,975 to 2,050 psi across the tested range of elastic moduli. For a cracking stress of 850 psi, the range is 2,225 to 2,295 psi. The elastic modulus has a minimal effect on the peak flexural stress, producing approximately 4% variation across the range of results, though it does influence the stiffness of the ascending branch of the flexural response.

To confirm that the UHPC exhibits strain hardening behavior, a ductility check is proposed based on the ratio of peak flexural stress to first-peak flexural stress (f_P / f_1). A minimum ratio of 1.25 is proposed, consistent with the ductility index used by PCI (Precast/Prestressed Concrete Institute 2022) for UHPC acceptance.

Based on the parametric results, the following flexural acceptance criteria are proposed for UHPC to meet the FHWA tensile performance requirements. For a UHPC designed to a minimum effective cracking stress of 750 psi, the peak flexural stress from ASTM C1609 testing should equal or exceed 2,000 psi. For UHPC designed to the higher threshold of 850 psi proposed in this study, the peak flexural stress should equal or exceed 2,300 psi. In both cases, the ductility ratio f_P / f_1 should be no less than 1.25 to ensure that the UHPC exhibits adequate post-cracking load carrying capacity. The full implementation of these criteria is addressed in Chapter 7.

5.9 Freeze-Thaw Durability Results

The freeze-thaw testing was conducted in accordance with AASHTO T 161 (2022) using specific UHPC mixtures to assess the freeze-thaw resistance of the non-proprietary UHPC produced in this study. The test was conducted using a Humboldt HC-3186S.4F freeze-thaw cabinet. The specimens used were 3 × 3 × 11.25 in. prisms with UHPC plugs filling the remaining space in each test chamber until it met AASHTO T 161 (2022) space requirements. The control specimen was made using a 3 × 3 × 14 in. UHPC specimen with no fibers. A 5/16-inch hole was used to embed the temperature probe in the control specimen, and it was sealed with silicon caulk. Dummy specimens were loaded into all remaining test chambers so that they were all full. Testing was conducted once the machine reached the end of an appropriate thaw cycle, either when new specimens were added or when specimens had approached 30 cycles since the last test. A target of 30 cycles was used to ensure that there was a buffer of 6 cycles before testing had to occur. To ensure all specimens experienced similar freeze-thaw conditions, the specimens were flipped end over end and moved one test chamber to the left.

Five UHPC blends of varying steel fiber dosages and two binary blends with different steel fiber dosages were tested. The results from all seven UHPC mixtures tested are shown in Figure 5-35. All the relative dynamic modulus readings remained above 98%, thus none of the 21 specimens tested failed within the 300 cycles. As such, testing shows that UHPC is inherently freeze-thaw resistant without the need for any air-entraining admixtures. This conclusion is similar to that of Thomas et al. (2012). This is very beneficial because the northern region of Alabama regularly experiences freezing temperatures, so UHPC without any air-entraining admixture can be used throughout Alabama. Furthermore, the 0.00% fiber blend achieving excellent freeze-thaw resistant shows that the cementitious matrix is dense and of low permeability, hence its freeze-thaw resistance.

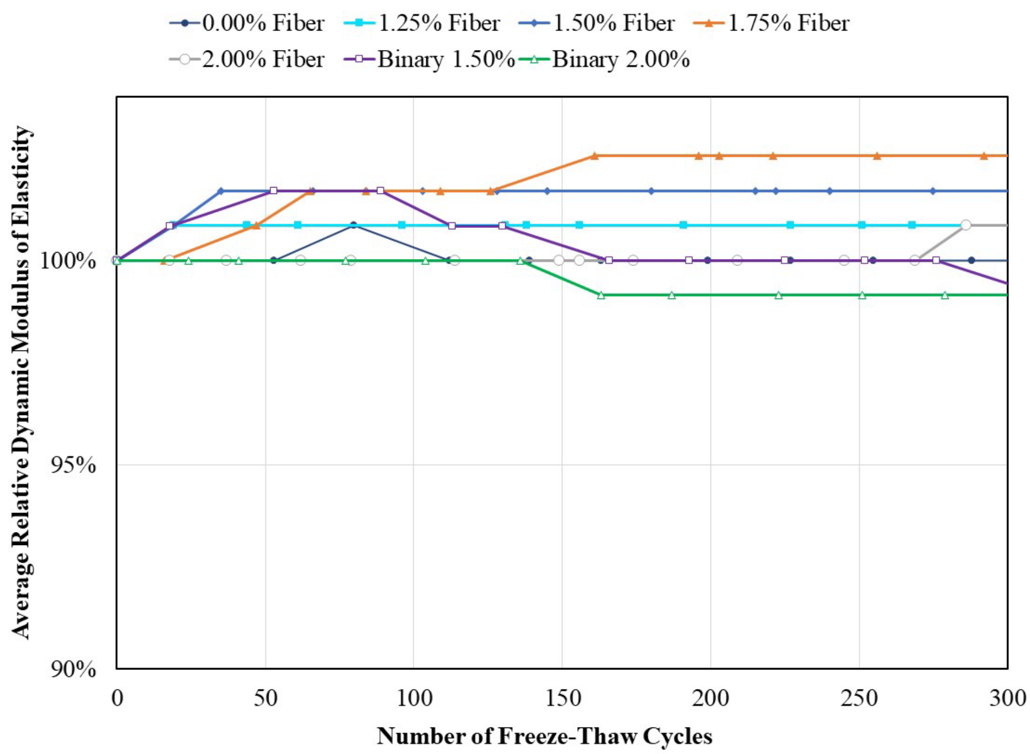

Figure 5-35: Freeze-Thaw Relative Dynamic Modulus of Elasticity of All Tested UHPC

5.10 COST ANALYSIS OF NON-PROPRIETARY UHPC

The unit cost of constituent materials were established from published government commodity data (USGS 2025), published literature (Wille and Boisvert-Cotulio 2013; Stewart et al. 2022), and records from when materials were procured for this project. Table 5-3 summarizes the unit costs adopted for the cost analysis and the corresponding sources.

Table 5-3: Unit Costs of UHPC Constituent Materials

Material	Unit Cost	Source
Portland Cement (Type IL)	$145/ton	USGS (2025)
Slag Cement	$140/ton	USGS (2025)
Silica Fume	$0.40/lb ($800/ton)	Procurement Records, 2025
Fine Aggregate	$14.25/ton	USGS (2025); Stewart et al. (2022)
Water	$3.50/1,000 gal	AL utility rate schedules, 2024
HRWR Admixture	$13 to $20/gal	Wille and Boisvert-Cotulio (2013); Stewart et al. (2022)
HCA (Delvo)	$13 to $20/gal	Graybeal (2013)
Steel Fiber	$2.00 to $2.50/lb	Stewart et al. (2022); Wille and Boisvert-Cotulio (2013); Procurement, 2025

Table 5-4 applies these unit cost to the baseline mixture with proportion using 1.5% steel fiber dosage by volume. Admixture weights were converted to volume using bulk specific gravities of 1.15 for the HRWR and 1.10 for the HCA. For the admixture and steel fiber cost, a range was used based on literature and procurement values. This establishes a range of prices for the non-proprietary UHPC as summarized in Table 5-4.

Table 5-4: Estimated Material Cost per Cubic Yard of UHPC (1.5% Steel Fiber)

Material	Quantity (lb/yd³)	Unit Cost	Cost/yd³
Portland Cement (Type IL)	1,180	$145/ton	$86
Slag Cement	590	$140/ton	$41
Silica Fume	177	$0.40/lb	$71
Fine Aggregate	1,498	$14.25/ton	$11
Water	389	$3.50/1,000 gal	<$1
HRWR Admixture	20.5	$13 to $20/gal	$28 to $43
HCA	5.4	$13 to $20/gal	$8 to $12
Steel Fiber (1.5%)	198	$2.00 to $2.50/lb	$396 to $495
Total			**~$640 to $760**

Table 5-5: Cost Distribution by Material

Material	Cost/yd³	Percent of Total
Portland Cement (Type IL)	$86	11% to 13%
Slag Cement	$41	5% to 7%
Silica Fume	$71	9% to 11%
Fine Aggregate (Sand)	$11	1% to 2%
Water	<$1	<0.1%
HRWR Admixture	$28 to $43	4% to 6%
HCA	$8 to $12	1% to 2%
Steel Fiber (1.5%)	$396 to $495	62% to 65%
Total	**$640 to $760**	**100%**

As seen in Table 5-5, at a 1.5% dosage, the steel fibers account for approximately 64% of the total material cost. The cementitious materials collectively represent about 28%, and the remaining constituents contribute less than 8%. At a 2% dosage, the fiber cost alone increases to approximately $585 per cubic yard, raising the total to roughly $829 per cubic yard, a difference of approximately $140 per cubic yard. As presented in Section 5.2, a 1.5% fiber dosage produced a post-cracking tensile strength above 1,000 psi at 28 days, exceeding the FHWA minimum of 750 psi. The 1.5% dosage therefore satisfies the performance requirement at a meaningfully lower cost, and this cost sensitivity was one of the factors that influenced the recommended fiber dosage.

5.11 SUMMARY

The material characterization program evaluated the effect of the following five variables on the mechanical properties of non-proprietary UHPC: steel fiber dosage, fine aggregate gradation, cementitious blend type, silica fume content, and water-binder ratio. More than twenty-five different UHPC batches were produced and tested in compression, flexure, and direct tension at 28 and 91 days to quantify the influence of each variable.

After considering the five variables, steel fiber dosage was the only variable that produced a significant and consistent effect on the tensile and flexural performance. Dosages at or above 1.00% exceeded the FHWA minimum post-cracking tensile strength of 750 psi, and increasing the dosage produced proportionally higher stresses in both test types. Compressive strength, on the other hand, was governed by the properties of the cementitious matrix and was not meaningfully affected by steel fiber content.

The remaining four variables had no significant influence on tensile or flexural strength within the ranges tested. Standard AASHTO M 6 river sand performed comparably to masonry sand and an optimized particle packing blend, which means that locally available concrete sand can be used without specialized sourcing or blending. Silica fume contents of 9%, 12%, and 15% of total binder all produced similar mechanical results, so the dosage can be selected based on economic and practical considerations rather than performance. Binary blends without silica fume matched the ternary blends in strength; however, the rapid loss of workability documented in Section 5.4 makes the binary blend impractical for field-scale placement of UHPC. The water-binder ratio affected compressive strength in the expected direction, with lower ratios producing higher values, but did not significantly change the tensile or flexural response across the 0.18 to 0.22 range tested.

The direct-tension testing program showed that stress-based metrics are reliable indicators of tensile performance, whereas strain-based metrics exhibited high variability across all batches and are not suitable for acceptance testing. This finding carried directly into the forward analysis presented in Section 5.8, where measured tensile properties and constitutive laws were used to estimate the required flexural response. The analysis demonstrated that for a UHPC meeting the FHWA minimum effective cracking stress of 750 psi in direct tension, the corresponding peak-flexural stress is 2,000 psi. For the higher direct-tension threshold of 850 psi proposed in this study, the corresponding peak-flexural stress is 2,300 psi. A ductility ratio of f_P / f_1 no less than 1.25, consistent with Precast Concrete Institute (PCI), is proposed as an additional acceptance check to ensure adequate post-cracking ductility is achieved.

All UHPC tested were inherently resistant to freeze-thaw degradation through 300 cycles without the need for air-entraining admixtures.

The cost analysis in Section 5.10 showed that steel fibers account for 62% to 65% of the total material cost at a 1.5% dosage, with the total estimated between $640 to $760 per cubic yard. No other constituent approaches that level of influence of cost. Reducing the fiber dosage from 2.0% to 1.5% by volume saves approximately $140 per cubic yard, while the 1.5% dosage still exceeds the FHWA minimum post-cracking tensile strength of 750 psi with adequate margin as presented in Section 5.2. The steel fiber dosage thus significantly affects both UHPC performance and the cost, and a 1.5% dosage provides the balance between meeting the structural requirements while minimizing the material cost component of UHPC.

These results collectively establish that the FHWA performance requirements for UHPC can be met using locally available Alabama materials. No specialized aggregates are needed, no air-entraining admixture is required, and the silica fume content can be held at 9% of total binder without sacrificing performance.

CHAPTER 6

FIELD-SCALE PRODUCTION OF NON-PROPRIETARY UHPC

6.1 OVERVIEW

The material characterization program documented in Chapters 3 through 5 was conducted in the laboratory, while producing approximately two cubic feet (2 ft^3) batches by using a planetary high-shear mixer. While the laboratory results established the performance of a baseline non-proprietary UHPC mixture, practical implementation requires production at volumes far greater than two cubic feet using ready mixed concrete trucks, which operate with a fundamentally different mixing action and energy input than laboratory mixers. The transition from laboratory to field introduces variables that can affect fresh properties, workability retention, fiber dispersion, and the overall quality of the finished UHPC element.

This chapter documents a series of three full-scale field trials conducted at an Alabama ready mixed concrete plant to evaluate the feasibility of producing the baseline non-proprietary UHPC at full-scale conditions. Each UHPC trial was made in a batch size of two cubic yards of UHPC in a ready mixed concrete truck. The primary objectives were to:

1. Develop an effective mixing procedure for ready mixed concrete plant production,
2. Identify and resolve challenges encountered during the transition from laboratory to field scale, and
3. Verify that the hardened properties of field-produced/large-scale UHPC are comparable to the laboratory baseline established in Chapter 5.

The mixture proportions used for all three trials matched the baseline mixture from Section 5: a ternary binder system with 1.50% steel fibers by volume, a water-binder ratio of 0.20, and with the AASHTO M 6 natural river sand as the fine aggregate.

6.2 MIXTURE PROPORTIONS AND FORMWORK

6.2.1 MIXTURE PROPORTIONS

The mixture proportions used for the field-scale trials are summarized in Table 6-1. The proportions are consistent with those recommended after the completion of the laboratory testing phase of this project.

Table 6-1: Field-Scale Mixture Proportions

Type IL Cement (lb/yd^3)	Slag Cement (lb/yd^3)	Silica Fume (lb/yd^3)	Water (lb/yd^3)	Fine Agg. (lb/yd^3)	HRWRA (fl oz/cwt)	HCA (fl oz/cwt)	Steel Fiber Vol. (%)
1180	590	177	389	1522	10.0	6	1.50

6.2.2 FORMWORK AND UHPC PLACEMENT PLAN

A predominant use of non-proprietary UHPC in transportation infrastructure is for bridge deck closure joints and partial-deck bridge deck overlays, which are typically 2 to 3 inches thick. To reflect these applications and to facilitate the extraction of test specimens, five flat slabs were built at the site, each measuring 4 ft x 8 ft. Two slabs (F1 and F2) were made at thicknesses of 2 in. and 3 in. and designated as primary test slabs for specimen extraction. The remaining three slabs (F3 through F5) were 3 in. thick and reserved for evaluating flow retention characteristics over the duration of UHPC placement.

The slab formwork was built from wood and sealed to prevent paste absorption. To obtain direct-tension and flexural test specimens from the test slabs, spacers were placed across the length of the slabs at intervals matching the slab depth (2 in. spacers for the 2 in. section, 3 in. spacers for the 3 in. slab section). This approach was chosen over saw-cutting along the length to preserve the tight geometric tolerances required for direct-tension testing specimens. Figure 6-1 shows these dimensions and the location of six direct-tension and flexural test specimens that we made in test slabs F1 and F2.

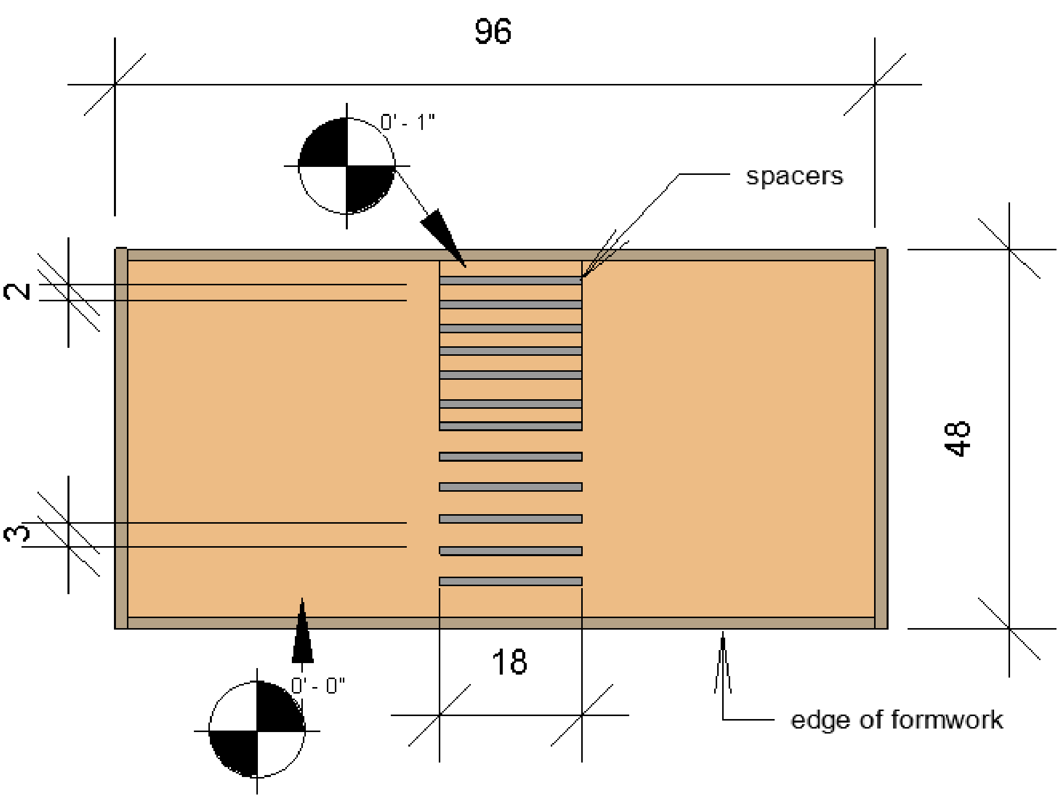

Figure 6-1: Plan View of Formwork (F1 and F2) with Dimensions in Inches

UHPC is regarded as a self-consolidating mixture, therefore a discharge (i.e., drop) location was chosen for the field study as shown in Figure 6-2. For all five slabs, the drop location was selected a few feet away from one end and the UHPC was allowed to flow and fill the slab from this location. This discharge location was selected to gauge how well the fibers align when UHPC is placed on a flat substrate and allowed to flow to the corners of the slab.

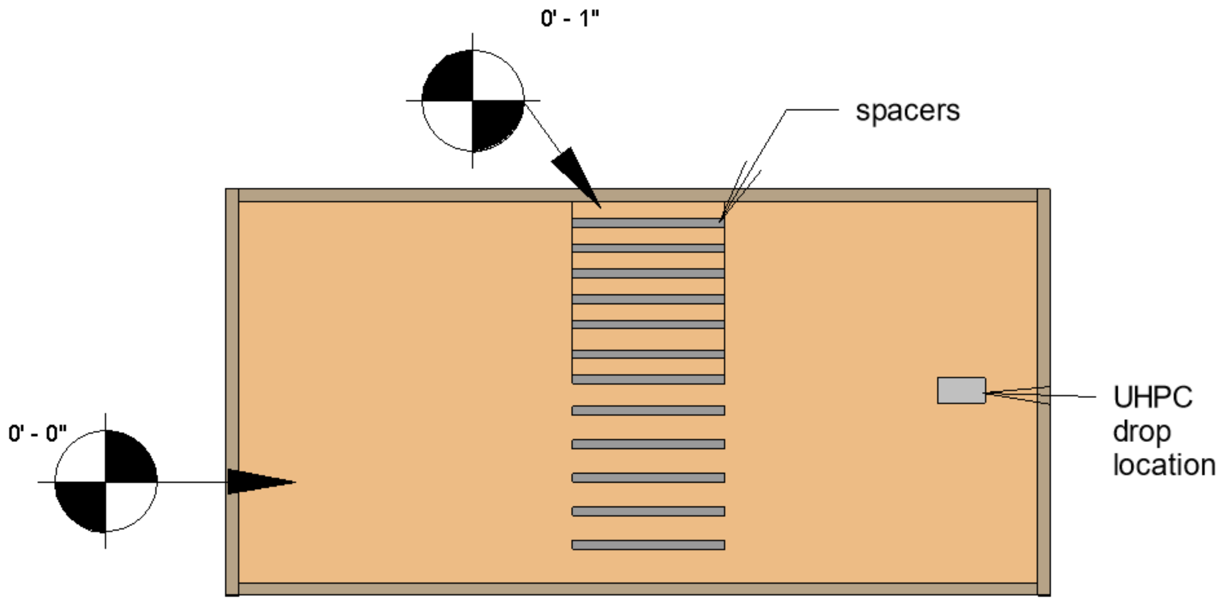

Figure 6-2: Plan View of Formwork for Slab F1 and F2 Showing the UHPC Drop Location

6.2.3 SPECIMEN PRODUCTION AND EXTRACTION

In the trials in which hardened concrete test specimens were made (Trials 1 and 3), the slab placement sequence was F5 first, followed by F1 and F2, then F3 and F4 and this can be seen in Figure 6-3. This sequence ensured that the initial portion of the batch was placed in a non-tested slab, while the middle portion of the batch filled the primary test formwork. In addition to the slab placements, eighteen cylinders, twelve direction-tension test prisms and six flexural prisms were cast from these trials. Following placement, the open surface of the UHPC in all formworks were coated with a resin-based curing compound (from WR Meadows) to mitigate evaporation and to provide final curing. The slabs were left to cure in laboratory conditions.

Twelve direct-tension and flexural test specimens were extracted from slabs F1 and F2. Specimens were extracted at an age of seven days using a standard concrete wet-saw blade to make transverse cuts, producing 18 in. long pieces that were then trimmed to final lengths of 17 in. for direct-tension testing and a length of 14 in. for flexural testing. Because the formwork depths were 2 in. and 3 in., the extracted specimens measured 2 x 2 x 17 in. and 3 x 3 x 14 in. Aluminum transfer plates were epoxied to the DTT specimen sides 12 to 24 hours before testing. Test ages of 28 and 91 days were selected to facilitate direct comparison with the laboratory scale batches from Chapter 5.

Figure 6-3: Formwork Constructed and Used in This Study

6.3 Development of the Full-Scale Mixing Procedure

The mixing procedure established in Chapter 3 uses a five-step sequence designed for a planetary high-shear mixer in a laboratory setting. The high-shear action of this mixer ensures thorough particle dispersion and prevents agglomeration of cementitious materials, even when they come into contact with moisture in the fine aggregate. A ready mixed concrete truck does not provide the same mixing energy. This difference in mixing action required the development of a field specific plant mixing and truck loading and sequence.

Three full-scale trials were conducted, each being 2 yd^3 of UHPC and produced at the same ready mixed concrete plant. The loading sequence was modified between trials based on the challenges observed in each preceding trial. The progression of trials and the reasoning behind each modification are described below.

6.3.1 Trial 1

The Trial 1 loading sequence was adapted directly from the laboratory procedure, with modifications to account for a two staged material loading approach at the concrete plant. During the first stage, the fine aggregate was loaded into the ready mixed truck. After the truck pulled out from under the plant, the research personnel then manually added silica fume from the slump rack. The drum was mixed at 50 percent of full speed (approximately 10 rpm) for 5 minutes. On the second pass, Type IL cement, slag cement, and 80% of the mixing water were added. The hydration-control admixture (HCA) was introduced, and the material mixed for 5 minutes at 50 percent of the full speed (approximately 10 rpm). It was observed during this phase that a higher initial drum speed simply traps the materials on the side of the drum without effectively mixing them, which is why the half full speed was adopted at the early stages. The total mixing time at the plant was approximately 25 minutes. The truck was then transported to the site which added 27 minutes of transport time.

At the site, the remaining 20% of the mixing water and 80% of the HRWRA were added, and the material mixed at 50% of full speed for 5 minutes. After visual inspection indicated sufficient fluidity, the remaining 20% of the HRWRA was added. Once the mixture reached the target consistency, all steel fibers were added, and the material mixed at the same speed for 5 minutes. A flow test performed per ASTM C1856 recorded an initial flow of 8.25 inches, within the acceptance range of 7 to 11 inches. Placement of all five slabs took approximately 20 minutes, after which a final flow test recorded 7.25 inches, indicating a 1-inch loss of flow during the placement operation. During this time eighteen cylinders and eighteen prisms were also molded for testing to compare to the specimens extruded from the slabs. The 5 fl oz/cwt HCA dosage was adequate to maintain workability throughout the full 90-minute sequence from starting of mixing through completion of placement.

The batch was a successful operation and demonstrated that non-proprietary UHPC can be effectively produced in a ready mixed concrete truck at production scale. However, a significant issue was observed: cement balls were present in the mixture as shown in Figure 6-4. These balls, ranging in size from approximately 0.25 to 1 inch in diameter, were composed of partially hydrated cement. The cement balls are hypothesized to have formed when cement came into contact with moisture in the fine aggregate during the loading process, before the cement particles became blended with the other powders. The formation of cement balls during field production has been documented by other researchers. Kim et al. (2021) observed the same phenomenon in their field trials. Giesler et al. (2016) reported that pre drying the fine aggregate eliminated the issue entirely, however, this is not a viable option in large-scale at a ready mixed concrete plant.

a)  **b)** 

Figure 6-4: a) Cement Ball from the Mixture and b) Split Cement Ball from the Mixture

6.3.2 TRIAL 2

In this trial, cement and sand were loaded together first, followed by the HCA and slag cement, then 80% of the mixing water, HRWRA and silica fume. Cement balls appeared again (see fig 6-5), though they were progressively mixed away with significant additional mixing. The total mixing time was about 120 minutes, which is too long for practical use. This increased mixing time required to break up the balling raised the mixture temperature to approximately 97°F. At this temperature, the UHPC lost all workability before placement could be completed. The batch was not usable for specimen production. This result demonstrated that while extended mixing can eventually disperse cement ball agglomerations in a ready mixed truck, the time required to do so depletes the available working window, particularly in warm weather conditions. A loading sequence that prevents the formation of cement balls in the first place is necessary, rather than relying on extended mixing to remove them after the fact.

Figure 6-5: Cement Balls Present in the Mixture

6.3.3 TRIAL 3

Trial 3 incorporated the lessons from the preceding trials into a revised loading sequence designed to prevent cement balls from forming. At the plant, the loading sequence was as follows: cement and sand were loaded with 60% of the total mixing water. Next, the HCA premixed with 10% of the total water was added, followed by 20% of the HRWRA premixed with an additional 10% of the total water to promote dispersion of the cementitious paste. The early introduction of 80% of water with some HRWRA was intended to provide sufficient workability to allow mixing of the fine aggregate and paste present. This mixture was mixed at full mixing speed for 4 minutes. Next, slag cement was then loaded with the remaining (80%) of the HRWRA and the remaining 20% of the total water. This mixture was mixed at full mixing speed for 4 minutes. Finally, all the silica fume was added and the mixture mixed at full mixing speed for 4 minutes. The silica fume was loaded last among the cementitious materials, which ensured it was added to an already wetted and workable mixture rather than being introduced in a mixture that is dry with very little workability. Figures 6-6 to 6-8 show these steps at the ready mixed concrete plant. The total plant mixing time was approximately 30 minutes, which is reasonable for UHPC production.

Figure 6-6: HRC Personnel Adding Silica Fume to the Ready Mixed Concrete Truck at the Plant

The transportation time for the ready mixed truck to reach the discharge location was approximately 15 minutes. At the site, the steel fibers were added, and the drum was mixed at full speed for 5 minutes (see Figure 6-7 and 6-8). The total time from initial mixing to placement was approximately 60 minutes.

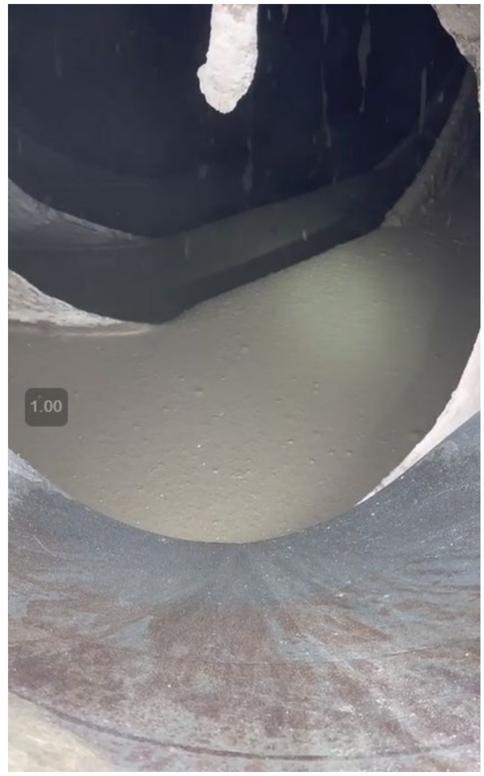

Figure 6-7: Steel Fibers in the Truck **Figure 6-8: Fluid UHPC at the end of Mixing**

Trial 3 produced no cement balls and achieved good flow. The UHPC was placed into the formwork, and specimens (cylinders and prisms) were cast for hardened property testing. The success of this trial confirmed that the cement ball issue can be resolved through a loading sequence that prevents dry cementitious materials from being exposed to moisture before adequate dispersion has occurred. The key principles include the following: introduce a large portion of the mixing water and HCA early to begin paste formation and add cementitious materials sequentially into an already wetted environment. A summary of these trials is covered in Table 6-2.

Table 6-2: Loading Sequences for All Three Field Trials

	Full-Scale Trials		
	Trial 1	**Trial 2**	**Trial 3**
At Plant	Fine agg. + Silica fume ➔ Mixed	Cement + Fine agg. + Delvo + Slag cement ➔ Mixed	Cement + Fine agg. + 60% water ➔ Mixed
	Cement + Slag cement + 80% of water + Delvo ➔ Mixed	80% water + 20% HRWRA + Silica fume ➔ Mixed	Delvo + 20% HRWRA + 20% water ➔ Mixed
			Slag cement + 40% HRWRA + 20% water ➔ Mixed
			Silica fume + 20% HRWRA ➔ Mixed
At Site	20% of water+ 80% of HRWRA ➔ Mixed	N/A	Steel fibers ➔ Mixed
	20% HRWRA + Steel fibers ➔ Mixed		
Time taken	25 min. (at plant) 27 min. (transport) 1.15 hr (placement completed)	N/A	30 min. (at plant) 15 min. (transport) 1 hr (placement completed)

6.4 Fresh Property Results

For Trial 1, the initial flow measured at the site was 8.25 inches and the final flow after completion of placement was 7.25 inches, representing a 1-inch loss of flow over the 15-minute placement period. Both measurements fell within the 7 to 11 in. acceptance range.

For Trial 3, a similar result was obtained with an initial flow of 8.25 inches, and a final flow after completion of 7.5 inches. Figures 6-9 and 6-10 show the flow test and placement of UHPC.

The HCA dosage of 6 fl oz/cwt was confirmed as adequate for maintaining workability throughout the full batching, transport, and placement operation for both Trial 1 (approximately 75 minutes total) and Trial 3 (approximately 60 minutes total).

below.

Figure 6-9: Flow Test Being Performed

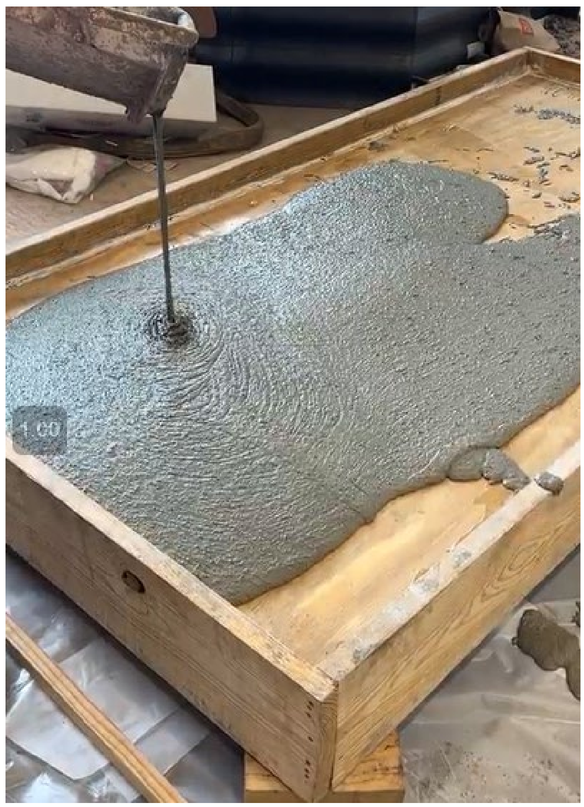

Figure 6-10: Placement of UHPC

6.5 Hardened Property Results

Hardened property testing was conducted on specimens from Trial 1 and Trial 3. The results are presented below.

6.5.1 COMPRESSIVE STRENGTH RESULTS

Compressive strength results from Trials 1 and 3 are presented in Table 6-3. Trial 3 batch with good mixing and workability exhibited a 56-day result greater than the 17,500 psi minimum, showing that large-scale production of UHPC is feasible with a ready mixed concrete truck. The impact of the cement balls on the compressive strength of the field-scale trial is best seen in the comparative result of Trial 1 and 3. As seen in Table 6-3 and Figure 6-11, the cement balls reduced the later age strength of Trial 1. This was evident in the cylinders to be tested with an example shown in fig. 6.17.

Table 6-3: Compressive Strength Results for Field-Scale Trials 1 and 3

		Concrete Age (days)				
Trial No.	**Property**	**1**	**7**	**28**	**56**	**91**
1	Compressive Strength (psi)	6,990	12,900	14,290	15,270	15,190
3	Compressive Strength (psi)	8,130	11,890	15,690	17,890	17,020

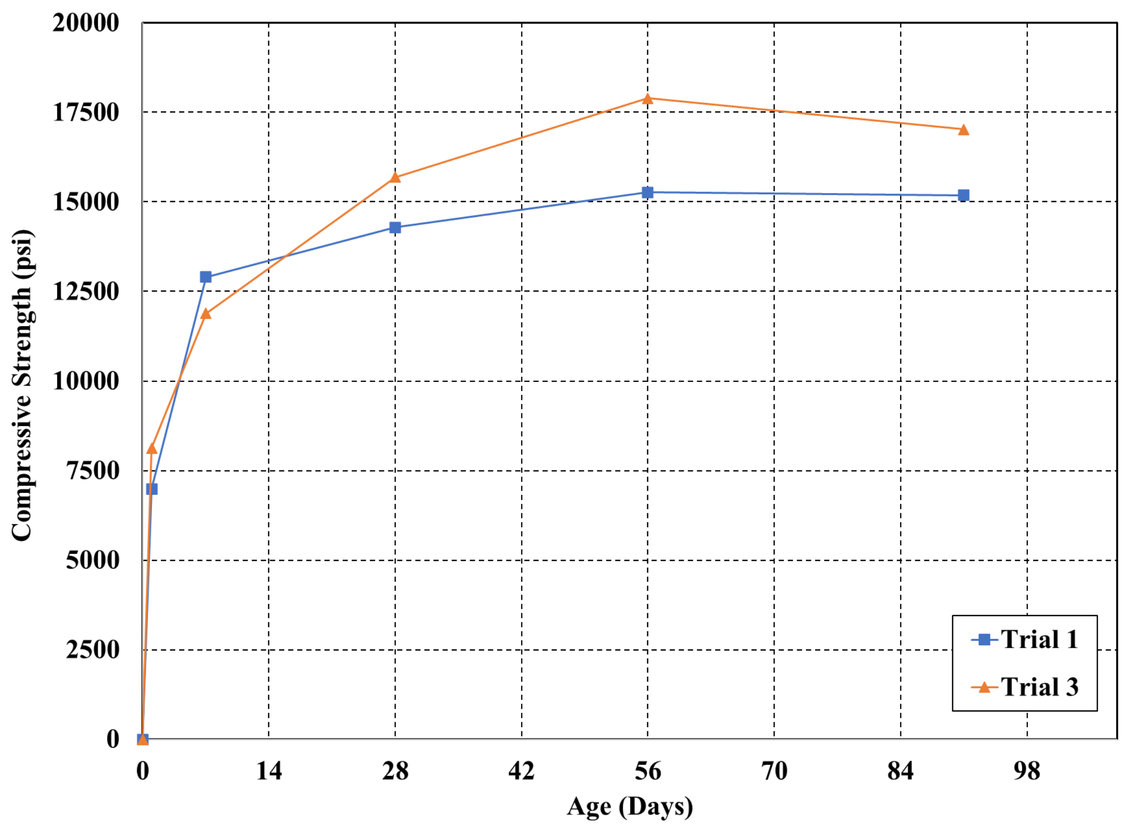

Figure 6-11: Compressive Strength Comparison between Trial 1 and 3

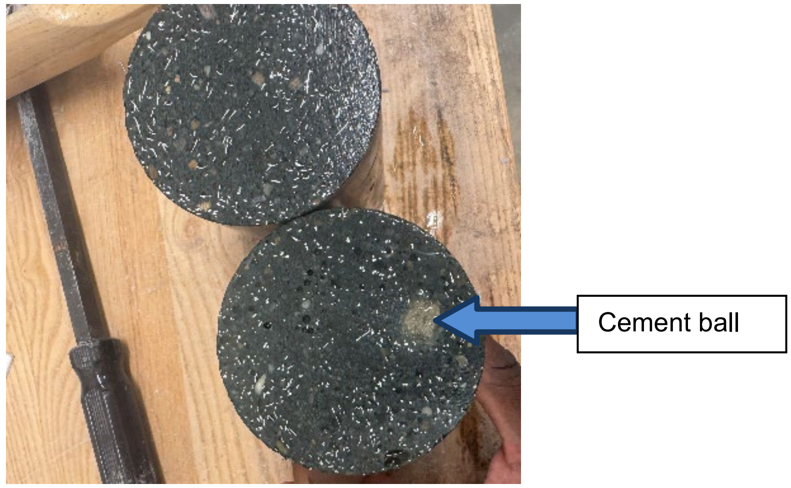

Figure 6-12: Cement Ball Seen in Trial 1 Cylinders.

6.5.2 FLEXURAL STRENGTH RESULTS

Flexural strength results from Trials 1 and 3 are presented in Table 6-4 and Figures 6-13 through 6-16. At 28 days, the extracted specimens reached a peak flexural stress of approximately 2,400 psi, while the molded specimens reached approximately 1,880 psi. At 91 days, the extracted specimens reached approximately 2,600 psi and the molded specimens approximately 1,880 psi. Both specimen types exhibited deflection hardening behavior, confirming that the fibers were effectively bridging cracks in the field produced material. However, the molded specimen results were lower than expected when compared to the established minimum (2000 psi and 2300 psi) from Chapter 5. This is attributed to the cement balls present in the Trial 1 mixture, which introduced localized weak zones in the matrix.

Trial 3, which produced no cement balls, showed improved results over Trial 1. At 28 days, the extracted specimens reached a peak flexural stress of approximately 2,700 psi and the molded specimens approximately 2,200 psi. Both values exceed the 2,000 psi peak flexural threshold corresponding to the FHWA minimum tensile requirement established in Section 5. The molded specimen result from Trial 3 is notably higher than the molded result from Trial 1 at the same age (2,200 psi versus 1,880 psi), which further supports the conclusion that the cement balls in Trial 1 had a measurable effect on the hardened flexural properties.

Regarding specimen success rates, the extracted specimens performed consistently across both trials. In Trial 1, all four extracted specimens tested at 28 days and all four tested at 91 days produced successful results, for a success rate of 100% at each age. Of the three molded specimens tested at 28 days, all three were successful; at 91 days, two of the three produced successful results. In Trial 3, all three extracted specimens tested at each age produced successful results. Of the three molded specimens tested at each age, two produced successful results.

Table 6-4: Flexural Strength Results for Field-Scale Trials 1 and 3

Trial No.	Property	Specimen Type	Concrete Age (days)			
			28		91	
			f_1	f_p	f_1	f_p
1	Flexural Strength (psi)	Molded	1,170	1,870	1,130	1,860
	Flexural Strength (psi)	Extracted	1,250	2,400	1,350	2,640
3	Flexural Strength (psi)	Molded	1,405	2,240	1,580	2,610
	Flexural Strength (psi)	Extracted	1,390	2,740	1,600	3,340

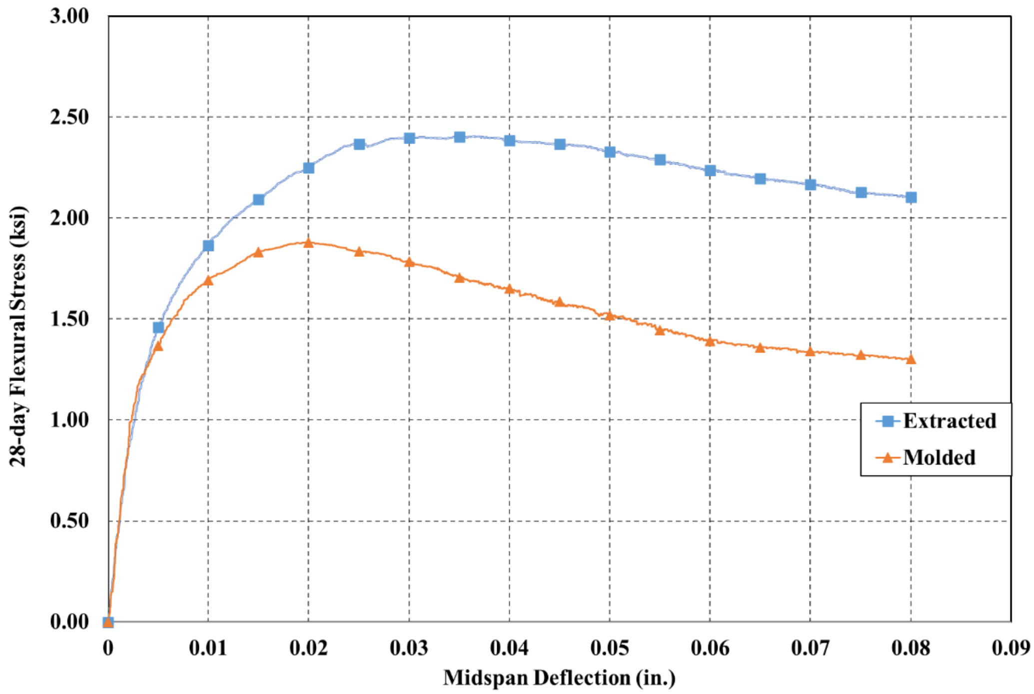

Figure 6-13: 28-Day Flexural Strength Result for Trial 1

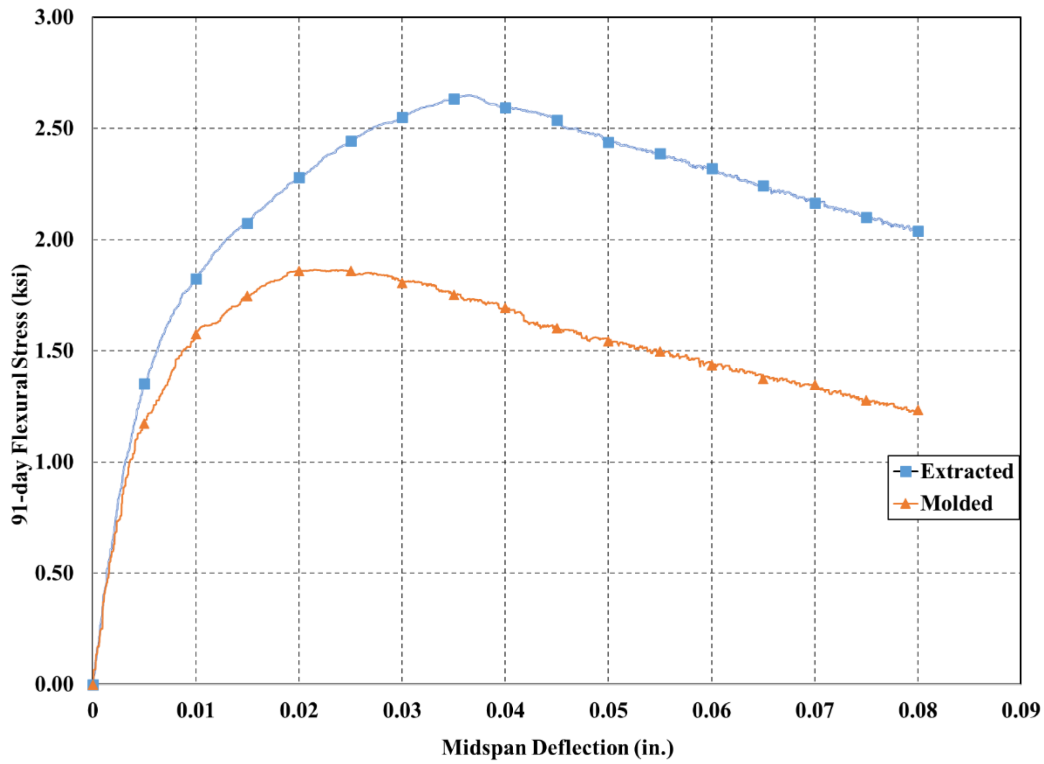

.

Figure 6-14: 91-Day Flexural Strength Result for Trial 1

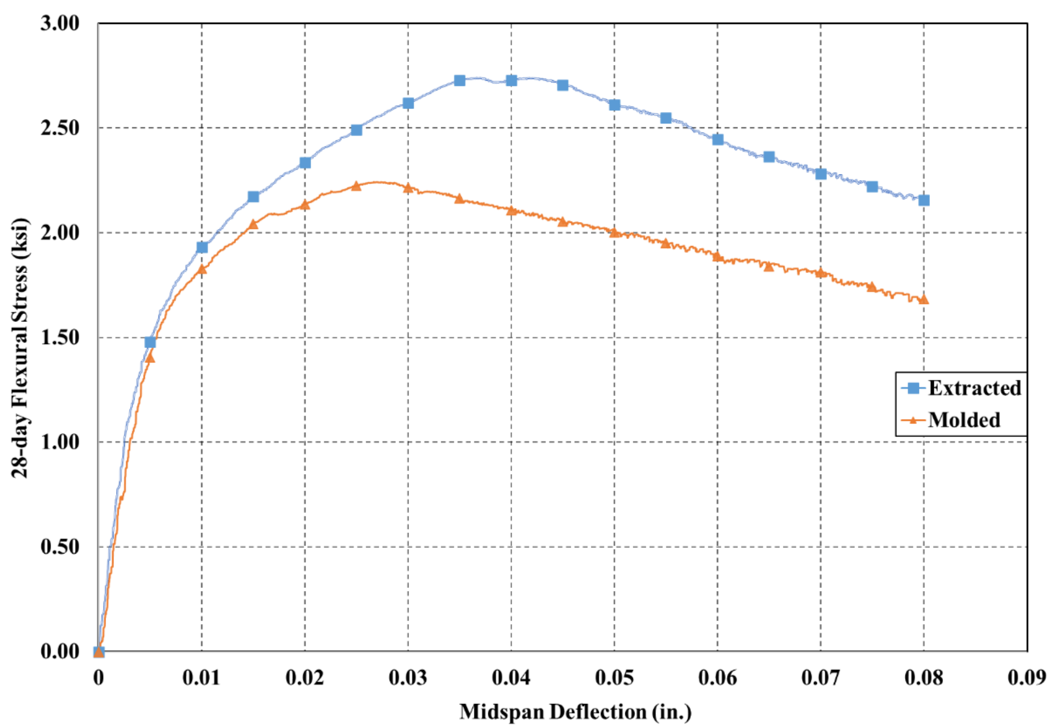

Figure 6-15: 28-Day Flexural Strength Result for Trial 3

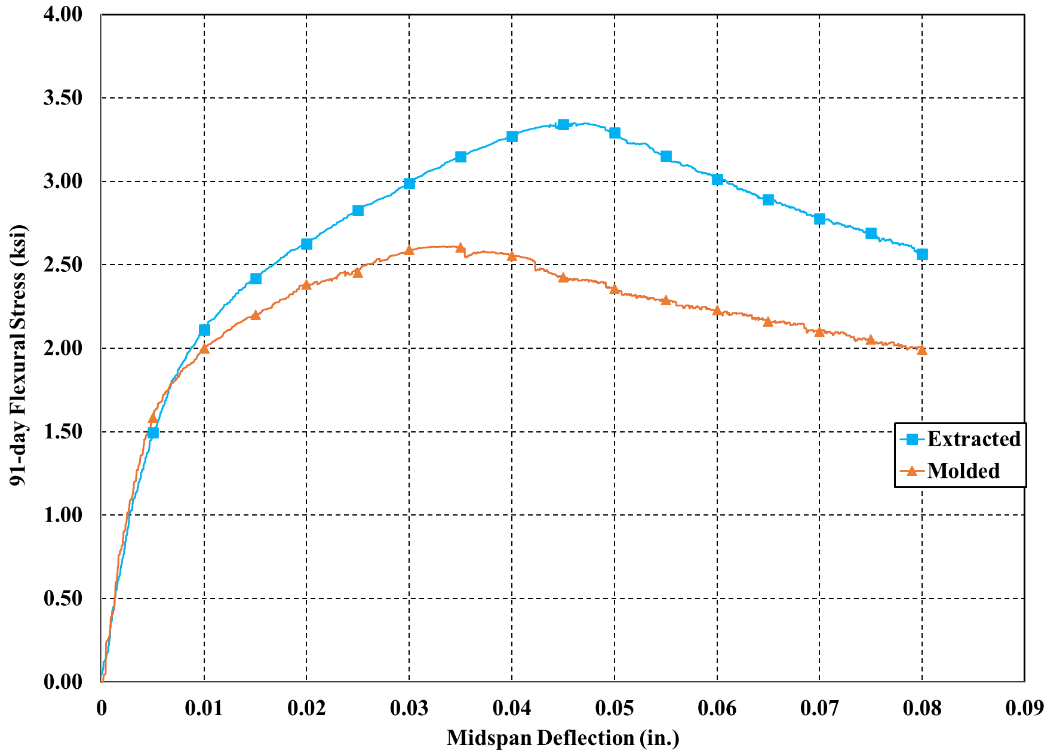

Figure 6-16: 91-Day Flexural Strength Result for Trial 3

6.5.3 DIRECT-TENSION RESULTS

Direct-tension results from Trials 1 and 3 are presented in Table 6-5 and Figures 6-17 through 6-20. At 28 and 91 days, the molded specimens exceeded the FHWA minimum effective cracking stress of 750 psi. However, the extracted specimen falls just short of the 750 psi minimum at both ages. This reduced performance is attributed to the presence of cement balls in the Trial 1 batch. The cement balls reduce the fibers from effectively bridging, hence its reduced capacity.

At 28 days, the molded specimens reached a peak tensile stress of over 900 psi and the extracted specimen of approximately 1,000 psi. Both values represent a meaningful increase over the Trial 1 results and are consistent with the improved result seen in the flexural specimen. The absence of cement balls in Trial 3 is the most likely explanation for the improved performance relative to Trial 1.

Regarding specimen success rates, Trial 1 extracted specimens yielded 4 successful tests out of 6 at 28 days and 2 successful tests out of 6 at 91 days. The reduced number of successful results at 91 days is attributed to the cement balls present in the Trial 1 mixture. Given the limited number of good specimens observed after batching, priority was given to 28-day testing, as this age forms the basis for specification compliance, and the remaining specimens were used for 91-day testing. Of the six molded specimens tested at each age, four were successful at 28 days and two at 91 days, with the reduced success at both ages again attributable to the cement balls.

Trial 3, which produced no cement balls, showed a marked improvement in success rates. Of the six extracted specimens tested at 28 days, four produced successful results. At 91 days, all five tested specimens produced successful results. Of the six molded specimens tested at each age, five were successful at both 28 and 91 days.

Table 6-5: Direct-Tension Results for Field-Scale Trials 1 and 3

		Direct-Tension Results							
		Concrete Age of 28 days				Concrete Age of 91 days			
Trial No.	**Specimen Type**	$f_{t,cr}$ (ksi)	$f_{t,peak}$ (ksi)	$f_{t,loc}$ (ksi)	ϵ_{loc} (in./in.)	$f_{t,cr}$ (ksi)	$f_{t,peak}$ (ksi)	$f_{t,loc}$ (ksi)	ϵ_{loc} (in./in.)
1	Molded	0.87	0.94	0.90	0.0020	0.89	0.95	0.93	0.0023
	Extracted	0.67	0.88	0.85	0.0025	0.74	0.86	0.86	0.0024
3	Molded	0.92	1.03	0.98	0.0028	0.90	1.06	1.02	0.0026
	Extracted	0.96	1.06	1.05	0.0034	0.94	1.11	1.08	0.0046

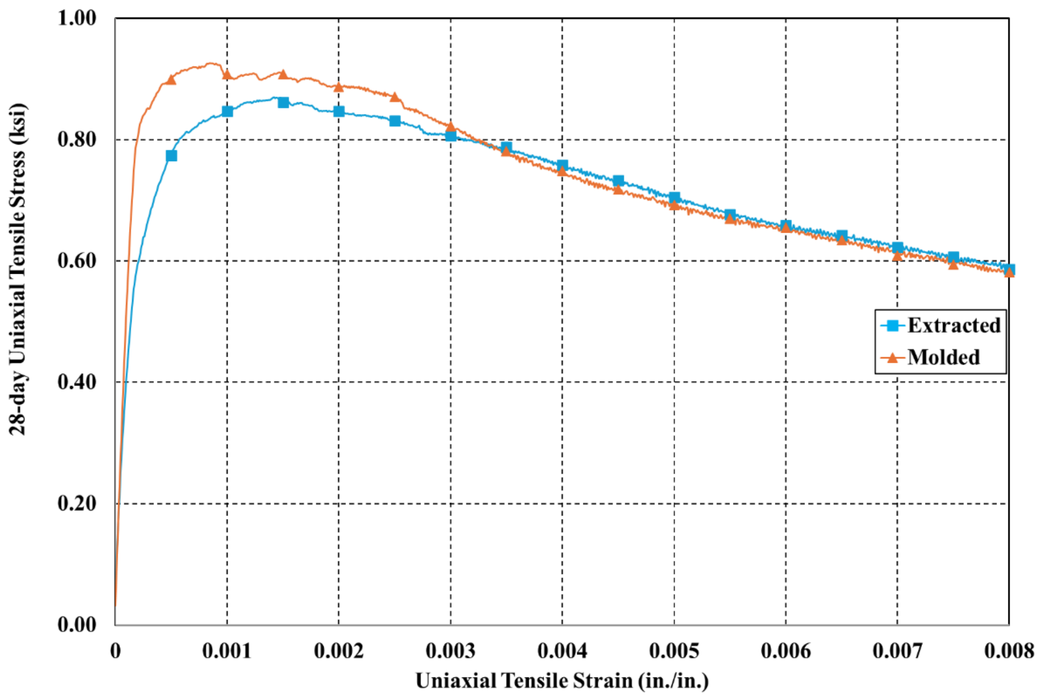

Figure 6-17: 28-Day Direct-Tensile Result for Trial 1

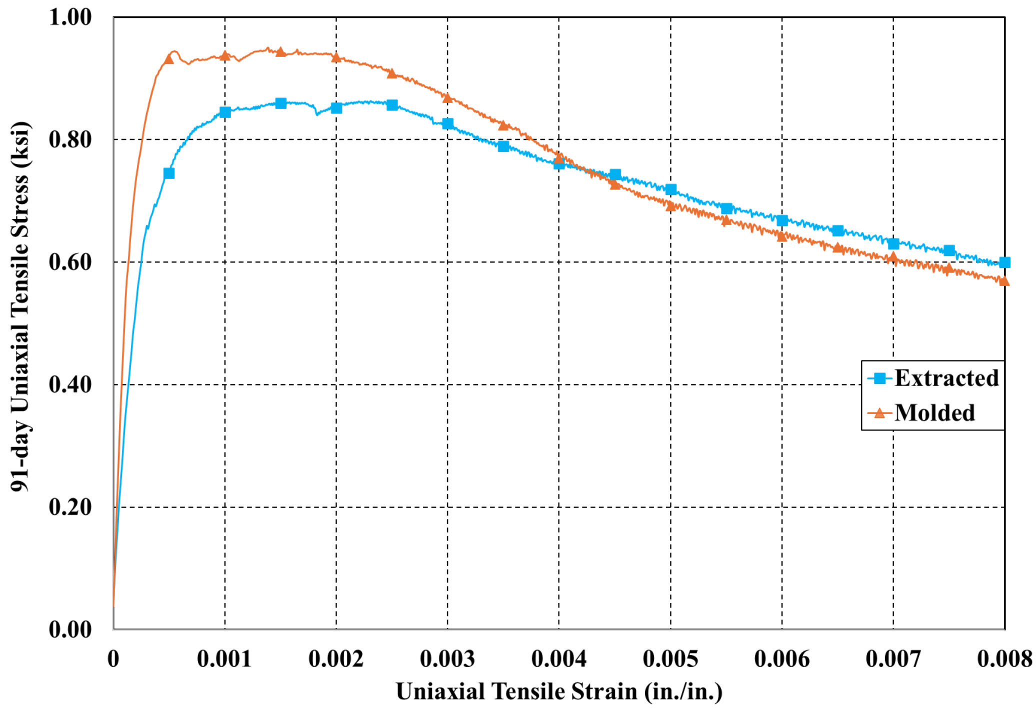

Figure 6-18: 91-Day Direct-Tensile Result for Trial 1

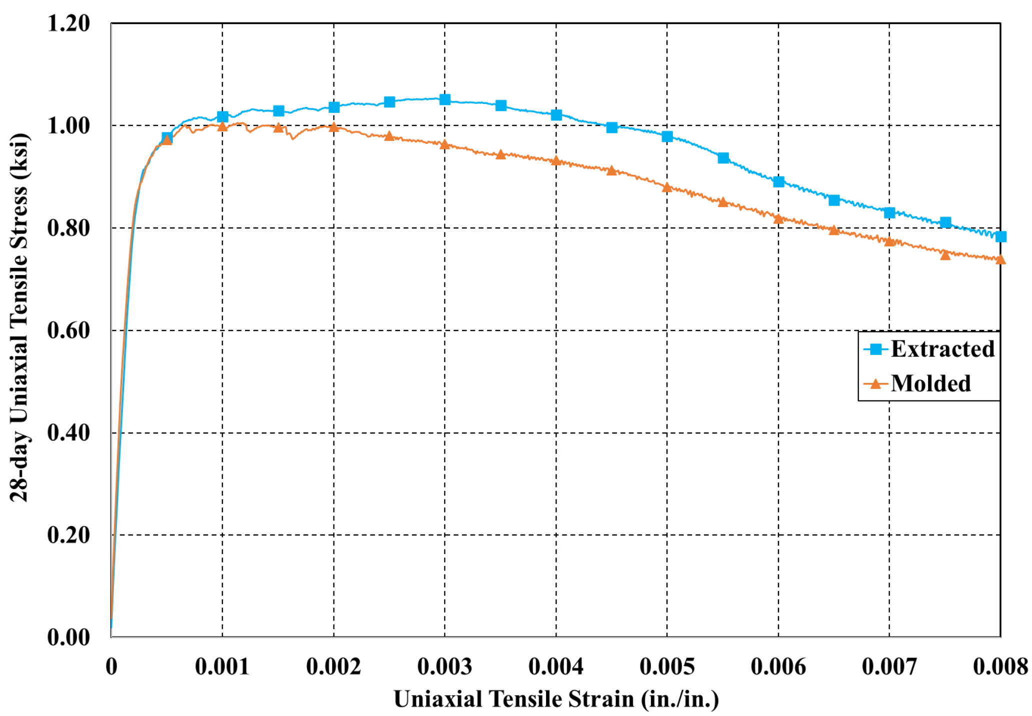

Figure 6-19: 28-Day Direct-Tensile Result for Trial 3

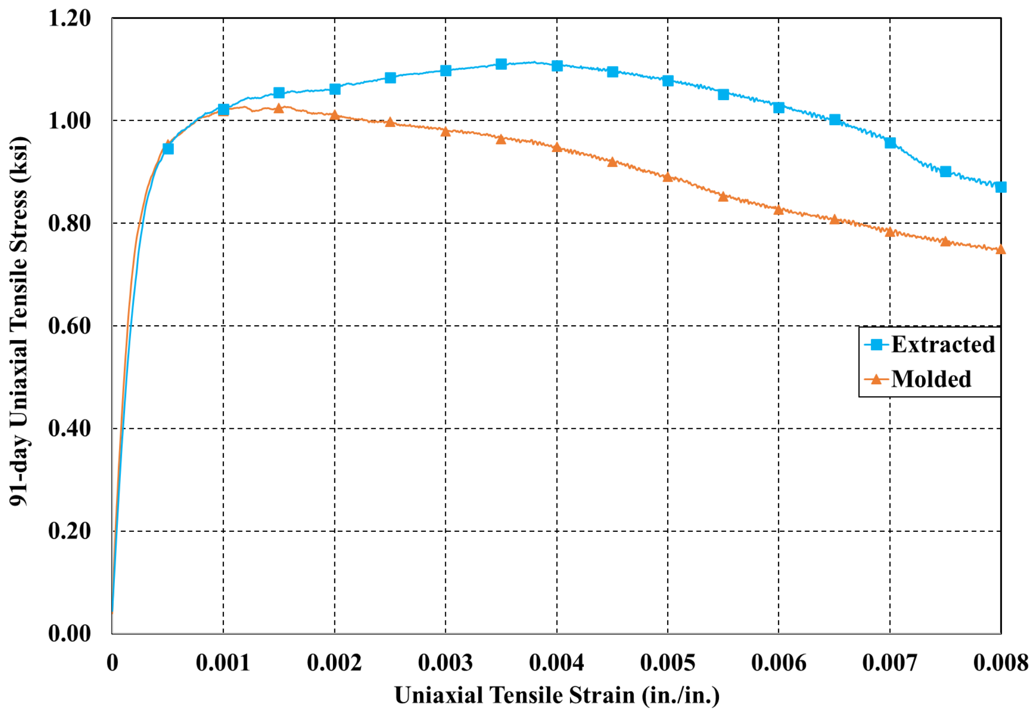

Figure 6-20: 91-Day Direct-Tensile Result for Trial 3

6.6 Comparison of Field-Scale and Laboratory Specimens

An important question for ALDOT implementation is whether UHPC produced at field scale in a ready mixed concrete truck achieves comparable hardened properties to the laboratory mixed UHPC baseline. In other words, can UHPC be successfully scaled from laboratory conditions to field-scale conditions. The following sections compare the compressive strength, flexural strength, and direct tensile performance of the field-scale Trial 3 UHPC against the laboratory result for the equivalent mixture (1.5% fiber, ternary blend, 0.20 water to binder ratio) from Chapter 5. Both molded and extracted specimens from the field-scale trial are included where applicable. Molded specimens were cast into standard molds alongside the field-scale placement and represent the same specimen casting protocol used for the laboratory baseline, making them the most direct basis for comparison. As a reminder, the slab specimens were cured in ambient laboratory conditions for 7 days, after which they were saw-cut to obtain the extracted specimens with the desired width and depth. After 7 days, the extracted specimens were cured in the temperature- and humidity-controlled room matching the description of ASTM C157 (2017) until testing at either 28 or 91 days.

6.6.1 Compressive Strength Results

Figure 6-21 compares the compressive strength development of the field-scale and laboratory mixed UHPC from 1 day through 91 days. At early ages, the two materials exhibited slight difference in strength development. The field-scale mixture achieved a slightly higher 1-day compressive strength of approximately 8,100 psi compared to approximately 6,600 psi for the laboratory mixture. By 7 days, however, the laboratory mixture had a higher strength compared to the field-scale result, reaching approximately 14,000 psi compared to approximately 11,900 psi. This reversal in early age behavior can be attributed to the differences in curing environment and heat generation between a 2 ft^3 laboratory batch and a 2 yd^3 field batch. The larger field-scale volume generates more heat of hydration in the first 24 hours, which accelerates initial strength gain relative to a smaller laboratory batch cured at a more moderate temperature.

By 28 days, the laboratory mixture reached approximately 17,600 psi while the field-scale mixture reached approximately 15,700 psi. The gap continued to narrow at 56 days, where the two materials were nearly equivalent at approximately 18,100 psi and 17,900 psi, respectively. The 91-day laboratory result continued to increase, reaching approximately 19,000 psi. The field-scale 91-day result, however, decreased to approximately 17,000 psi, falling below the 56-day value. This apparent decrease is not believed to reflect an actual loss of compressive strength. Rather, it is attributed to challenges associated with cylinder end preparation and specimen condition at the time of testing. Regardless, both the laboratory and field-scale compressive strengths reached the 17,500 psi threshold of UHPC at 56 days, confirming that field-scale production in a ready mixed concrete truck does not compromise the compressive performance of this UHPC.

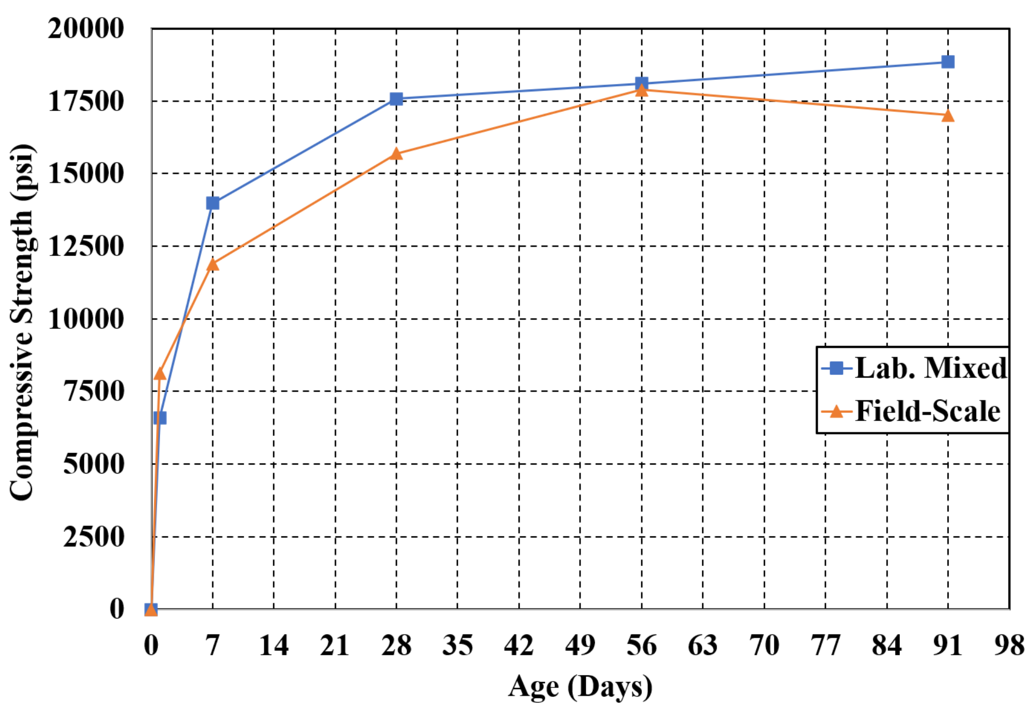

Figure 6-21: Compressive Strength Comparison of Field-Scale and Laboratory Mix

6.6.2 FLEXURAL STRENGTH RESULTS

Figures 6-22 and 6-23 present the 28-day and 91-day flexural stress versus midspan deflection responses for the laboratory-mixed molded prisms, field-scale molded prisms, and field-scale extracted prisms. Table 6-6 summarizes the first-peak stress (f_1) and peak flexural stress (f_P) for each.

Because both the laboratory and field-scale molded specimens were cast into 3 x 3 in. prismatic molds, the molded-to-molded comparison provides the most controlled evaluation of whether field-scale production affects flexural performance. At 28 days, the field-scale molded specimens reached a peak flexural stress of 2,240 psi compared to 2,650 psi for the laboratory molded specimens. At 91 days, the field-scale molded specimens reached a peak of 2,610 psi, within 2% of the laboratory result of 2,660 psi. This convergence indicates that the field-scale UHPC achieves equivalent flexural capacity to the laboratory mixed material at later ages, and that the 28-day difference reflects a slightly slower rate of strength development rather than a significant difference in the UHPC performance.

The first-peak stress for the field-scale molded specimens was lower than the laboratory baseline at both ages (1,405 psi versus 2,025 psi at 28 days, and 1,580 psi versus 2,000 psi at 91 days). These values represent the onset of matrix cracking as identified from the flexural stress versus midspan deflection curve which are sensitive to the specific rate of loading during the test, which can vary within the permissible range of ASTM C1609/C1609M (2019). The peak flexural stress, which governs the structural contribution of the steel fibers, is a meaningful metric for evaluating field-scale performance. The extracted specimens exhibited the highest peak flexural stress of all three specimen types, reaching 2,740 psi at 28 days and 3,340 psi at 91 days. This difference across the molded and extracted specimens tracks across the field-scale result of Trial 1 and 3. Although the reason for the higher flexural strength is unknown, the following mechanism might have contributed to this difference. Placement in a full-scall slab provided approximately 35 in. of uninterrupted flow from the discharge point to the spacers, compared to roughly 1 in. in the cast prism molds, which provide a longer flow path that might have provided an improvement in fiber orientation in the longitudinal (principal stress) direction. This allowed the UHPC to arrive at zone where the specimens were extracted to have improved steel fiber alignment as compared to the small cast prisms.

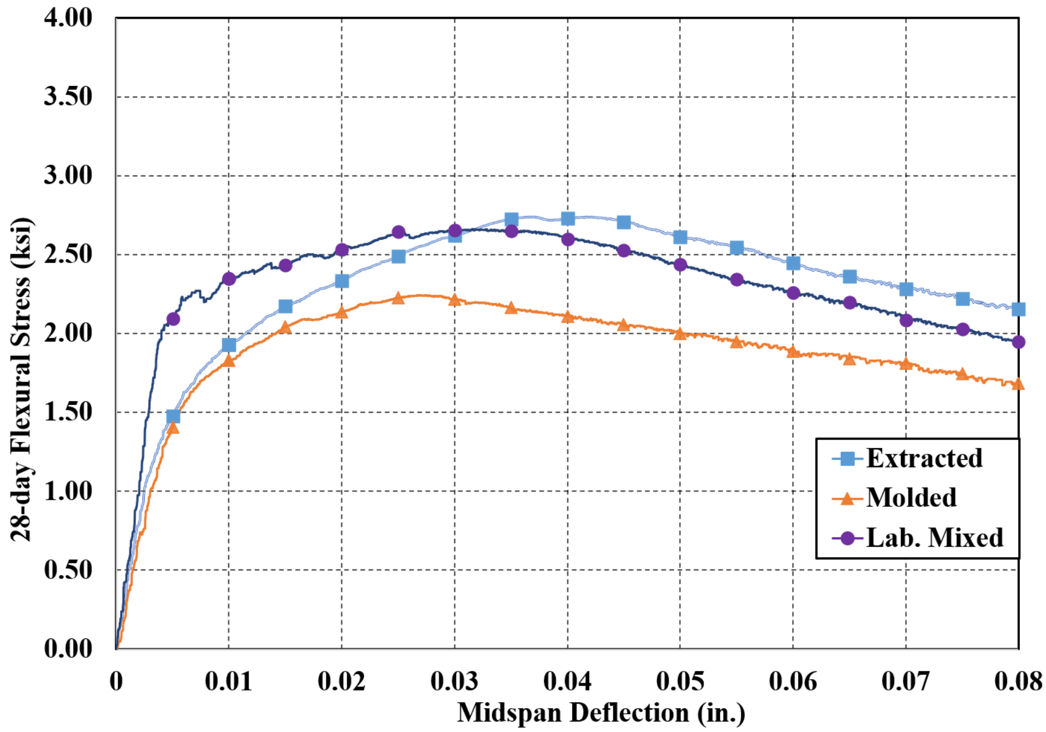

Figure 6-22: Comparison of Field-Scale and Laboratory 28-Day Flexural Strength Result

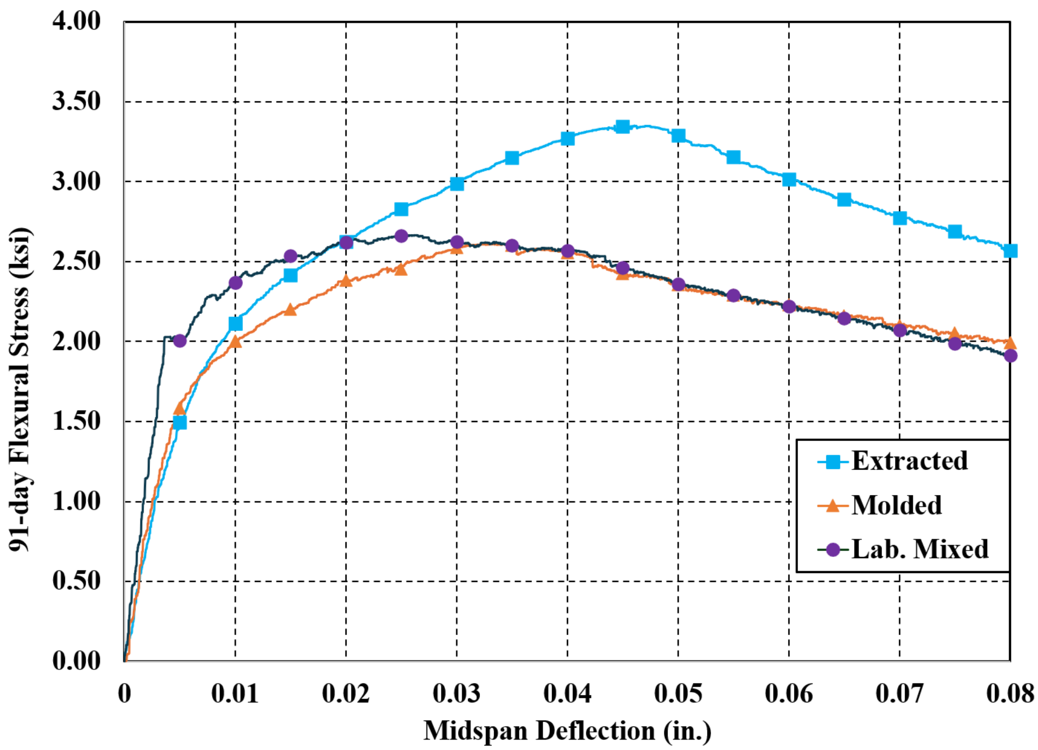

Figure 6-23: Comparison of Field-Scale and Laboratory 91-Day Flexural Strength Result

Table 6-6: Flexural Strength Comparison for Laboratory Mixed and Field-Scale UHPC

		Flexural Strength (psi)			
		28 days		91 days	
Test Type	**Specimen Type**	f_1	f_P	f_1	f_P
Lab. Mixed	Molded	2025	2650	2000	2660
Large Scale: Trial 3	Molded	1405	2240	1580	2610
	Extracted	1390	2740	1600	3340

6.6.3 DIRECT-TENSION RESULTS

Figures 6-24 and 6-25 present the 28-day and 91-day direct-tension results for the laboratory-mixed molded prisms, field-scale molded prisms, and field-scale extracted prisms. Table 6-7 summarizes the direct-tension cracking stress, peak stress, localization stress, and localization strain for each specimen type.

The three curves in Figures 6-24 and 6-25 align closely at both ages. At 28 days, the field-scale molded specimens tracked the laboratory result through the elastic and post-cracking regions of the response, reaching comparable peak stresses of approximately 1,030 psi versus 1,080 psi for the laboratory mixture. The field-scale, extracted specimens reached a marginally higher peak of approximately 1,060 psi and maintained a marginally higher post-peak response. All three specimen types exceeded the FHWA minimum post-cracking tensile strength of 750 psi and the 850 psi threshold proposed in this study.

At 91 days, similar results were observed. The laboratory mixture reached marginally higher peak stress of approximately 1,180 psi, followed by the field-scale extracted specimens at 1,110 psi and the field-scale molded specimens at 1,060 psi. However, these differences are not significant if one considers the precision associated with direct-tension testing.

This comparison confirms that the non-proprietary UHPC developed in this research can be produced at field scale in a ready mixed concrete plant and achieve tensile performance that is comparable to laboratory-produced material, provided that the mixing procedure prevents the formation of cement balls.

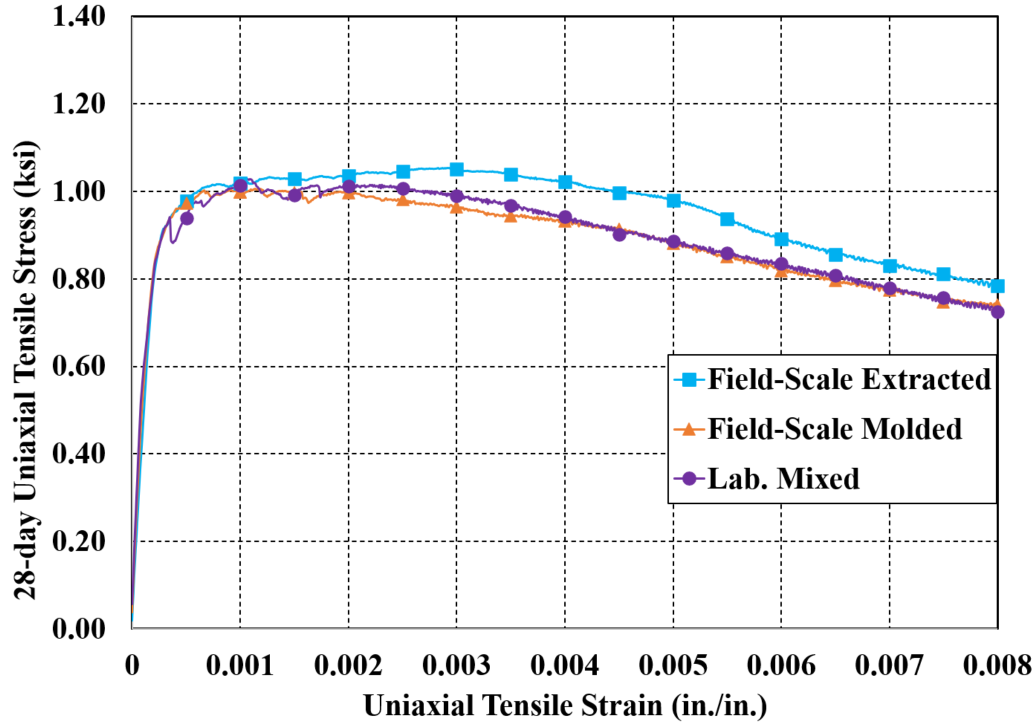

Figure 6-24: Comparison of Field-Scale and Laboratory 28-Day Direct Tensile Results

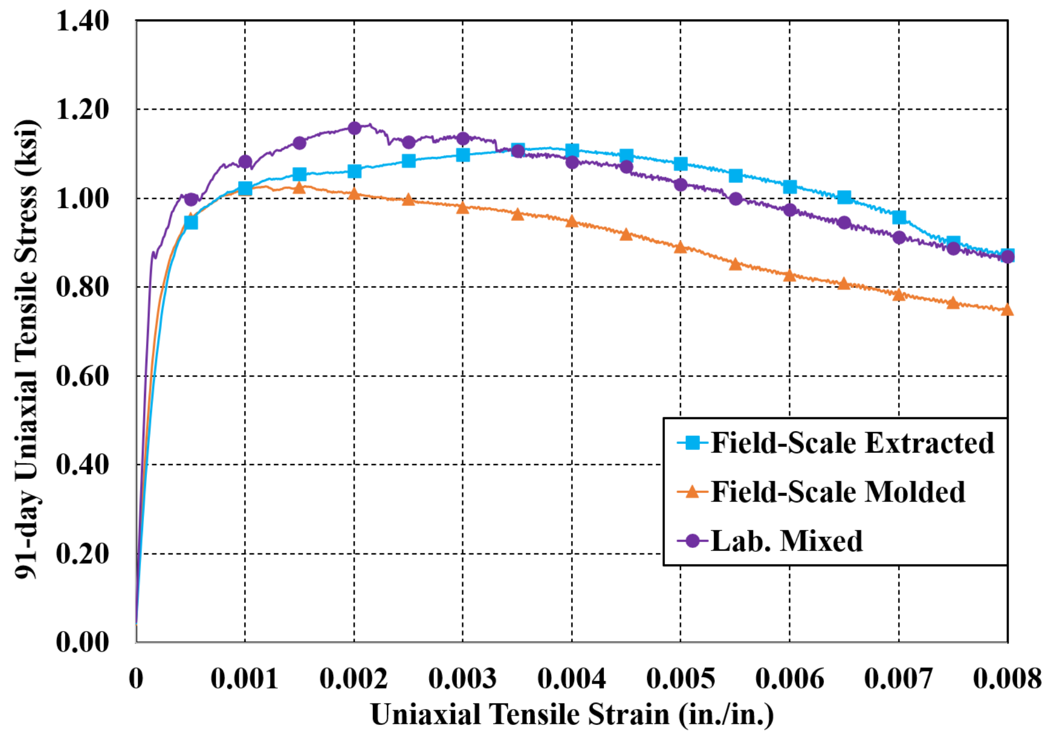

Figure 6-25: Comparison of Field-Scale and Laboratory 91-Day Direct Tensile Results

Table 6-7: Direct Tension Comparison for Laboratory Mixed and Field-Scale UHPC

		Direct-Tension Results							
		Concrete Age of 28 days				Concrete Age of 91 days			
Test Type	**Specimen Type**	$f_{t,cr}$ (ksi)	$f_{t,peak}$ (ksi)	$f_{t,loc}$ (ksi)	$\epsilon_{t,loc}$ (in./in.)	$f_{t,cr}$ (ksi)	$f_{t,peak}$ (ksi)	$f_{t,loc}$ (ksi)	$\epsilon_{t,loc}$ (in./in.)
Lab. Mixed	Molded	0.87	1.08	1.00	0.0028	1.00	1.18	1.10	0.0040
Large-Scale: Trial 3	Molded	0.92	1.03	0.98	0.0028	0.90	1.06	1.02	0.0026
	Extracted	0.96	1.06	1.05	0.0034	0.94	1.11	1.08	0.0046

6.7 Summary

The field-scale production trials demonstrated that non-proprietary UHPC can be produced at field scale in a ready mixed concrete plant using materials that are locally available in Alabama. Three trials were conducted to develop a loading and mixing sequence that prevents cement balling, which was the primary challenge encountered when transitioning from laboratory to field-scale production of UHPC. The final loading sequence from Trial 3, detailed in Section 6.3.3, successfully eliminated cement balls and produced UHPC with the desired flow and workability throughout mixing, transportation, and placement.

All hardened property results from the successful full-scale trial, Trial 3, were similar when compared to those obtained from the laboratory-scale testing phase covered in Chapter 5. In contrast, Trial 1, which contained cement balls, produced measurably lower flexural and tensile results, confirming that cement balls have a detrimental effect on hardened performance and must be prevented by using effective batching and mixing procedures.

CHAPTER 7
DISCUSSION OF IMPLEMENTATION RECOMMENDATIONS

7.1 Introduction

The purpose of this chapter is to provide implementation recommendations for the use of non-proprietary UHPC on ALDOT projects. These recommendations are based on the material characterization results covered in Chapter 5, the field-scale production trials documented in Chapter 6, and specifications reviewed from various state departments of transportation. These recommendations include a *draft* special provision for the use of UHPC that is included in Appendix A.

7.2 Materials

The UHPC developed in this study was produced from materials available to the Alabama concrete industry, with the majority of the materials from Alabama. Only materials that are compliant with the Build America, Buy America Act were considered. Type IL portland-limestone cement produced by Argos Cement in Alabama was used. Slag cement was obtained from Heidelberg Materials. Silica fume (also referred to as microsilica) was Elkem Microsilica, procured through Elkem Materials. The fine aggregate was natural river sand meeting AASHTO M 6 (2022), sourced locally from near Montgomery, Alabama. The high-range water-reducing admixture (Master Glenium 7920) and the hydration control admixture (MasterSet DELVO) were obtained from Master Builders Solutions. Steel fibers were sourced from Tokusen fiber and Sumiden Wire, both providing straight high tensile strength fibers (>400 ksi) conforming to ASTM A820 with a nominal length of 0.51 in. and a nominal diameter of 0.008 in.

Different materials can be adopted to produce UHPC depending on the producer's capability and local materials to meet ALDOT requirement. Therefore, it is recommended that ALDOT adopt a performance-based approach to UHPC acceptance rather than prescribing specific mixture proportions. The results from Chapter 5 demonstrate that the FHWA performance requirements can be met with a range of constituent proportions, provided the materials meet the applicable ASTM and AASHTO standards. Note that some ASTM standards are necessary because some of these are not covered by AASHTO. The producer should have the flexibility to proportion UHPC to meet the performance thresholds established in Section 7.5 using locally available materials. The mixture proportions used in this study, as documented in Chapter 3, can serve as a reference mixture that has been validated through both laboratory and field testing.

7.3 Mixing and Production

7.3.1 Laboratory-Scale Mixing

It is recommended that laboratory mixing of UHPC be performed using a planetary high-shear mixer. The high-shear action is necessary to disperse fine cementitious particles, particularly silica fume, and prevent agglomeration. Conventional drum or pan mixers do not provide sufficient mixing energy for UHPC and are therefore not recommended.

The laboratory mixing sequence used in this study is as follows. Sand and silica fume are combined and mixed for 5 minutes. Cement and slag cement are added and mixed for 5 minutes. Eighty percent of the mixing water, combined with the HCA, is introduced and mixed for 3 minutes. The remaining 20% of the water and the HRWRA are added, and then mixing continues for 5 to 15 minutes until the mixture reaches a fluid consistency. Steel fibers are then added at the end and mixed for 5 minutes to achieve uniform dispersion. The flow should be verified per ASTM C1856 after fiber addition, with a target of 7 to 11 inches.

7.3.2 Field-Scale (Ready Mixed Concrete Truck) Production

A ready mixed concrete truck does not provide the same shear energy as a planetary mixer. The drum rotation blends constituents effectively but cannot break up all agglomerations once they have formed. As documented in Chapter 6, when having a mixture with a very low water content as is the case with UHPC, loading dry cementitious materials directly onto moist fine aggregate in a ready mixed concrete truck produced cement ball agglomerations that should be avoided. The loading sequence must therefore be designed to prevent cement balling rather than relying on the mixing energy to break up the cement balls.

The recommended field-loading sequence, developed through three full-scale trials covered in Chapter 6, is as follows:

- At the Concrete Plant:
  Moisture corrections are determined to adjust the water and aggregate batch weights based on the moisture content of the fine aggregate. All portland cement and fine aggregate are loaded with 60% of the total mixing water. The HCA is premixed with 10% of the total water and added to promote early hydration control. An additional 10% of the total water is premixed with 20% of the HRWRA and added to aid early dispersion to avoid cement balling. This initial load in the truck is mixed for 4 minutes at full mixing speed. Next, slag cement is then loaded with 80% of the HRWRA and the remaining 20% of the total water and all this material mixed for 4 minutes at full mixing speed. Next, the silica fume is added and the material mixed for 4 minutes at full mixing speed. Once mixing is complete, the truck is ready to leave for the job site. The total plant mixing time is approximately 30 minutes.

- At the Jobsite:

  If by visual inspection the flow appears insufficient, additional HRWRA can be added and mixed in for 4 minutes at full mixing speed. The addition of additional HRWRA can be expected because the flow could be impacted by changes in temperature and transport time. Steel fibers are then added to the fluid mixture and the material mixed for an additional 5 minutes.

Three principles govern this procedure. First, a portion of the mixing water and the HCA should be introduced early to the portland cement form a paste with sufficient fluidity and to delay the rate of cement hydration. Second, cementitious materials should be added sequentially to material already in a semi-workable state. Third, steel fibers are added only after the mixture has reached a fluid state.

Throughout the mixing procedure, full mixing speed is preferred. However, if the material quantity in the drum is low, the mixing speed should be reduced to ensure that the drum is effectively mixing the materials rather than simply tossing it to the sides of the drum. The temperature of the mixture, measured in accordance with AASHTO T 309, should remain below 90°F to prevent accelerated hydration of the large quantity of cementitious material. Flow should be tested as per ASTM C1437 with modifications from ASTM C1856 after fiber addition, with the allowable flow from 7 in. to 11 in. During the field trials conducted in this study in the summer months, an HCA at a dosage of 6 fl oz/cwt of the total cementitious materials content maintained adequate workability throughout the full 90-minute batching and placement window.

Therefore, the recommended time limit for placement is 1 hour and 45 minutes, measured from the first addition of water to the cementitious materials until placement of the load is completed. Since UHPC is produced with hydration-control admixtures and requires additional mixing no limit on revolutions is recommended. .

7.4 Formwork, Placement, Finishing, and Curing

UHPC is a self-consolidating, thixotropic material that fills and consolidates without vibration, ; therefore, any unsealed gaps in the formwork could provide paths for paste or mortar to leak out of the form. Loss of paste at a form joint could potentially lead to surface voids and honeycombing. The forms are therefore required to be non-absorbent and leak-tight, sealed to contain the UHPC. Formwork should be made from with non-absorptive materials such as metal or sealed plywood so they do not draw water from the mixture at the formed face. This requirement follows the practice reviewed in Section 2.9. The Texas special specification requires non-absorptive formwork sealed to contain UHPC, and the draft special provision adopts the same approach by requiring leak-tightness to be demonstrated during the mock placement before the first production placement.

With an allowable flow range of 7 to 11 inches, the UHPC is self-consolidating and requires no external vibration. Placement is performed by discharging directly into the formwork. Because UHPC is thixotropic, the exposed surface begins to stiffen relatively quickly after placement, which narrows the window for screeding and finishing. If evaporation is also occurring, particularly in warm or windy conditions, the stiffening surface can develop a wrinkled texture known as "elephant skin," as discussed in Section 2.8. Surface finishing should therefore be completed as quickly as feasible, and a resin-based curing compound meeting ASTM C309 should be applied at the manufacturer's recommended coverage rate immediately after screeding. In this study, a curing compound sourced in Alabama was applied on that basis and no cracking or surface defects, including elephant skin, were observed on the field-placed slabs.

Prior to the first production placement, a full-scale representative mockup is required to confirm that the formwork, crew, equipment, mixing procedure, and construction methods result in UHPC that is acceptable for the intended application. The mockup provides the setting to verify form leak-tightness and to demonstrate that the UHPC producer and contractor can execute the approved placement plan. After curing, two cross sections of the hardened mockup could be cut and examined for segregation or non-uniformity that would not be apparent from the surface alone.

7.5 Acceptance and Quality Control Testing Requirements

The UHPC acceptance criteria recommended for ALDOT are performance based and are summarized in Table 7-1. Either the direct-tension or flexural requirement needs to be met, not both. This option is provided, because in some laboratories flexural strength testing might be preferred over direct-tension testing.

Table 7-1: Recommended Mixture Design Approval Criteria for UHPC

Requirement	Test	Specification	Specimen Size	Number of Specimens	Acceptance Requirement
Yes	Compression	ASTM C39 per ASTM C1856	3 x 6 in. cylinder	3 (At least 2 valid results)	≥ 17,500 psi at 56 days
Select either direct-tension or flexural testing	Direct Tension	AASHTO T 397	2 x 2 x 17 in. prism	4 (At least 2 valid results)	$f_{t,cr}$ ≥ 850 psi at 28 days and $f_{t,loc} > f_{t,cr}$
	Flexural	ASTM C1609 per ASTM C1856	3 x 3 x 14 in. prism	3 (At least 2 valid results)	f_P ≥ 2,300 psi and f_P/f_1 ≥ 1.25 at 28 days

7.5.1 Compressive Strength Testing

Compressive strength is governed by the cementitious matrix; steel fiber dosage does not significantly influence the compressive result (Section 5.2). Compressive testing therefore confirms the quality of the batching process and the cementitious system. The minimum compressive strength of 17,500 psi is consistent with the FHWA definition of UHPC (Graybeal and El-Helou 2023) and the ACI 239 report (ACI PRC-239.1-24). The compressive strength should be tested on 3 x 6 in. cylinders with both ends ground flat, in accordance with the modifications specified in ASTM C1856 for UHPC. It is recommended to produce three cylinders per test age, with the average of the results used for acceptance. For the results to be valid, at least two specimens should meet the precision statement of AASHTO T 22.

The compressive strength acceptance age of 56 days is recommended because UHPC contains a large volume of silica fume and slag cement that contribute to later-age strength development. The results from Chapter 5 showed that several batches did not consistently exceed 17,500 psi at 28 days but reached this threshold by 56 days. UHPC continues to gain significant compressive strength between 28 and 56 days due to ongoing hydration and pozzolanic reactions, and the 56-day acceptance age captures this behavior.

7.5.2 Flexural Testing for Mixture Design Approval

As discussed earlier in this section, either direct-tension or flexural testing need to be performed for UHPC to ensure that it meets the tensile stress requirements. Flexural testing per ASTM C1609 on 3 x 3 x 14 in. prisms loaded at the third points is recommended as the primary mixture design approval test for mixture prequalification. This test is simpler to perform, has a higher success rate, and produces less variability than the direct-tension test. Three specimens per test age are recommended, with a minimum of two specimens required for the test to be considered valid.

The forward analysis in Section 5.8 established that flexural stress results can serve as an indirect verification of tensile performance. The flexural minimum of 2,300 psi for peak stress corresponds to the 850 psi direct-tension test threshold based on the parametric analysis in Section 5.8.4. The ductility ratio of f_P / f_1 ≥ 1.25, consistent with PCI practice, confirms that the UHPC exhibits adequate post-cracking load carrying behavior. A ratio below 1.25 indicates that the contribution of the steel fibers is insufficient to sustain post-cracking capacity, regardless of the absolute peak stress value.

7.5.3 Direct-Tension Testing For Mixture Design Approval

Considering that the length of the steel fibers is approximately 0.5 inches, direct-tension testing should be performed on2 x 2 x 17 in. prisms in accordance with AASHTO T 397 and with the testing protocol refinements as discussed in Chapter 4 to improve the number of successful tests.

It is recommended to produce four specimens per test age, with the average of the results used for acceptance. For the results to be valid, at least two specimens should yield valid results. This accounts for the inherent variability and lower success rate of the direct-tension test documented in Chapter 4. Acceptance should be based on stress-based metrics only. Strain based results exhibit high variability (Section 5.7) and are not recommended for specification limits. Instead, ductility should be confirmed by ensuring the ratio of the localization stress to the effective cracking stress is greater than 1.0.

A minimum direct-tension stress of 850 psi is recommended, providing a safety margin above the FHWA requirement of 750 psi. This higher threshold accounts for the variability inherent in the direct-tension test and the increased variability associated with field-produced concrete. As confirmed by the results in Section 5.2, a 1.5% fiber dosage produces effective cracking stresses above 850 psi at 28 days.

The direct-tension and flexural testing requirements described herein are intended for prequalification of the UHPC proportions prior to field production. Once the mixture proportions have been prequalified through these tests, field quality assurance testing can be performed by only using compressive strength testing. This is practical for two reasons. First, compressive strength testing is straightforward to perform with the equipment and expertise currently available in Alabama, making it an immediately implementable requirement at this early stage of UHPC adoption in the state. Second, the purpose of field quality assurance testing is to confirm that individual batches have been produced correctly. Errors or variability in batching primarily affect the cementitious matrix, and compressive strength is directly sensitive to these changes. Tensile performance, by contrast, is governed primarily by the steel fiber type and dosage (Section 5.2), which are established during prequalification. Compressive strength testing can therefore serve as a practical indicator of batch-to-batch production acceptance. This approach is consistent with the practice of other state DOTs as reviewed in Section 2.9, where field testing requirements are typically limited to flow, temperature, and compressive strength testing.

7.6 Cost Considerations

The cost analysis in Section 5.10 showed that steel fibers account for 62% to 65% of the total material cost of non-proprietary UHPC at a 1.5% dosage, with the total estimated between $640 to $760 per cubic yard. The fiber dosage is driven by the tensile and flexural performance requirements, which means the required performance level effectively drives the cost of the UHPC.

In applications requiring the full FHWA tensile performance (closure pours, connections, overlays), the fiber dosage is the primary cost driver and should be optimized to meet the performance threshold without excess. For the non-proprietary UHPC produced in this study, a 1.5% steel fiber dosage provides adequate margin above the 850 psi effective cracking stress threshold recommended in Section 7.5.

The performance-based approach recommended in this report allows ALDOT to specify the required mechanical properties and let the producer optimize the mixture to meet the performance-based requirements at the lowest cost.

7.7 Draft Special Provision

A draft special provision for ALDOT to consider was developed for this project as is available in Appendix A. It was developed after considering the laboratory and field-scale findings from this study, and the specifications reviewed from state departments of transportation as presented in Section 2.9. This draft special provision is intended for field-cast UHPC applications that include applications such as closure pours, joint repairs, link slabs, and beam-end repairs. By using performance-based requirements, this draft special provision accommodates both proprietary (prepackaged) and non-proprietary UHPC.

CHAPTER 8
SUMMARY, CONCLUSIONS, AND RECOMMENDATIONS

The work performed during this study is aimed at developing, characterizing, and ensuring effective implementation of non-proprietary UHPC for the Alabama transportation industry. In this chapter, the work performed is summarized, conclusions are offered, and recommendations are provided based on the completed work.

8.1 Summary of Work Performed

This study developed and characterized non-proprietary UHPC using locally available Alabama materials, with the objective of meeting the FHWA performance requirements at a much-reduced cost when compared to commercially available proprietary UHPC.

The laboratory phase of the work produced more than twenty-five batches of non-proprietary UHPC to evaluate the influence of the following five constituent variables on the fresh and hardened properties: steel fiber dosage, fine aggregate gradation, cementitious blend type, silica fume dosage, and water-binder ratio. Each variable was assessed through compressive, flexural, and direct-tension testing at 28 and 91 days, and select mixtures were tested for freeze-thaw durability through 300 cycles. During this testing program, the direct-tension test (AASHTO T 397) implemented with a 220-kip, wedge-grip machine initially exhibited a low success well below what would be practical for use as a quality control test. A systematic protocol was thus developed to address specimen preparation, crosshead alignment, and gripping sequence, which improved the success rate from 44% to 75% without requiring any additional equipment beyond what is required in AASHTO T 397. The direct-tension testing also revealed that stress-based metrics were reliable and consistent across all mixture variables, whereas strain-based metrics exhibited high scatter with no discernible dose-response relationship.

Findings from the direct-tension testing motivated the development of a forward analysis to relate the direct-tension stress results to the more practical and reliable flexural test results. The analysis established equivalent flexural acceptance criteria corresponding to the FHWA tensile requirements, providing ALDOT with an option to use flexural testing for quality assurance purposes. A cost analysis was also performed to quantify the material cost per cubic yard and identify the dominant cost driver within the mixture.

With the laboratory testing phase complete, three field-scale trials were conducted at an Alabama ready mixed concrete plant. During these full-scale trials two cubic yards of UHPC were produced in a ready mixed concrete truck. During each full-scale trial the mixing and loading sequence was progressively adjusted to eliminate cement balling during mixing. The fresh and hardened properties of the UHPC were tested during the field trials on molded specimens and specimens extracted from slabs cast with the UHPC.

8.2 CONCLUSIONS

From the material characterization program, the following conclusions are drawn regarding materials and mixture proportioning as it relates to producing non-proprietary UHPC in Alabama:

- Steel fiber dosage was the constituent variable that most significantly affected the tensile and flexural performance of UHPC. Compressive strength was influenced by the cementitious matrix and was not meaningfully affected by steel fiber content.
- A fiber dosage of 1.50% by volume produced a peak flexural stress above 2,800 psi, and a post-cracking tensile strength above 850 psi at 28 days, providing adequate margin above the FHWA minimum of 750 psi.
- Standard AASHTO M 6 natural river sand performed comparably when compared to masonry sand and an optimized gradation of fine particles. No specialized aggregates or gradation optimization is required for non-proprietary UHPC in Alabama.
- Binary blends without silica fume matched the strengths obtained from the ternary blends; however, the binary blends exhibited rapid loss of workability that makes them impractical for field production. A ternary blend that contains portland cement, silica fume, and slag cement is recommended.
- Silica fume dosages of 9%, 12%, and 15% of total binder content produced acceptable mechanical property results; therefore, the minimum dosage of 9% is sufficient.
- The water-to-binder ratio affected compressive strength as expected but did not significantly change the tensile or flexural response across the 0.18 to 0.22 range evaluated. A ratio of 0.20 is recommended, but this can be adjusted to meet specified performance requirements.
- All UHPC mixtures tested were inherently resistant to freeze-thaw degradation through 300 cycles without need for any air entraining admixture.

From the laboratory testing program to evaluate the tensile and flexural response of UHPC, the following conclusions are drawn:

- Stress-based metrics from the direct-tension test (effective cracking stress, peak stress, and localization stress) in accordance with AASHTO T 397 showed clear, repeatable trends across all mixture variables. Strain-based metrics from the direct-tension test exhibited high variability and are not suited for specification or acceptance.
- The testing protocol refinements developed for AASHTO T 397 in this study improved the success rate from 44% to 75% using the same wedge-grip equipment, with no additional capital investment required.
- A forward analysis was developed to reliably estimate the flexural stress response of UHPC from the direct-tension test stress results.
- A minimum peak flexural stress of 2,000 psi corresponds to the FHWA minimum effective cracking stress of 750 psi. A minimum peak flexural stress of 2,300 psi corresponds to the minimum effective cracking stress 850 psi threshold proposed in this study.

- A ductility ratio of the peak flexural stress to the first-peak flexural stress (f_P / f_1) no less than 1.25, consistent with PCI practice, is proposed as an additional acceptance criterion to confirm adequate post-cracking behavior when testing the flexural response of UHPC.

From the cost analysis, the following conclusions are drawn:

- Steel fibers account for 62% to 65% of the total material cost at a 1.5% dosage, with the total cost of non-proprietary UHPC estimated between $640 to $760 per cubic yard.
- Reducing the fiber dosage from 2.0% to 1.5% saves approximately $140 per cubic yard while still exceeding the FHWA tensile requirement with adequate margin.

From the field-scale production trials, the following conclusions are drawn:

- Non-proprietary UHPC can be produced under full-scale conditions in a ready mixed concrete plant using materials available to the Alabama concrete industry.
- Cement balls formed when dry cementitious materials came into contact with moisture in the fine aggregate before adequate dispersion had taken place. These cement balls had a measurable detrimental effect on the hardened properties of the placed UHPC. Extended mixing to break up cement balls after they have formed is not a viable remedy, as the time required raises the mixture temperature and depletes the available working window.
- The loading sequence from full-scale Trial 3, in which the mixing water and hydration-control admixture are introduced early and cementitious materials are added sequentially into an already wetted environment, successfully eliminated cement balls.
- The hardened properties of the field produced UHPC from Trial 3 were comparable to the laboratory baseline, confirming that non-proprietary UHPC can reliably be produced under full-scale conditions using the procedures developed in this study.

8.3 Recommendations

From the results of the study the following recommendations are made:

- ALDOT adopts a performance-based approach to UHPC acceptance rather than prescribing specific mixture proportions.
- Since flexural testing per ASTM C1609 is easier to perform and produces more reliable results than AASHTO T 397, flexural testing is recommended as the primary test prequalification of the UHPC proportions. Once the mixture proportions have been prequalified through either flexural or direct-tension testing, routine field quality control can rely on compressive strength testing alone.
- To characterize either tensile behavior, the following 28-day mixture design approval requirement is recommended for ALDOT that provides a safety margin above the FHWA minimums and accounts for the variability inherent in field produced UHPC:

  - a minimum effective cracking stress of 850 psi in direct tension in accordance with AASHTO T 397, or
  - a minimum peak flexural stress of 2,300 psi with a ductility ratio of f_P / f_1 no less than 1.25 in accordance with ASTM C1609.
- A minimum steel fiber dosage of 1.5% by volume is recommended for applications that are required to meet the FHWA tensile performance requirements.
- The field mixing procedure from Trial 3 (Section 6.3.3) is recommended for ready mixed concrete delivery of UHPC.

8.4 Recommendations for Future Research

From the work conducted the following recommendations for future research are offered:

- ALDOT should consider pursuing a full-scale pilot project using non-proprietary UHPC in an actual bridge closure pour or partial-depth bridge deck application. The laboratory and field production results from this study should be used to evaluate the draft special provision under actual construction conditions.
  - Trial projects should evaluate both a flowable UHPC application (such as a closure pour) and a low-flow UHPC application (such as a partial-depth bridge deck) to assess the specification across the range of field conditions ALDOT may encounter.
- Conduct a comprehensive shrinkage study to characterize the autogenous and drying shrinkage behavior of the non-proprietary UHPC developed in this study. This is necessary for designing connections and overlays where restrained shrinkage may induce cracking or affect bond with adjacent elements.
- Perform testing to evaluate the structural performance of UHPC in full-scale elements in applications representative of ALDOT bridge construction.

REFERENCES

AASHTO M 6. 2022. Standard Specification for Fine Aggregate for Hydraulic Cement Concrete. Washington, DC: American Association of State Highway and Transportation Officials.

AASHTO M 45. 2024. Standard Specification for Aggregate for Masonry Mortar. Washington, DC: American Association of State Highway and Transportation Officials.

AASHTO R 119. 2024. Standard Practice for Making and Curing Concrete Test Specimens in the Laboratory. Washington, DC: American Association of State Highway and Transportation Officials.

AASHTO T 22. 2022. Standard Method of Test for Compressive Strength of Cylindrical Concrete Specimens. Washington, DC: American Association of State Highway and Transportation Officials.

AASHTO T 161. 2022. Standard Method of Test for Resistance of Concrete to Rapid Freezing and Thawing. Washington, DC: American Association of State Highway and Transportation Officials.

AASHTO T 277. 2023. Standard Method of Test for Electrical Indication of Concrete's Ability to Resist Chloride Ion Penetration. Washington, DC: American Association of State Highway and Transportation Officials.

AASHTO T 309. 2022. Standard Method of Test for Temperature of Freshly Mixed Hydraulic-Cement Concrete. Washington, DC: American Association of State Highway and Transportation Officials.

AASHTO T 397. 2022. Standard Method of Test for Uniaxial Tensile Response of Ultra-High Performance Concrete. Washington, DC: American Association of State Highway and Transportation Officials.

Abokifa, M., and M. A. Moustafa. 2021. "Mechanical Characterization and Material Variability Effects of Emerging Non-Proprietary UHPC Mixes for Accelerated Bridge Construction Field Joints." Construction and Building Materials 308 (November): 125064.

AFGC (Association Française de Génie Civil). 2013. Ultra High Performance Fibre-Reinforced Concretes: Interim Recommendations. Paris: AFGC.

Alkaysi, M., S. El-Tawil, Z. Liu, and W. Hansen. 2016. "Effects of Silica Powder and Cement Type on Durability of Ultra High Performance Concrete (UHPC)." Cement and Concrete Composites 66 (February): 47-56.

ACI Committee 239. 2018. *Ultra-High Performance Concrete: An Emerging Technology Report (ACI 239R-18).* Farmington Hills, MI: American Concrete Institute.

ACI Committee 239. 2024. ACI PRC-239.1-24: What is Ultra-High-Performance Concrete (UHPC)?-TechNote. Farmington Hills, MI: American Concrete Institute.

American Concrete Institute. 2025. ACI Concrete Terminology. Farmington Hills, MI: American Concrete Institute.

Andreasen, A. H. M., and J. Andersen. 1930. "Ueber die Beziehung zwischen Kornabstufung und Zwischenraum in Produkten aus losen Körnern (mit einigen Experimenten)." Kolloid-Zeitschrift 50

(3): 217-28.

ASTM A820/A820M. 2022. Specification for Steel Fibers for Fiber-Reinforced Concrete. West Conshohocken, PA: ASTM International.

ASTM C39/C39M. 2021. Test Method for Compressive Strength of Cylindrical Concrete Specimens. West Conshohocken, PA: ASTM International.

ASTM C78/C78M. 2022. Test Method for Flexural Strength of Concrete (Using Simple Beam with Third-Point Loading). West Conshohocken, PA: ASTM International.

ASTM C157/C157M. 2017. Test Method for Length Change of Hardened Hydraulic-Cement Mortar and Concrete. West Conshohocken, PA: ASTM International.

ASTM C192/C192M. 2019. Practice for Making and Curing Concrete Test Specimens in the Laboratory. West Conshohocken, PA: ASTM International.

ASTM C494/C494M. 2024. Specification for Chemical Admixtures for Concrete. West Conshohocken, PA: ASTM International.

ASTM C595/C595M. 2025. Specification for Blended Hydraulic Cements. West Conshohocken, PA: ASTM International.

ASTM C670. 2015. Practice for Preparing Precision and Bias Statements for Test Methods for Construction Materials. West Conshohocken, PA: ASTM International.

ASTM C1064/C1064M. 2023. Test Method for Temperature of Freshly Mixed Hydraulic-Cement Concrete. West Conshohocken, PA: ASTM International.

ASTM C1202. 2022. Test Method for Electrical Indication of Concrete's Ability to Resist Chloride Ion Penetration. West Conshohocken, PA: ASTM International. https://doi.org/10.1520/C1202-22.

ASTM C1437. 2020. Test Method for Flow of Hydraulic Cement Mortar. West Conshohocken, PA: ASTM International.

ASTM C1609/C1609M. 2019. Test Method for Flexural Performance of Fiber-Reinforced Concrete (Using Beam With Third-Point Loading). West Conshohocken, PA: ASTM International.

ASTM C1812/C1812M. 2015. Standard Practice for Design of Journal Bearing Supports to Be Used in Fiber Reinforced Concrete Beam Tests. West Conshohocken, PA: ASTM International.

ASTM C1856/C1856M. 2017. Standard Practice for Fabricating and Testing Specimens of Ultra-High Performance Concrete. West Conshohocken, PA: ASTM International.

Bache, H. H. 1981. Densified Cement Ultra-Fine Particle-Based Materials. Aalborg: Aalborg Portland.

Baby, F., B. Graybeal, P. Marchand, and F. Toutlemonde. 2013. "UHPFRC Tensile Behavior Characterization: Inverse Analysis of Four-Point Bending Test Results." *Materials and Structures* 46 (8): 1337–1354.

Berry, M., R. Snidarich, and C. Wood. 2017. Development of Non-Proprietary Ultra-High Performance Concrete. Helena: Montana Department of Transportation.

Blais, P. Y., and M. Couture. 1999. "Precast, Prestressed Pedestrian Bridge-World's First Reactive Powder Concrete Bridge." PCI Journal 44 (5): 60-71.

Chen, Y., F. Matalkah, W. Rankothge, A. Balachandra, and P. Soroushian. 2017. "Improvement of the Surface Quality and Aesthetics of Ultra-High-Performance Concrete." Proceedings of the Institution of Civil Engineers-Construction Materials 172 (5): 246-55.

de Larrard, F., and T. Sedran. 1994. "Optimization of Ultra-High-Performance Concrete by the Use of a Packing Model." Cement and Concrete Research 24 (6): 997-1009.

El-Tawil, S., Y.-S. Tai, B. Meng, W. Hansen, and Z. Liu. 2018. Commercial Production of Non-Proprietary Ultra High Performance Concrete. RC-1670. Ann Arbor: University of Michigan.

El-Tawil, S., M. A. Saqif, and D. Rogers. 2023. "Lab-Mixed versus Truck-Mixed UHPC-What's the Difference?" Concrete International 45 (1).

Florida Department of Transportation. 2023. Developmental Specification 349: Non-Proprietary Ultra-High Performance Concrete (UHPC). Tallahassee: Florida Department of Transportation.

Floyd, R. W., J. S. Volz, M. Zaman, et al. 2023. Design and Monitoring of Non-Proprietary UHPC Joints of Precast Elements. FHWA-OK-23-01. Norman: University of Oklahoma.

Floyd, R. W., J. S. Volz, M. Zaman, et al. 2024. Development of Non-Proprietary UHPC Mix. ABC-UTC-2016-C2-OU01-Final.

Funk, J. E., and D. R. Dinger. 2013. Predictive Process Control of Crowded Particulate Suspensions: Applied to Ceramic Manufacturing. New York: Springer Science & Business Media.

Gali, S., and S. Sritharan. 2024. "Evaluation of AASHTO T 397: Standard Method of Test for Uniaxial Tensile Response of Ultra-High-Performance Concrete." ACI Materials Journal 121 (1).

Giesler, A. J., S. B. Applegate, and B. D. Weldon. 2016. "Implementing Nonproprietary, Ultra-High-Performance Concrete in a Precasting Plant." PCI Journal 61 (6).

Graybeal, B. 2006. Material Property Characterization of Ultra-High Performance Concrete. FHWA-HRT-06-103. Washington, DC: Federal Highway Administration.

Graybeal, B. 2008. "UHPC in the U.S. Highway Transportation System." Paper presented at the Second International Symposium on Ultra High Performance Concrete, Kassel, Germany, March 5.

Graybeal, B. 2011. Ultra-High Performance Concrete. FHWA-HRT-11-038. Washington, DC: Federal Highway Administration.

Graybeal, B. 2013. Development of Non-Proprietary Ultra-High Performance Concrete for Use in the Highway Bridge Sector. FHWA-HRT-13-100. Washington, DC: Federal Highway Administration.

Graybeal, B. 2014a. Design and Construction of Field-Cast UHPC Connections. FHWA-HRT-14-084. Washington, DC: Federal Highway Administration.

Graybeal, B. 2014b. Tensile Mechanical Response of Ultra-High-Performance Concrete. FHWA-HRT-14-089. Washington, DC: Federal Highway Administration.

Graybeal, B. 2018. Ultra-High Performance Concrete Connections for Precast Concrete Bridge Decks. TechBrief FHWA-HRT-18-013. Washington, DC: Federal Highway Administration.

Graybeal, B. A., and R. G. El-Helou. 2023. Structural Design with Ultra-High Performance Concrete. FHWA-HRT-23-077. Washington, DC: Federal Highway Administration.

Graybeal, B., and F. Baby. 2013. "Development of Direct Tension Test Method for Ultra-High-Performance Fiber-Reinforced Concrete." ACI Materials Journal 110 (2).

Graybeal, B., E. Brühwiler, B.-S. Kim, F. Toutlemonde, Y. L. Voo, and A. Zaghi. 2020. "International Perspective on UHPC in Bridge Engineering." Journal of Bridge Engineering 25 (11): 04020094.

Green, B. H., R. D. Moser, D. A. Scott, and W. R. Long. 2015. "Ultra-High Performance Concrete History and Usage by the Corps of Engineers." Advances in Civil Engineering Materials 4 (2): 132-43.

Haber, Z. 2016. *Ultra-High-Performance Concrete*. Presentation at the 2016 Florida Department of Transportation Design Training Expo, Daytona Beach, Florida.

Han, M.-C., and C.-G. Han. 2010. "Use of Maturity Methods to Estimate the Setting Time of Concrete Containing Super Retarding Agents." Cement and Concrete Composites 32 (2): 164-72.

Huang, H., X. Gao, K. H. Khayat, and A. Su. 2021. "Influence of Fiber Alignment and Length on Flexural Properties of UHPC." Construction and Building Materials 290 (July): 122863.

Khayat, K. H., and M. Valipour. 2018. Design and Performance of Cost-Effective Ultra High Performance Concrete for Bridge Deck Overlays. CMR 18-006. Rolla: Missouri University of Science and Technology Center for Infrastructure Engineering Studies.

Kim, H., B. Moon, X. Hu, et al. 2021. "Construction and Performance Monitoring of Innovative Ultra-High-Performance Concrete Bridge." Infrastructures 6 (9): 121.

Looney, T., A. McDaniel, J. Volz, and R. Floyd. 2019. "Development and Characterization of Ultra-High Performance Concrete with Slag Cement for Use as Bridge Joint Material." British Journal of Civil and Architecture Engineering 1 (2): 1-14.

López, J. Á., P. Serna, J. Navarro-Gregori, and H. Coll. 2016. "A Simplified Five-Point Inverse Analysis Method to Determine the Tensile Properties of UHPFRC from Unnotched Four-Point Bending Tests." *Composites Part B: Engineering* 91 (April): 189–204.

Maalej, M., and V. C. Li. 1994. "Flexural/Tensile-Strength Ratio in Engineered Cementitious Composites." Journal of Materials in Civil Engineering 6 (4): 513-28.

Martínez López, Á. 2017. "Characterisation of the Tensile Behaviour of UHPFRC by Means of Four-Point Bending Tests." PhD diss., Universitat Politècnica de València.

Master Builders Solutions. 2024. "MasterSet DELVO." Accessed November 8, 2024. https://master-builders-solutions.com/en-us/products/masterset/masterset-delvo/.

Mendonca, F., M. Abo El-Khier, G. Morcous, and J. Hu. 2020. Feasibility Study of Development of Ultra-High Performance Concrete (UHPC) for Highway Bridge Applications in Nebraska. SPR-P1(18) M072. Lincoln: Nebraska Department of Transportation.

Mohr, B. J., M. S. E. Maleque, M. S. Islam, T. Huff, and R. C. Henderson. 2025. Development of Tennessee UHPC for Bridge Applications. Nashville: Tennessee Department of Transportation.

Precast/Prestressed Concrete Institute. 2022. Guidelines for the Use of Ultra-High-Performance Concrete (UHPC) in Precast and Prestressed Concrete. TR-9-22. Chicago: PCI.

Rahman, S., T. Molyneaux, and I. Patnaikuni. 2005. "Ultra High Performance Concrete: Recent

Applications and Research." Australian Journal of Civil Engineering 2 (1): 13-20.

Richard, P., and M. Cheyrezy. 1995. "Composition of Reactive Powder Concretes." Cement and Concrete Research 25 (7): 1501-11.

Riding, K. A., C. C. Ferraro, H. R. Hamilton, M. S. Voss, and R. S. Alrashidi. 2019. Requirements for Use of Field-Cast, Proprietary Ultra-High-Performance Concrete in Florida Structural Applications. Report No. 210. Gainesville: University of Florida.

Riding, K. A., C. C. Ferraro, H. R. Hamilton, J. Harley, R. S. Alrashidi, M. S. Voss, D. Alabi, and R. Zamzami. 2022. Ultra-High-Performance Concrete (UHPC) Use in Florida Structural Applications. BDV31-977-105. Gainesville: University of Florida.

Rigaud, S., G. Chanvillard, and J. Chen. 2012. "Characterization of Bending and Tensile Behavior of Ultra-High Performance Concrete Containing Glass Fibers." In *Ultra-High Performance Concrete and Nanotechnology in Construction: Proceedings of Hipermat 2012.*

Russell, H. G., and B. A. Graybeal. 2013. Ultra-High Performance Concrete: A State-of-the-Art Report for the Bridge Community. FHWA-HRT-13-060. Washington, DC: Federal Highway Administration.

Sbia, L. A., A. Peyvandi, I. Harsini, J. Lu, S. U. Abideen, R. R. Weerasiri, A. M. Balachandra, and P. Soroushian. 2017. "Study on Field Thermal Curing of Ultra-High-Performance Concrete Employing Heat of Hydration." ACI Materials Journal 114 (5): 733-43.

Scott, J. D., R. J. Peterman, B. T. Beck, A. A. Robertson, K. A. Riding, and C.-H. J. Wu. 2018. "Determining the Remaining Prestress Force in a Prestressed Concrete Railroad Tie Through Loading in Direct Tension." Paper presented at the 2018 Joint Rail Conference, Pittsburgh, PA, April 18. V001T01A011.

Shafei, B., and R. Karim. 2021. Development of Non-Proprietary Ultra-High Performance Concrete (UHPC) for Iowa Bridges. Ames: Iowa State University.

Shafei, B., and R. Karim. 2022. Non-Proprietary Ultra-High Performance Concrete Mix Design for ABC Applications. Ames: Iowa State University.

Stewart, L. K., L. Kahn, K. Kurtis, and G. Loreto. 2022. Development of GDOT Ultra-High Performance Concrete for Bridge Deck Closure Pours. Atlanta: Georgia Department of Transportation.

Tackett, A. M., and W. M. Hale. 2010. "Examining the Effects of Mixer Type and Temperature on the Properties of Ultra-High Performance Concrete." MS thesis, University of Arkansas.

Thomas, M., B. Green, E. O'Neal, V. Perry, S. Hayman, and A. Hossack. 2012. "Marine Performance of UHPC at Treat Island." In Ultra-High Performance Concrete and Nanotechnology in Construction: Proceedings of Hipermat 2012, 3rd International Symposium on UHPC and Nanotechnology for High Performance Construction Materials. Kassel: Kassel University Press.

U.S. Geological Survey. 2025. Mineral Commodity Summaries 2025. Reston, VA: U.S. Geological Survey.

Voss, M. S., K. A. Riding, R. S. Alrashidi, C. C. Ferraro, and H. R. Hamilton. 2022. "Comparison between Direct Tension, Four-Point Flexure, and Simplified Double-Punch Tests for UHPC Tensile Behavior." Journal of Materials in Civil Engineering 34 (9): 04022229.

Wille, K., A. E. Naaman, and G. J. Parra-Montesinos. 2011a. "Ultra-High Performance Concrete with Compressive Strength Exceeding 150 MPa (22 Ksi): A Simpler Way." ACI Materials Journal 108 (1).

Wille, K., A. E. Naaman, S. El-Tawil, and G. J. Parra-Montesinos. 2011b. "Ultra-High Performance Concrete and Fiber Reinforced Concrete: Achieving Strength and Ductility without Heat Curing." Materials and Structures 45 (3): 309-24.

Wille, K., and C. Boisvert-Cotulio. 2013. Development of Non-Proprietary Ultra-High Performance Concrete for Use in the Highway Bridge Sector. Report No. PB2013-110587.

Wu, Z., K. H. Khayat, and C. Shi. 2019. "Changes in Rheology and Mechanical Properties of Ultra-High Performance Concrete with Silica Fume Content." Cement and Concrete Research 123 (September): 105786.

Xia, J., T. Chan, K. R. Mackie, M. A. Saleem, and A. Mirmiran. 2018. "Sectional Analysis for Design of Ultra-High Performance Fiber Reinforced Concrete Beams with Passive Reinforcement." Engineering Structures 160 (April): 121-32.

Yalçınkaya, Ç., and O. Çopuroğlu. 2021. "Elephant Skin Formation on UHPC Surface: Effects of Climatic Condition and Blast Furnace Slag Content." Construction and Building Materials 268 (February): 121126.

Yu, R., P. Spiesz, and H. J. H. Brouwers. 2014. "Mix Design and Properties Assessment of Ultra-High Performance Fibre Reinforced Concrete (UHPFRC)." Cement and Concrete Research 56: 29-39.

Yuan, S., V. T. Nguyen, F. Yang, and J. Li. 2023. "Investigation of 'Elephant Skin' on UHPC Surface via a New Test Method: Influencing Factors, Formation Mechanism and Control Measures." Construction and Building Materials 409 (December): 134152.

Zhou, M., W. Lu, J. Song, and G. C. Lee. 2018. "Application of Ultra-High Performance Concrete in Bridge Engineering." Construction and Building Materials 186 (October): 1256-67.

Zhu, Y., Y. Zhang, H. Hussein, and S. Qu. 2021. "Existing Inverse Analysis Approaches for Tensile Stress-Strain Relationship of UHPC with Treated Steel Fibers." Journal of Materials in Civil Engineering 33 (6): 04021118

APPENDIX A

DRAFT ALDOT SPECIAL PROVISION

ALDOT 5XY

ULTRA-HIGH-PERFORMANCE CONCRETE (UHPC)

5XY.01 Description.

This work consists of furnishing and placing ultra-high-performance concrete (UHPC) as indicated on the plans. UHPC is a fiber-reinforced, cementitious composite material that consists of cementitious materials, water, fine aggregate, chemical admixtures, and steel fibers.

UHPC shall be either a proprietary product or a non-proprietary mixture. Regardless of source, the UHPC shall meet the performance requirements of this Special Provision.

5XY.02 Materials.

(a) General Requirements.

The UHPC mixture proportions shall have a maximum water-to-cementitious materials ratio of 0.25. The UHPC shall be self-consolidating and shall not require internal vibration for placement.

(b) Constituent Materials.

UHPC shall consist of any combination of the following constituent materials:

(1) Cement: Portland cement conforming to ALDOT Section 815 is permitted.
(2) Mineral Admixtures: Only mineral admixtures conforming to ALDOT Section 806 are permitted in non-proprietary UHPC. Other mineral admixtures may be used if approved by the Engineer.
(3) Fine Aggregate: Fine aggregate conforming to ALDOT Section 802 or meeting the gradation requirements of AASHTO M 6. No coarse aggregates are permitted. Optimized gradations that do not meet the gradation requirements given in Section 802 are permitted; however, these shall be submitted to the Materials and Tests Engineer for approval prior to use.
(4) Water: Water conforming to ALDOT Section 807 is permitted.
(5) Chemical Admixtures: Only chemical admixtures conforming to ALDOT Section 809 are permitted. The use of calcium chloride will not be permitted. No air-entraining admixture is required.
(6) Steel Fibers: Straight steel fibers shall be used that conform to ASTM A820. Steel fibers shall have a minimum tensile strength of 300 ksi and a nominal length of approximately 0.5 inches.

(c) Mixture Requirements for Non-Proprietary UHPC.

Non-proprietary UHPC producers shall submit mixture designs and certified test reports from an independent AASHTO-accredited laboratory demonstrating that the product meets the requirements of Tables 1 and 2. Any change of materials or material sources requires new testing and certification. The mixture design submittal shall include constituent material sources, proportions, yield, batching and mixing procedures, allowable temperature ranges, and the fresh and hardened properties of the UHPC.

Table 1: UHPC Mixture Design Prequalification Test Requirements

Property	Test Method	Requirement
Flow	ASTM C1437 per ASTM C1856	7 to 11 inches
Temperature	AASHTO T 309	≤ 90°F {32°C}
Compressive Strength*	ASTM C39 per ASTM C1856	≥ 17,500 psi at 56 days
Shrinkage**	ASTM C157 per ASTM C1856	≤ 800 microstrain at 28 days

Note: * Make three 3 in. x 6 in. cylindrical specimens for all compressive strength testing.
** Specimens demolded after 24 hours, and lime cured for 24 hours.

Table 2: UHPC Mixture Design Prequalification Tensile Test Requirements

Property*	Acceptance Requirement	Number of Specimens	Test Method
Effective Cracking Strength	≥ 850 psi at 28 days	4 (At least 2 valid results)	AASHTO T 397
Localization Stress	> $f_{t,cr}$ at 28 days		
Flexural Strength (peak)	≥ 2,300 psi at 28 days	3 (At least 2 valid results)	ASTM C1609 per ASTM C1856
Ratio of Flexural Strength to First-Peak Strength	≥ 1.25 at 28 days		

Note: * The Contractor shall use either AASHTO T 397 or ASTM C1609 for tensile prequalification. The selected method shall be identified in the UHPC submittal and consistently used throughout the project.

(d) Mixture Requirements for Proprietary UHPC.

Proprietary UHPC products shall be delivered in original, unopened, moisture-proof packaging with the manufacturer's name, date of manufacture, material expiration date, and storage requirements clearly marked. All materials must be used within the manufacturer's recommended shelf life and in accordance with manufacturer's instructions. The manufacturer shall provide a product data sheet that includes mixture proportions, yield, batching and mixing procedures, placement methods, curing methods, and allowable temperature ranges. In addition, the manufacturer shall provide for the proposed proprietary UHPC the results for the properties listed in Tables 1 and 2.

5XY.03 Submittals.

Submit the following to the Engineer at least 60 days prior to the first placement of UHPC:

(1) UHPC Placement Plan: The placement plan shall include the proposed method of surface preparation and required surface profile texture; proposed forming methods; proposed batching sequence and mixing procedure (including order of introduction of materials and mixing times); proposed placement sequence and schedule; details of all equipment to be used; curing procedures and minimum cure times; testing procedures; and quality control/assurance testing.

(2) UHPC mixture design and certified test results from an AASHTO-accredited laboratory demonstrating compliance with Tables 1 and 2. For proprietary UHPC, the manufacturer's product data sheet and certified independent test reports shall be submitted. For non-proprietary products, the mixture proportions, material sources, and independent test data shall be submitted.

(3) A list of projects in which the proposed UHPC product has been used in similar applications as the intended ALDOT project. The Engineer reserves the right to reject UHPC material that lacks a demonstrated record of field performance in the intended ALDOT application.

(4) Credentials and experience of the UHPC representative who will be on site during all placements.

5XY.04 Equipment.

Furnish all materials, tools, equipment, transportation, storage, access, labor, and supervision required for the proper batching, mixing, transport, placement, finishing, and curing of UHPC.

For proprietary UHPC, use mixing equipment recommended by the manufacturer. For non-proprietary UHPC, use a high-shear mixer or equipment demonstrated to achieve adequate dispersion of fibers and cementitious constituents. Ready mixed concrete trucks may be used if demonstrated during trial batching to produce UHPC meeting the specified fresh and hardened properties.

Provide equipment necessary to test fresh UHPC properties (flow and temperature) and to cast and cure compressive strength specimens at the project site.

5XY.05 UHPC Mockup.

(a) Mockup Requirements.

The Contractor shall construct a UHPC mockup between 60 and 365 calendar days prior to placement of UHPC in the intended ALDOT project. The UHPC mockup shall be a full-scale representation of the intended UHPC application and if applicable, shall replicate the interface between UHPC and any existing concrete (i.e., cast-in-place or precast concrete). The mockup shall replicate the form pressure created by the liquid UHPC. All form joints will be sealed to prevent leakage of any paste or mortar, and leak-tightness will be assessed by the Engineer during placement of the mockup.

The Contractor shall schedule a pre-pour meeting prior to field casting the mockup. The meeting shall address the placement and finishing plan, testing plan, experience with previous UHPC placements, and the Engineer's expectations for a successful mockup. The Engineer's approval of the mockup is required before field casting of UHPC in the mockup may proceed.

The mockup shall use the same UHPC materials, equipment, and procedures proposed for the project. During placement the Contractor shall demonstrate that the UHPC can be properly mixed and placed while meeting the requirements of this specification. The testing required for the mockup is covered in Subarticle 5XY.05(b).

After a minimum of 14 days of curing, the Contractor shall cut the hardened mockup at two locations determined by the Engineer. The Engineer shall conduct visual inspection of two cross sections that could include the joint interface. Any signs of leakage, segregation, or non-uniformity of the constituent materials will be unacceptable.

If the UHPC produced for the mockup does not produce the required results, the Contractor shall make adjustments to the UHPC and produce another mockup. No separate payment will be made for additional mockups.

(b) Testing Requirements for Mockup.

Perform testing for the mockup to ensure that the UHPC meets the performance requirements defined in Table 1.

(1) Flow: One test per ASTM C1437 with modifications from ASTM C1856.
(2) Temperature of freshly mixed UHPC: One test per batch, per AASHTO T 309.
(3) Compressive Strength: Cast one set of three 3 in. x 6 in. cylinders for testing at 28 and 56 days. Include additional sets when other test ages are specified in the Contract Documents. Test per ASTM C39 with modifications from ASTM C1856. The average compressive strength of each 56-day set of three cylinders shall equal or exceed 17,500 psi. No individual cylinder shall fall below 90% of the specified minimum strength.

5XY.06 Construction Requirements.

The following is part of UHPC construction:

(1) The UHPC material supplier shall be on site during all UHPC placement operations. The material supplier shall be knowledgeable in the supply, mixing, delivery, placement, and curing of the UHPC material.
(2) Perform forming, batching, placing, and curing in accordance with the approved UHPC Placement Plan and manufacturer's instructions.
(3) During batching, maintain the temperature of freshly mixed UHPC below 90°F {32°C}. Ice may be used as part of the mixture water to control temperature, provided the total water content does not exceed the allowable water-to-cementitious materials ratio.
(4) The delivery and placement of UHPC shall be completed within 1 hour and 45 minutes, measured from the time water is first added to the cementitious materials until placement of the load is complete. Where the work requires a longer window, the Contractor shall establish it by trial batching at the anticipated placement temperature, using the qualified hydration-control admixture dosage, and submit the results to the Engineer for review and approval.
(5) Formwork in contact with the UHPC shall be made from non-absorptive materials (e.g., sealed plywood or steel). Seal all form joints to prevent leakage of any paste or mortar. Design and construct forms for the maximum formwork pressure associated with UHPC and its placement. Follow the manufacturer’s recommendations for the design and fabrication of forms.
(6) Prewet and maintain in a saturated-surface dry condition all existing concrete surfaces that will be in contact with UHPC. Remove all standing surface water immediately before placement.
(7) Keep connections and surfaces free of oil, dirt, and debris.
(8) Do not vibrate UHPC. Discharge all succeeding UHPC placements into fluid UHPC. When pouring long or intersecting joints, ensure that the leading edge of the pour does not dry out or form a cold joint.

(9) Do not remove formwork prior to 24 hours after UHPC placement or until the UHPC has achieved a compressive strength of 10,000 psi, whichever is later.
(10) Cure non-proprietary UHPC with a resin-based curing compound applied at the manufacturer's recommended coverage rate. Cure proprietary UHPC by following the manufacturer's recommendations. Curing shall be applied as soon as possible after finishing is completed.
(11) Cure and protect the UHPC from moisture loss until it has achieved a compressive strength of at least 10,000 psi or 50% of the specified 28-day compressive strength, whichever is lower.
(12) If grinding of the UHPC surface is specified, then the UHPC surface shall be slightly overfilled. Do not perform grinding until the UHPC has achieved a compressive strength of at least 14,000 psi (unless a different value is specified in the Contract Documents). If significant fiber pullout is observed during grinding, suspend operations and obtain written approval from the Engineer before resuming.
(13) The structural element may be loaded or opened to traffic when the UHPC has attained a minimum compressive strength of 14,000 psi, unless a different value is specified in the Contract Documents.

5XY.07 UHPC Testing Requirements During Production.

(a) Testing.

UHPC lot is defined as 10 cubic yards or fraction thereof. Perform testing for each lot and determine if the UHPC meets the performance requirements defined in Table 1, excluding shrinkage:

(1) Flow: One test per batch.
(2) Temperature: One test per batch.
(3) Compressive Strength: Cast three sets of three 3 in. x 6 in. cylinders per lot. Take one set at the beginning, one at the midpoint, and one at the end of the lot. Cure all specimens in an environment representative of the placed UHPC. Track all sets to lot numbers for traceability.
Test compressive strength cylinders as follows: one set when form removal or loading is desired; one set at 56 days to verify achievement of specified compressive strength listed in Table 1; and one set reserved.

(b) Quality Acceptance.

The average compressive strength of each 56-day set of three cylinders shall equal or exceed 17,500 psi. No individual cylinder shall fall below 90% of the specified minimum strength. If the 56-day compressive strength does not meet the specified requirements, the Engineer will evaluate the placement and may require coring, load testing, or removal and replacement.

Record all flow results, temperatures, compressive strengths, batch quantities, lot numbers, and placement locations. Submit a copy of all records to the Engineer as part of the as-built documentation.

5XY.08 Method of Measurement.

Measurement will be by the cubic yard of UHPC placed and accepted. The quantity of UHPC to be paid for will be the Plan Quantity, in cubic yards, in place.

5XY.09 Basis of Payment.

(a) Unit Price Coverage.

UHPC unit price shall constitute full compensation for all work including surface preparation, mixing, supplying, transporting, mockups, placing, finishing, curing, grinding (if required), accessories, all items cast into the concrete, and for all other materials, equipment, labor, and incidentals required to make the UHPC part of the completed project.

(b) Payment will be Made under Item No.:

5XY Ultra-High-Performance Concrete (UHPC), ____ cubic yard

APPENDIX B
FLEXURAL CONVERSION FROM DIRECT-TENSION TEST

MATLAB CODE

```
% UHPC Flexural Forward Analysis
% Sectional equilibrium approach
% Inputs: E and stresses in ksi | Outputs: stress in psi, displacement in inches

clear; clc; close all;

% Material Parameters (AASHTO T 397 results)
E_ksi       = 5720;
ft_cr_ksi   = 0.88;
ft_peak_ksi = 1.08;
ft_loc_ksi  = 1.01;

et_cr   = 0.000346727;
et_peak = 0.000991123;
et_loc  = 0.002401507;

% Convert to psi
p.E        = E_ksi * 1000;
p.ft_cr    = ft_cr_ksi * 1000;
p.ft_peak  = ft_peak_ksi * 1000;
p.ft_loc   = ft_loc_ksi * 1000;
p.ft_final = p.ft_cr;
p.et_cr    = et_cr;
p.et_peak  = et_peak;
p.et_loc   = et_loc;
p.et_fail  = et_loc + 0.0003;

% Specimen Geometry: 3 x 3 x 14 in., 12 in. span, third-point loading
p.b = 3.0;
p.h = 3.0;
p.L = 12.0;
```

```
% Section Analysis
n_points = 400;
phi_cr  = 2 * p.ft_cr / (p.E * p.h);
phi_max = phi_cr * 60;
phi_vec = linspace(0, phi_max, n_points);

M_vec        = zeros(size(phi_vec));
yn_vec       = zeros(size(phi_vec));
converged    = false(size(phi_vec));
ec_solutions = zeros(size(phi_vec));

options = optimset('Display', 'off', 'TolX', 1e-10, 'TolFun', 1e-8);

for i = 1:length(phi_vec)
    phi = phi_vec(i);

    if phi < 1e-10
        M_vec(i)     = 0;
        yn_vec(i)    = p.h / 2;
        converged(i) = true;
        continue;
    end

    % Initial guess for compression fiber strain
    if i == 1
        ec_guess = -phi * p.h / 2;
    elseif converged(i-1)
        ec_guess = ec_solutions(i-1);
    else
        prev = find(converged(1:i-1), 1, 'last');
        if ~isempty(prev)
            ec_guess = ec_solutions(prev) * (phi / phi_vec(prev));
        else
            ec_guess = -phi * p.h / 2;
        end
    end
```

```
force_eq = @(ec) integral(@(y) get_stress(ec + phi*y, p) * p.b, ...
                    0, p.h, 'AbsTol', 1e-10, 'RelTol', 1e-8);

guess_mults = [1.0, 0.5, 1.5];
for attempt = 1:3
   if converged(i), break; end
   try
      ec_sol = fzero(force_eq, ec_guess * guess_mults(attempt), options);
      yn_sol = -ec_sol / phi;
      if yn_sol > 0 && yn_sol < p.h
         M_int = @(y) get_stress(ec_sol + phi*y, p) .* (y - yn_sol) * p.b;
         M = integral(M_int, 0, p.h, 'AbsTol', 1e-10, 'RelTol', 1e-8);
         if M >= 0
            M_vec(i)      = M;
            yn_vec(i)     = yn_sol;
            converged(i)  = true;
            ec_solutions(i) = ec_sol;
         end
      end
   catch
      if attempt == 3 && ~converged(i)
         try
            ec_sol = fzero(force_eq, [-phi*p.h*2, phi*p.h], options);
            yn_sol = -ec_sol / phi;
            if yn_sol > 0 && yn_sol < p.h
               M_int = @(y) get_stress(ec_sol + phi*y, p) .* (y - yn_sol) * p.b;
               M = integral(M_int, 0, p.h, 'AbsTol', 1e-10, 'RelTol', 1e-8);
               if M >= 0
                  M_vec(i)      = M;
                  yn_vec(i)     = yn_sol;
                  converged(i)  = true;
                  ec_solutions(i) = ec_sol;
               end
            end
         catch
         end
      end
```

```
    end
  end
end

% Load-Displacement Transformation (Martinez Lopez 2017)
valid = converged & M_vec > 0 & ~isnan(M_vec) & ~isinf(M_vec);
phi_v = phi_vec(valid);
M_v   = M_vec(valid);

P        = (6 * M_v) / p.L;
delta_lin = (23 * p.L^2 / 216) .* phi_v + ...
            (12 * P * p.L) / (25 * p.E * p.b * p.h);
delta_log = (5  * p.L^2 / 72 ) .* phi_v + ...
            (P / (6 * p.E * p.b)) .* (p.L / p.h)^3 + ...
            (12 * P * p.L) / (25 * p.E * p.b * p.h);
delta = min(delta_lin, delta_log);
sigma = (6 * M_v) ./ (p.b * p.h^2);

% Critical Points
peak_stress = max(sigma);

% Initial stiffness: linear regression over 20-60% of peak load range
mask = sigma > 0.20 * peak_stress & sigma < 0.60 * peak_stress & delta > 0;
k0   = sum(delta(mask) .* sigma(mask)) / sum(delta(mask).^2);

% Elastic limit: first point above 50% of peak with stiffness deviation exceeding 5%
idx_el = length(sigma);
for i = 1:length(delta)
  if k0 * delta(i) > 0 && sigma(i) > 0.50 * peak_stress
    if (sigma(i) - k0 * delta(i)) / (k0 * delta(i)) * 100 < -5
      idx_el = i;
      break;
    end
  end
end
f1     = sigma(idx_el);
disp_el = delta(idx_el);
```

```
% Peak
[fp, pk_idx] = max(sigma);
disp_pk = delta(pk_idx);

% Stiffness reference line
d_line = linspace(0, max(delta), 100);
s_line = k0 * d_line;

fprintf('f1  = %.0f psi  at  delta = %.4f in\n', f1, disp_el);
fprintf('fp  = %.0f psi  at  delta = %.4f in\n', fp, disp_pk);

% Plot
figure('Position', [100, 100, 900, 650]);
hold on;

plot(delta, sigma, 'b-', 'LineWidth', 2, ...
    'DisplayName', 'Calculated');
plot(d_line, s_line, '--', 'Color', [0.5 0.5 0.5], 'LineWidth', 1.2, ...
    'DisplayName', 'Initial Stiffness');
plot(disp_el, f1, 'o', 'MarkerSize', 9, ...
    'MarkerFaceColor', [0 0.6 0], 'MarkerEdgeColor', [0 0.6 0], ...
    'DisplayName', sprintf('f_{1} = %.0f psi', f1));
plot(disp_pk, fp, 'o', 'MarkerSize', 9, ...
    'MarkerFaceColor', 'b', 'MarkerEdgeColor', 'b', ...
    'DisplayName', sprintf('f_{P} = %.0f psi', fp));
plot([disp_el disp_el], [0 f1], '--', 'LineWidth', 0.5, ...
    'Color', [0 0.6 0], 'HandleVisibility', 'off');

xlim([0, max(delta) * 1.05]);
ylim([0, peak_stress  * 1.10]);

set(gca, 'FontName', 'Times New Roman', 'FontSize', 20);
xlabel('Midspan Deflection (in.)',  'FontName', 'Times New Roman', 'FontSize', 20, 'FontWeight', 'bold');
ylabel('Flexural Stress (psi)',     'FontName', 'Times New Roman', 'FontSize', 20, 'FontWeight', 'bold');
```

```
legend('Location', 'best', 'FontName', 'Times New Roman', 'FontSize', 20);
grid on;
set(gca, 'GridLineStyle', '--', 'GridAlpha', 0.3);
box on;

% Four-stage piecewise linear stress-strain constitutive model
function sigma = get_stress(epsilon, p)
    sigma = zeros(size(epsilon));
    for i = 1:numel(epsilon)
        e = epsilon(i);
        if e < 0
            sigma(i) = p.E * max(e, -0.003);
        elseif e <= p.et_cr
            sigma(i) = p.E * e;
        elseif e <= p.et_peak
            sigma(i) = p.ft_cr + (p.ft_peak - p.ft_cr) * ...
                       (e - p.et_cr) / (p.et_peak - p.et_cr);
        elseif e <= p.et_loc
            sigma(i) = p.ft_peak - (p.ft_peak - p.ft_loc) * ...
                       (e - p.et_peak) / (p.et_loc - p.et_peak);
        elseif e <= p.et_fail
            sigma(i) = p.ft_loc - (p.ft_loc - p.ft_final) * ...
                       (e - p.et_loc) / (p.et_fail - p.et_loc);
        else
            sigma(i) = max(p.ft_final * exp(-5 * (e - p.et_fail)), 100);
        end
    end
end
```